

THERMOMECHANICAL AND THERMOCHEMICAL BEHAVIOR
OF A HAFNIUM-20 PERCENT TANTALUM ALLOY

by

JAMES PRESTON HOWELL


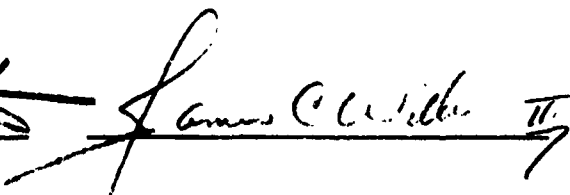


A thesis submitted to the Graduate Faculty of
North Carolina State University at Raleigh
in partial fulfillment of the
requirements for the Degree of
Doctor of Philosophy

DEPARTMENT OF MATERIALS ENGINEERING

(NASA-TM-X-68339) THERMOMECHANICAL AND N72-25524
THERMOCHEMICAL BEHAVIOR OF A HAFNIUM-20
PERCENT TANTALUM ALLOY Ph.D. Thesis -
North Carolina State Univ., Raleigh J.P. Unclas
Howell (NASA) 1971 171 p CSCL 11D G3/17 30540
RALEIGH

1 9 7 1

APPROVED BY:

 
 
Chairman of Advisory Committee

ABSTRACT

HCWELL, JAMES PRESTON. Thermomechanical and Thermochemical Behavior of a Hafnium-20 Percent Tantalum Alloy. (Under the direction of CHARLES R. MANNING, JR.)

An investigation was conducted to determine the thermomechanical and thermochemical behavior of a high temperature oxidation resistant hafnium-20 percent tantalum alloy. The elastic and shear moduli of this alloy were determined in air up to 1000°C and in vacuum up to 2000°C using a mechanical resonance technique. The internal friction of the alloy was measured up to temperatures greater than 1400°C . Room temperature stress-strain behavior of the oxidized and unoxidized alloy was established. The effect of annealing on the elastic and shear moduli of the extruded rod material was investigated. The martensitic-type phase transformation occurring in the alloy was studied using hot stage metallography and electron microscopy. Static oxidation tests were conducted on the alloy at temperatures from 1000°C to 1700°C with weight gain measurements made as a function of time and temperatures. Surface morphology studies were conducted on the oxide coatings formed at the different temperatures using scanning electron microscopy and X-ray diffraction techniques.

The elastic modulus of the hafnium-20 percent tantalum extruded rod material as received was found to be 17×10^6 psi with a shear modulus of $6.8 - 7.0 \times 10^6$ psi at room temperature. Annealing the alloy at 1200°C for 4 hours was found to increase the elastic modulus to 18.6×10^6 psi and the shear modulus to 7.4×10^6 psi. The lower moduli of the as received material was attributed to the preferred

orientation of the extruded rod specimens. Poisson's ratio of the annealed alloy was found to be 0.27.

The elastic and shear moduli decreased linearly with increasing temperatures up to about 1020° C. Above this temperature the moduli dropped very rapidly and was accompanied by a rapid increase in the internal friction. At 1400° C the internal friction was 133 times greater than the room temperature value of $Q^{-1} = 9.1 \times 10^{-5}$ and continuing to rise. At 1979° C the elastic modulus decreased to 3.5×10^6 psi or less than 20 percent of its room temperature value.

Ultimate tensile strength of the as received alloy averaged 151,000 psi with failure being that of ductile fracture. Annealing lowered the strength to 120,400 psi while oxidation at 1000° C caused a 75-percent decrease in strain-to-failure which was characterized by a typical brittle fracture.

Results of static oxidation studies indicate a typical parabolic oxidation behavior for times up to 3 hours, tending to become linear beyond that point. Surface oxide morphology studies show that oxide coatings formed at temperatures below 1400° C are mixtures of monoclinic and stabilized tetragonal HfO_2 , and $\beta-Ta_2O_5$. They are typically white in color and are susceptible to severe cracking in cooling from elevated temperatures. In contrast, coatings formed above 1400° C were bluish/gray in color, predominantly stabilized tetragonal HfO_2 and $\beta-Ta_2O_5$. Individual oxide needles formed in coatings above 1400° C and sintered together forming a smooth, molten, tightly adherent coating.

Results of this investigation indicate the potential of the hafnium-20 percent tantalum alloy for use in high temperature oxidizing

environments. It is, however, limited to relative short time applications, has low elastic and shear moduli at elevated temperatures, and is embrittled by preferred oxidation at the grain boundaries.

BIOGRAPHY

The author was born [REDACTED] [REDACTED] [REDACTED] [REDACTED]. He attended public schools in that city, graduating in 1958. He entered in University of South Carolina in September 1958 and received his Bachelor of Science degree in Mechanical Engineering in January 1963. Upon graduation the author entered the United States Navy as an Ensign where he served 2 years of sea duty on the U.S.S. Luce (DLG-7). Upon release from active military duty, he accepted a position as an Aerospace Technologist with NASA-Langley Research Center. He returned to the University of South Carolina in September 1966, receiving his Master of Science degree in Mechanical Engineering in August 1967. The author completed an additional year of study toward the Ph.D at South Carolina, returning to NASA in June 1968. He entered North Carolina State University in January 1969 and completed his Ph.D course requirements in Materials Engineering. The author returned to Langley Research Center to his present position as an Aerospace Materials Engineer. He is a member of the American Society of Metals and Sigma Xi honorary society.

The author was married in 1963 to the former Elizabeth Ann Mills, and they have two children, James, Jr. and Kristin Elizabeth.

ACKNOWLEDGMENTS

The author extends his deepest appreciation to Dr. Charles R. Manning, Jr., under whose guidance and encouragement this research was conducted. Special thanks and sincere appreciation is expressed for the time and effort given by the Advisory Committee: Dr. William W. Austin, Dr. J. C. Williams, Dr. A. A. Fahmy, and Dr. Manning.

The author would also like to extend appreciation to the engineering technicians: Mr. Beryl Abicht, Mr. Albert Shearin, Mr. Gene Rollins, Mr. Charles Whitehead, Mr. Ashby Lawson, Mrs. Alberta Saunders, and Mrs. Elsie Illg, each of whom assisted the author in carrying out the experimental aspects of this investigation. Mrs. Sue K. Seward deserves special appreciation for her help in conducting the literature survey.

Many thanks go to Mrs. Mary Edwards for her expedient typing of this final manuscript.

The author would like to thank his wife, Elizabeth Howell, for the encouragement which she provided him during the many months of this investigation.

Finally, the author expresses his appreciation to the National Aeronautics and Space Administration for support of this project.

TABLE OF CONTENTS

	Page
LIST OF TABLES	vi
LIST OF FIGURES	vii
INTRODUCTION	1
REVIEW OF LITERATURE	4
General Development	4
Hafnium-Tantalum Phase Diagram	9
Oxidation Behavior	11
X-Ray Diffraction	20
Elasticity Fundamentals	21
Introduction	
Concept of Stress-Strain	22
Dynamic Elasticity Fundamentals	26
Internal Friction Review	33
Internal Friction Resulting from Thermal Effects	37
Internal Friction Resulting from Point Defects	39
Internal Friction Resulting from Dislocations	40
Internal Friction Resulting from Grain Boundaries	42
Other Sources of Internal Friction	45
Internal Friction Measurements	45
Torsional Pendulum Method	46
Ultrasonic Pulse Method	46
Resonant Bar Method	47
MATERIALS	49
EQUIPMENT AND EXPERIMENTAL PROCEDURE	53
Dynamic Elasticity and Internal Friction Measurements	53
Stress-Strain Behavior	71
Phase Transformation Study	75
Static Oxidation Behavior	83
Metallographic Techniques	87

TABLE OF CONTENTS (continued)

	Page
RESULTS AND DISCUSSION	89
Room Temperature Dynamic Elasticity Measurements	89
Room Temperature Stress-Strain Behavior	93
Room Temperature Internal Friction	97
Elevated Temperature Dynamic Elasticity and Internal Friction	101
Annealing Behavior	131
Phase Transformation Study	134
Static Oxidation Tests	140
CONCLUSIONS	159
LIST OF REFERENCES	163

LIST OF TABLES

	Page
1. Hafnium-tantalum final ingot analysis	50
2. Hafnium crystal bar analysis	51
3. Tantalum analysis	51
4. Room temperature elastic moduli of hafnium-20% tantalum alloy	90
5. Summary of static tensile test data for hafnium-20% tantalum alloy	94
6. Summary of room temperature measured internal friction data for a hafnium-20% tantalum alloy	102
7. Elevated temperature elastic and shear moduli of hafnium-20% tantalum alloy	104
8. Elevated temperature elastic and shear moduli of hafnium-20% tantalum alloy	105
9. Elevated temperature elastic and shear moduli of hafnium-20% tantalum alloy	106
10. Elevated temperature elastic and shear moduli of hafnium-20% tantalum alloy	107
11. Elevated temperature elastic and shear moduli of pure hafnium metal	108
12. Elevated temperature elastic and shear moduli of hafnium-20% tantalum alloy	109
13. Elevated temperature elastic and shear moduli of hafnium-20% tantalum alloy	110
14. Elevated temperature elastic modulus of hafnium-20% tantalum alloy	111
15. Elevated temperature elastic and shear moduli of hafnium-20% tantalum alloy	112
16. Elevated temperature dependency ratio of the elastic and shear moduli of a preoxidized hafnium-20% tantalum alloy	113
17. Elevated temperature internal friction ratio for hafnium-20% tantalum alloy	127

LIST OF FIGURES

	Page
1. Hafnium-tantalum equilibrium diagram	10
2. Microstructure of hafnium-20% tantalum alloy oxidized by oxygen-hydrogen torch at 1925° C for 10 minutes . . .	12
3. High magnification of subscale-interstitial contamination zone	14
4. Oxidation rate of hafnium-20% tantalum alloys at 1700°-1925° C	16
5. Oxide growth rate for hafnium-20% tantalum alloy	18
6. Typical stress-strain diagram for a ductile, elastic material	25
7. Typical resonant frequency curve for specimen undergoing constant forced vibration	35
8. Magnaflux SR-200 Elastomat for dynamic elasticity measurements up to 1000° C	54
9. Block diagram of Magnaflux SR-200 dynamic elasticity equipment	55
10. Rectangular specimen test setup for Elastomat furnace . . .	57
11. Room temperature sonic resonant frequency system	63
12. Lissajous figure phase relationships for various modes of vibration	63
13. Vacuum high-temperature dynamic elasticity apparatus . .	64
14. Furnace and suspension system for dynamic elasticity apparatus	65
15. Block diagram schematic of vacuum high-temperature dynamic elasticity equipment	66
16. Detail of suspension system for round specimen	68
17. Room temperature damping apparatus	72
18. Detail view of room temperature damping test setup	73

19. Instron static tensile test setup	74
20. X-ray diffraction test setup	76
21. Knoop microhardness measurements test setup	78
22. Hot stage metallograph for phase transformation study . . .	79
23. Vacuum hot stage chamber	80
24. Cambridge scanning electron microscope	82
25. Overall test setup for static oxidation tests	84
26. Specimen suspension system for static oxidation tests . . .	85
27. Hafnium-20% tantalum stress-strain diagram	95
28. Typical ductile and brittle fractures for as received and oxidized hafnium-20% tantalum alloy	96
29. Typical room temperature damping curve for the hafnium-20% tantalum alloy	98
30. Temperature dependency of the elastic modulus of hafnium-20% tantalum up to 1000° C in air	115
31. Temperature dependency of the shear modulus of hafnium-20% tantalum up to 1000° C in air	116
32. Oxidized hafnium-20% tantalum dynamic elasticity test specimen after cooling from 1000° C	118
33. Oxidized pure hafnium dynamic elasticity test specimen after cooling for one and four cycles from 1000° C . . .	119
34. Average values of Poisson's ratio versus temperature up to 1000° C in air for hafnium-20% tantalum alloy	120
35. Elevated temperature elastic modulus and internal friction ratio of an annealed hafnium-20% tantalum alloy	122
36. Elevated temperature shear modulus of an annealed hafnium-20% tantalum alloy	123
37. Elevated temperature elastic modulus ratio for an oxidized and annealed hafnium-20% tantalum alloy	125

38. Elevated temperature shear modulus ratio for an oxidized and annealed hafnium-20% tantalum alloy	126
39. Relative internal friction ratio versus temperature for a hafnium-20% tantalum alloy in air	129
40. Elevated temperature relative internal friction ratio of an annealed and preoxidized hafnium-20% tantalum alloy	130
41. Change in elastic modulus with time at a constant annealing temperature of 1112° C	132
42. Change in relative internal friction ratio with time at a constant annealing temperature of 1112° C	133
43. Scanning electron micrographs of an as received hafnium-20% tantalum alloy	135
44. Hot stage metallography showing hafnium-20% tantalum phase transformation	138
45. Scanning electron micrograph of hafnium-20% tantalum specimen after diffusionless transformation	139
46. Replica electron micrograph showing surface distortions after diffusionless transformation	139
47. Oxidation behavior of a hafnium-20% tantalum alloy in static air	141
48. Static oxidation tests at 1000° C	143
49. Static oxidation tests at 1255° C	144
50. Static oxidation tests at 1470° C	145
51. Static oxidation tests at 1688° C	146
52. Scanning electron micrographs of cross section of specimen oxidized at 1688° C	147
53. Microstructure of hafnium-20% tantalum oxidized at 1000° C	149
54. Microstructure of hafnium-20% tantalum oxidized at 1000° C using polarized light	149

55. Oxide particle formation on heating in air at temperature from 1000° C to 1600° C for 3 minutes	152
56. Needle-like oxide crystals formed at oxidation temperature of 1740° C for 3 minutes	153
57. Oxide crystals sintering at 1700° C after 30-minute exposure	154
58. Oxide whisker formation at 1685° C after 10-minute exposure	156
59. Cracking of oxide coating formed after 30-minute exposure at 1150° C in air	157

INTRODUCTION

With the advent of the space age and the development of hypersonic vehicles, demands for the development of new materials have been increasing at a rapid pace. Extreme temperature aerodynamic environments have been a primary driving force for the development of materials with good oxidation resistance at temperatures above 2000°C , yet having room temperature ductility that will allow forming by techniques used for refractory metals. Refractory metals, in general, are plagued by their very high oxidation rates at elevated temperatures, but encouraging results have been obtained by alloying these high melting point materials with each other.

One such combination of refractory metals which seems to be a promising candidate for a wide variety of applications is the hafnium-tantalum alloy system. Initial investigations of this alloy system suggest potential usage as a coating or a free-standing structure in such applications as reentry vehicle leading edges, ramjet engine structures, rocket thrust chambers and nozzle inserts, and other applications requiring high temperature oxidizing atmospheres.

The early development work in the hafnium-tantalum alloy system has been concentrated in the 20 to 30 percent tantalum, 70 to 80 percent hafnium composition range. Preliminary oxidation data indicates that the greatest oxidation resistance of this alloy system lies within this composition range. Maynard Hill of Johns Hopkins University (1968) has reported coatings of a 20 percent tantalum-hafnium system

to be superior among candidates for small-radius leading edges for hypersonic vehicles.

Prior to the design of high temperature structures, the fundamental mechanical and chemical behavior of the material must be well understood. The mechanical properties of the material must be available as a function of temperature to properly size structures. The degradation of the mechanical behavior of the material in a high temperature oxidizing environment is important, as this alloy's greatest potential usage will be under this condition. Because of high material cost and limited industrial experience in its fabrication, many of the questions on the fundamental behavior of the hafnium-20% tantalum system have not been answered.

The purpose of this investigation was to provide a basic understanding of the thermomechanical and thermochemical behavior of the hafnium-20% tantalum alloy system. The specific objectives were to (1) characterize the fundamental elastic properties of Young's or elastic modulus shear modulus, and Poisson's ratio, of the hafnium-20% tantalum alloy as a function of temperature, up to 2000° C using a mechanical resonance technique; (2) determine the temperature dependence of the internal friction of the alloy system; (3) evaluate the ultimate and yield strength of the alloy at room temperature; (4) study the degradation of mechanical behavior due to extended exposure in an oxidizing environment; (5) study the annealing behavior of the alloy through the mechanical resonance technique; (6) conduct a qualitative structural analysis of the metal alloy and its high and low temperature oxide through X-ray diffraction techniques; (7) study the oxidation

characteristics of the alloy as a function of temperature and time;
and (8) study the martensitic phase transformation of the alloy with
hot stage metallography techniques.

REVIEW OF LITERATURE

General Development

A historical review of the development of the hafnium-tantalum alloy system begins with the discovery of the two metallic elements comprising this system as related by Hempel (1961). Tantalum was discovered in 1802 by the Swedish scientist, Ekeberg, who named it after Tantalus in Greek mythology because of the difficulty of dissolving the oxide. Because of the similarity of the properties of the compounds of columbium and tantalum, the two were regarded as identical for over forty years. The first ductile tantalum was produced in Berlin in 1903 and it was the first metallic filament for incandescent lamps. It has been commercially produced in the United States since 1922.

Tantalum is located in group VB of the periodic table. It has a body-centered cubic crystal structure, an atomic number of 73, and atomic weight of 180.95. It ranks fifty-fourth in order of concentration of elements in the earth's crust, and is always found associated with its sister element, columbium, which is about eleven times as prevalent. It is always found in mineral form, the most important mineral source being a ferrous manganese tantalate-columbate, $(\text{Fe, Mn}) (\text{Ta, Cb})_2 \text{O}_6$.

Extraction processes are used to separate the tantalum from ores or concentrates. The reduction of the compounds to metal can be accomplished by one of several techniques, such as electrolysis, sodium reduction, and interaction of tantalum oxide and tantalum carbide.

Consolidation and purification processes such as sintering, arc melting, and electron beam melting are used to convert powders to massive form.

Tantalum is a strong ductile metal, characterized by (1) high density, 16.6 g/cc; (2) high melting point, 2996°C (third highest among the metals, exceeded only by rhenium, 3180°C , and tungsten, 3410°C); and (3) its extreme inertness to attack by all acids except hydrofluoric and sulfuric, at ordinary temperatures.

Martin and Pizzolato (1961) relate the history of the other major constituent in this alloy system. Hafnium was not discovered until 1923 by Coster and von Hevesy in a careful X-ray study of various zirconium-containing minerals. They announced the discovery of element 72, proposing the name hafnium (from *Hafnia*, Latin for Copenhagen) in honor of the city in which the discovery was made.

Hafnium is located in group **IVA** of the periodic table, and has an atomic number of 72, an atomic weight of 178.6, and crystallizes in the hexagonal, close-packed structure. It occurs in nature in small to moderate amounts associated with zirconium in all types of zirconium-bearing minerals. It is estimated that there are four parts per million of hafnium in the earth's crust. This is about the same as the content of beryllium or uranium, and more than the quantities of tantalum, silver, or mercury. The principal commercial sources of hafnium are the minerals, zircon, $(\text{Zr, Hf})\text{SiO}_4$, and baddeleyite, $(\text{Zr, Hf})\text{O}_2$, primarily processed for their zirconium content.

The main problem in production of hafnium, or reactor grade zirconium, is the separation of these metals, as they react chemically

the same. Several extraction methods have been developed for this separation. Production of the hafnium metal is done by a modified Kroll process in which hafnium tetrachloride is reduced by magnesium or sodium. A hot-wire process is used to refine the hard, brittle sponge hafnium into crystal bar. Vacuum and inert arc melting techniques are used to obtain the finished product material.

Metallic hafnium is characterized by (1) a high melting point, $2222 \pm 30^{\circ}$ C; (2) high density, 13.29 g/cc; (3) good corrosion resistance; and (4) allotropic transformation from HCP crystal structure to body-centered cubic (BCC) at elevated temperature. The physical and chemical properties of this material are greatly dependent on impurity content.

A search of the literature revealed that Elliot (1954) prepared an alloy of the two refractory metals having the composition HfTa_2 . He reported that the alloy could not be fractured or crushed and had a crystal structure composed of a mixture of the BCC and HCP structures.

As the demand for development of materials to meet new high temperature requirements increased during the early 1960's, new programs were initiated to develop unique high temperature, oxidation resistant materials. Because of their high melting points, refractory metals were prime candidates for use in coating materials in the temperature regime between 1650° C and 2200° C for protection of tantalum and tungsten alloys. It is in this temperature range that the strength advantages of these alloys become significant if they can be protected from catastrophic oxidation. Preliminary studies by Marnoch (1965) and Dickinson et al., (1963) indicated that only four of the

refractory metals produced refractory oxides which showed sufficient stability at high temperatures to be considered candidate base materials. These oxides were thoria (ThO_2), hafnia (HfO_2), zirconia (ZrO_2), and beryllia (BeO_2). Thoria was radioactive and beryllia was toxic, leaving hafnia and zirconia as prime candidates. Even though these materials were very similar, hafnia was selected by Marnoch as the base oxide for development of a high temperature coating system.

Hafnium metal by itself will not produce a slow-growing, adherent and stable oxide at elevated temperatures. However, by alloying with other elements, the high temperature oxidation resistance of pure metals can be improved. Marnoch (1965) chose tantalum as his basic alloying element because its oxide stabilizes the high temperature form of hafnia, and because it would form a ductile alloy with hafnium. An extensive program was carried out by the Marquart Corporation in the development of this alloy system. Primary emphasis was placed on developing the oxidation resistance of the system. The oxidation characteristics of the hafnium-tantalum alloys as affected by composition, impurity content, alloying additions, temperature, time, and environment, were investigated. The results indicated that the Hf-20% Ta and Hf-27% Ta binary alloys and Hf-30% Ta-2% Mo ternary alloy offered significant potential for protection of tungsten and alloys of columbium, tantalum, and molybdenum for relatively extended time periods at temperatures up to 2200°C .

In addition to the investigation of Marquart Corporation, Hill and Rausch (1966) of IITRI stimulated more interest in the hafnium-tantalum alloy system in a program for the development of protective

coatings for tantalum base alloys for temperatures above 1950°C . In this program, good oxidation resistance was demonstrated for short times in hafnium alloys containing 15 to 30 weight percent tantalum.

As a result of this IITRI program, Van Thyne, Hess, and Rausch (1966) demonstrated the potential of the Hf-20% tantalum alloy as a cladding material on a Ta-10W liquid fuel rocket nozzle throat. A 0.020-inch cladding of the hafnium-tantalum withstood several restarts and nearly 15 minutes of engine firing at a 2000°C flame temperature.

Van Thyne (1966) continued development of oxidation resistant hafnium alloys under sponsorship of the United States Naval Air Systems Command. The aim of this program was to develop hafnium alloys which could be employed in oxidizing environments in the temperature range of 1200° to 1650°C . The initial goal was an uncoated structural material capable of withstanding at least 100 hours of service. Primary interest was placed on the development and evaluation of oxidation resistant composition. Binary alloys of Hf-Ta and Hf-Cb were shown to oxidize rather severely in less than 20 hours at 1370°C , but ternary additions, such as chromium, aluminum, and boron considerably improved oxidation resistance.

Marnoch (1967) reported on some of the thermal and mechanical properties of the hafnium-tantalum alloys. Thermal conductivity and thermal expansion were reported for the hafnium-20% tantalum-2% molybdenum composition. A limited amount of shear strength data was reported along with some of the bending properties of this alloy. Ultimate tensile strength properties of a Hf-27% Ta alloy were given based on a limited number of tests.

After making significant progress in the development of the hafnium-tantalum alloy system as a potential high temperature coating material under the programs already discussed, a program on fabrication and processing technology was sponsored by NASA. From September 1965 through February 1969, Mash et al., (1968), of Fansteel, Inc., developed optimum processing parameters for the production of clad sheet and tubing. Electron beam and tungsten inert gas arc welding fabrication techniques were investigated. Form spinning and shear spinning techniques were developed. In addition to developing large scale metallurgical processing technology, several hafnium-20% tantalum clad rocket nozzles were produced.

The general historical development of the hafnium-tantalum alloy system having been covered in the preceding pages, a review of the theoretical aspects of behavior of this alloy system and the general fundamentals involved in elasticity and internal friction measurements are presented.

Hafnium-Tantalum Phase Diagram

Some insight into the nature of the hafnium-tantalum alloy system and its behavior can be gained from the phase diagram. This diagram, shown in Figure 1, represents the work of Oden et al., (1964), at the U.S. Bureau of Mines in Albany, Oregon. The BCC allotrope of hafnium forms a continuous series of solid solutions with tantalum. These solid solutions, which exist at elevated temperatures, are designated beta solid solutions. At 24 weight percent tantalum and 1050° C, hafnium rich beta decomposes in a monotectoid reaction to yield a

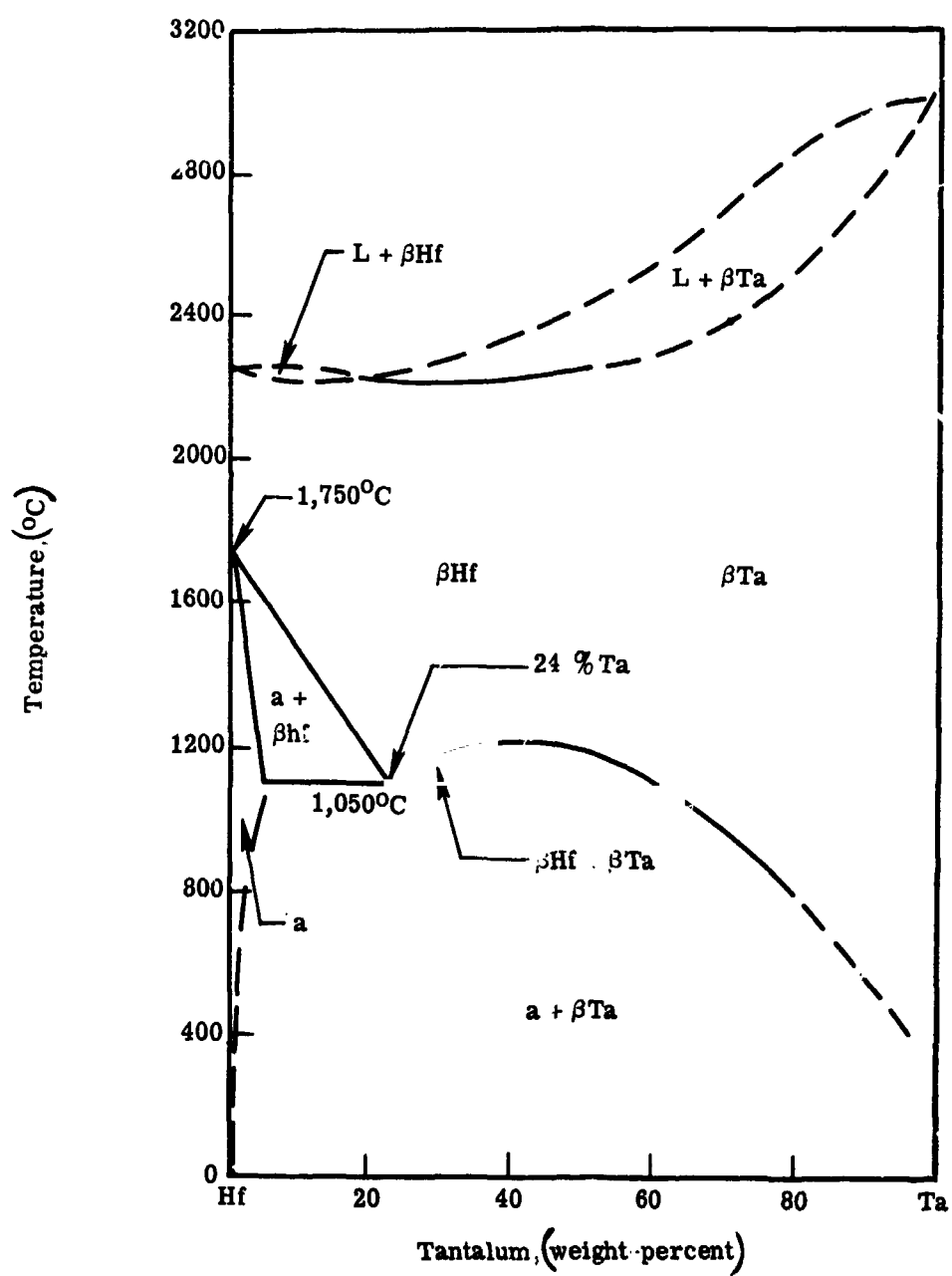


Figure 1. Hafnium-tantalum equilibrium diagram

two-phase region of alpha and tantalum rich beta solid solutions. Russian scientists Svechnikov et al., (1964), obtained somewhat similar results, however, they placed the eutectoid temperature at $1020 \pm 10^{\circ}$ C at 17 weight percent tantalum. On rapid cooling of the alloy they reported the existence of a supersaturated solid solution of Ta in alpha Hf and called it alpha prime (α'), characterized by an acicular appearance.

Oxidation Behavior

The hafnium-tantalum alloy system provides an oxidation-resistant coating system which, according to Marnoch (1965), has relatively high temperature resistance to oxygen, diffusion, freedom from breakaway modes, mechanical and chemical compatibility with several refractory substrata, and some self-healing characteristics. Acting as a reservoir for the protective hafnium-tantalum oxide coating which is formed, excellent protection is afforded to the substrata until the virgin alloy is completely converted to oxide.

The oxidation behavior of the hafnium-20% tantalum alloy is quite complex. Hill and Rausch (1966) have demonstrated that oxidation exposure at high temperatures (1600° C and higher) results in the formation of three basic zones in the alloy: (1) a fully oxidized outer scale; (2) a lamellar metal and oxide subscale; and (3) a two-phase $\alpha + \beta$ zone of interstitial oxygen contamination.

Figure 2 shows a typical metallographic examination as obtained by Hill and Rausch. Electron microprobe analysis of the alloy at Marquart (1965) studied the composition of the various phases visible

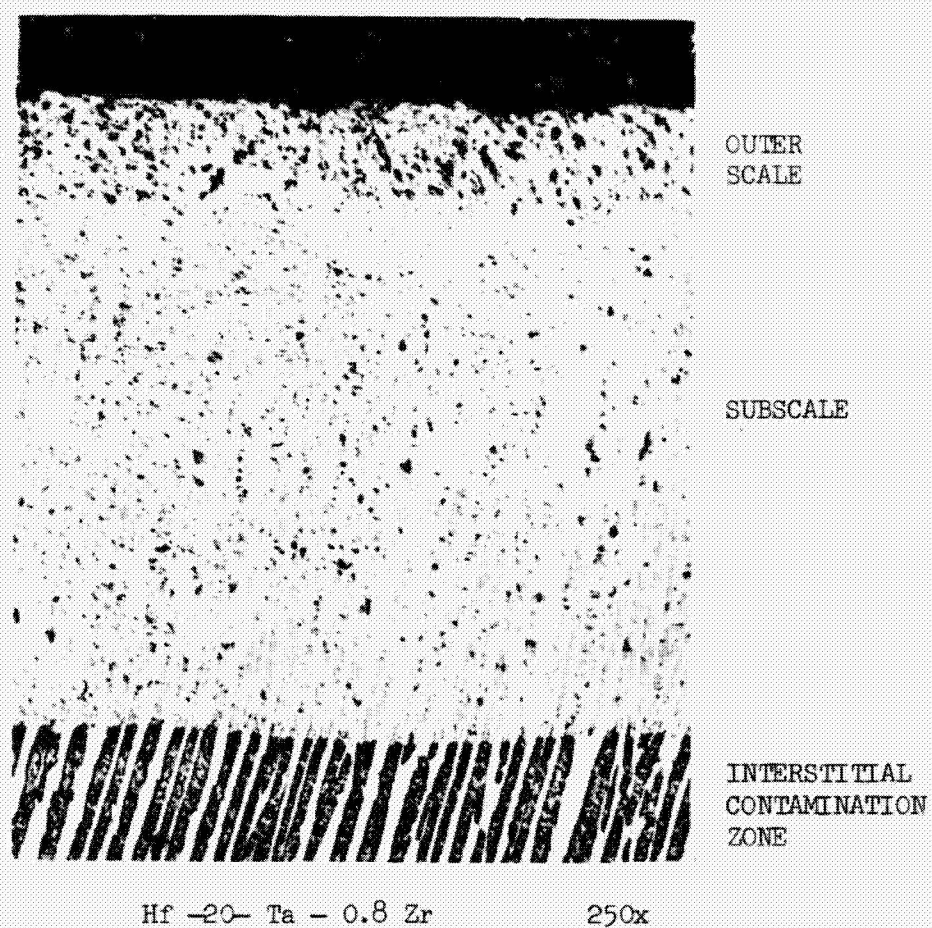


Figure 2. Microstructure of hafnium-20% tantalum alloy oxidized by oxygen-hydrogen torch at 1925° C for 10 minutes. Reproduced from Hill and Rausch (1966)

in the three basic zones. The analysis revealed that in the subscale, the oxide stringers were hafnium rich and the metal stringers were tantalum rich. These stringers are apparently instrumental in the observed tenacity of the oxide. In the oxygen contamination zone, the dark etching lamellae were hafnium rich and the light etching stringers were tantalum rich, but the ratios were different from that of the corresponding lamellae in the subscale; the separation is greater in the oxide stringers of the subscale.

Hill and Rausch reported that the α hafnium and β tantalum equilibrium structures in the subscale and oxygen contamination zone in hafnium-20% tantalum alloys show a preferential oxidation. Marquart Corporation suggests that the dark etching phase in the oxygen contamination zone is primarily alpha hafnium, the light etching phase being primarily beta tantalum. In the subscale, the oxide stringers are probably primarily HfO_2 and the metal stringers possibly oxygen saturated beta tantalum. Figure 3 shows the interface of the subscale-interstitial contamination zone along with the oxide and metallic stringers.

In the production of the hafnium-tantalum alloys, there is always a small percentage of zirconium present in the hafnium. In general, this represents the largest impurity content of the hafnium-20% tantalum alloys. Hill and Rausch demonstrated, however, that impurity contents ranging from 0.78-percent zirconium to 2.5-percent zirconium had no appreciable effect on the oxidation rate and scale plus subscale thickness at 1925°C . They conducted other oxidation rate testing with the hydrogen-oxygen torch at temperatures from 1700°C to 1925°C with

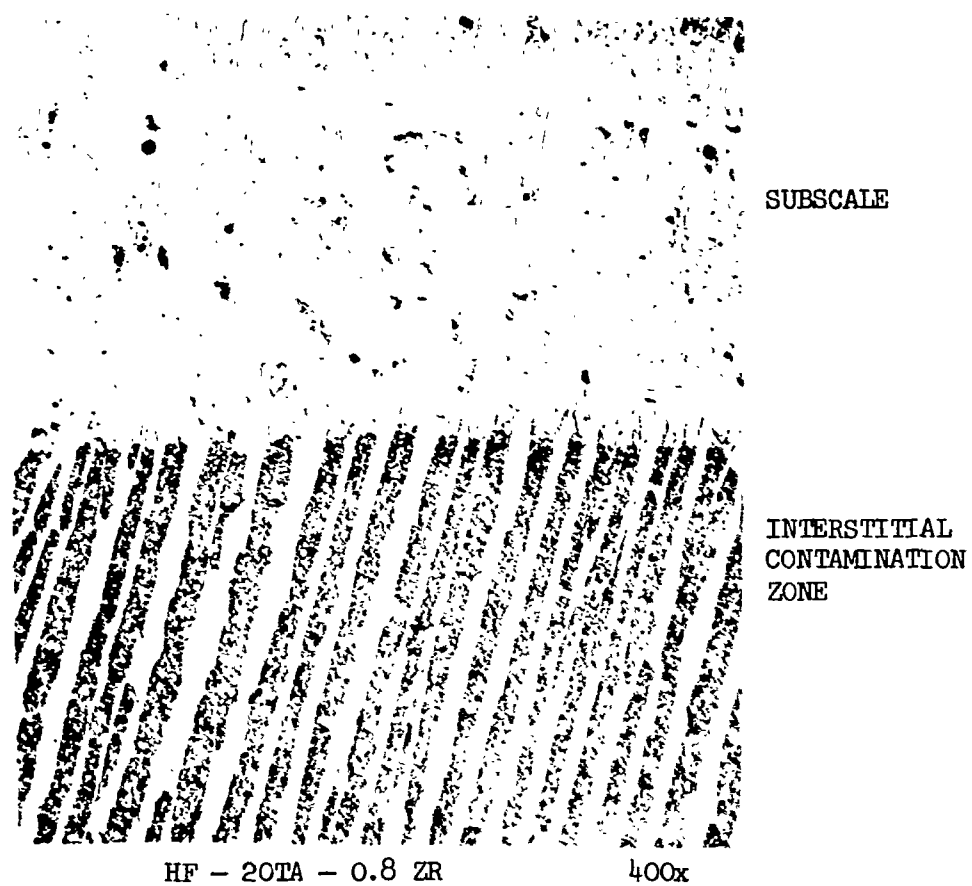


Figure 3. High magnification of subscale-interstitial contamination zone shown in Figure 2. Reproduced from Hill and Rausch (1966)

results shown in Figure 4. These curves indicate a parabolic growth rate, or the possibility of two different linear rate processes being operative.

The growth of the metal-plus-oxide structure in the subscale zone is the most significant feature in the oxidation process. In general, the total scale thickness increase with time in the "high" temperature oxidation tests is due to subscale growth. Hill and Rausch postulate that during the initial exposure period, an outer scale of significant thickness is formed rapidly without the formation of an equivalent subscale. This is due to the fact that the lamellar oxide structure is the result of competition for the available oxygen by the hafnium-rich and tantalum-rich phases. The partitioning of the oxygen is not prevalent initially because of the availability of excess oxygen during the initial exposure period. Their hypothesis suggests that subscale formation becomes important only when the available oxygen is reduced by the formation of a continuous outer oxide. Their test indicated in most cases, a fairly constant ratio of scale-to-subscale of approximately 1:4.

During Marnoch's study (1965), the effect on oxidation behavior of oxygen content in the as-cast alloy was noted. The amount of oxygen in the alloy strongly influenced the stabilization of alpha hafnium. This effect has been noticed by Oden et al., (1964), and Rudy and Stecher (1963). Consequently, Marnoch reports that the two-phase alpha and beta structure may be retained above the normal transformation temperature. He indicates that although the amount of alpha is small, it is retained as needles, or platelets, along beta cubic planes in a

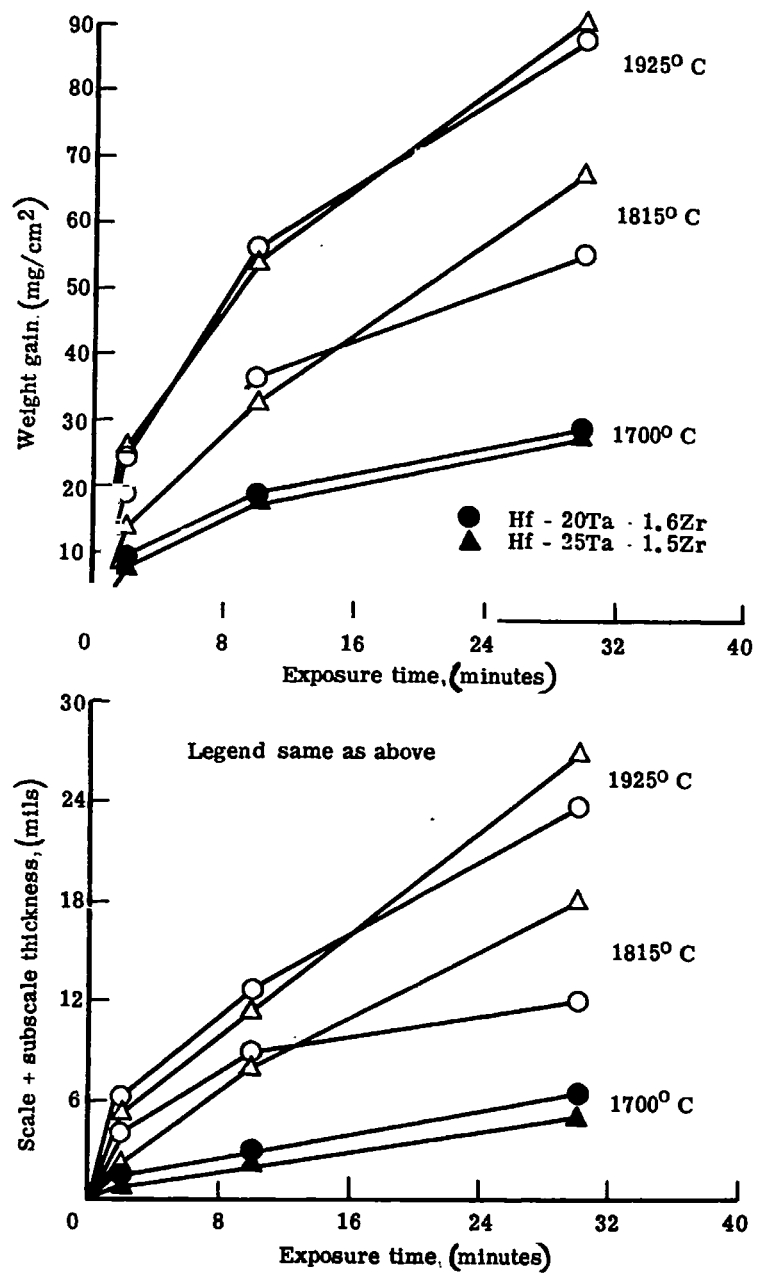


Figure 4. Oxidation rate of hafnium-20% tantalum alloys at 1700 - 1925° C. Reproduced from Hill and Rausch (1966)

typical Widmanstätten structure. Oxygen attack of the alloy then takes place preferentially along the alpha hafnium platelets to produce the segregated stringers characteristic of those seen in his oxyacetylene torch-tested alloys.

Marnoch proposed a dual concept to describe the oxidation behavior: oxygen diffusion through dense surface oxide which governs the kinetics of oxidation, and oxygen attack preferentially along alpha hafnium platelets in the two-phase alpha plus beta alloy matrix which governs the formation of the reaction zone (subscale plus oxidation contamination zone).

The results of Marnoch's oxyacetylene torch tests on the hafnium-20% tantalum alloy are shown in Figure 5. This figure shows the oxide growth as a function of time. The growth rate appears parabolic up to about 10 minutes, after which it becomes somewhat linear at uncorrected surface temperatures up to about 1975°C . Using radiant or induction heating at 1925°C uncorrected surface temperature, and metering in air at flow rates of 25 SCFH on a hafnium-27% tantalum alloy in a 40-torr vacuum, Marnoch found some significant results. He found that oxygen pressure did not significantly affect the rate of internal oxidation of the alloy, but the rate of total conversion of metal to oxide was slower, as the supply of oxygen atoms to the surface of the sample was only slightly faster than the diffusion rate of oxygen through the metal, resulting in incomplete conversion. Thus, he concludes that conversion of metal to oxide takes longer at low oxygen pressure than at high oxygen pressure.

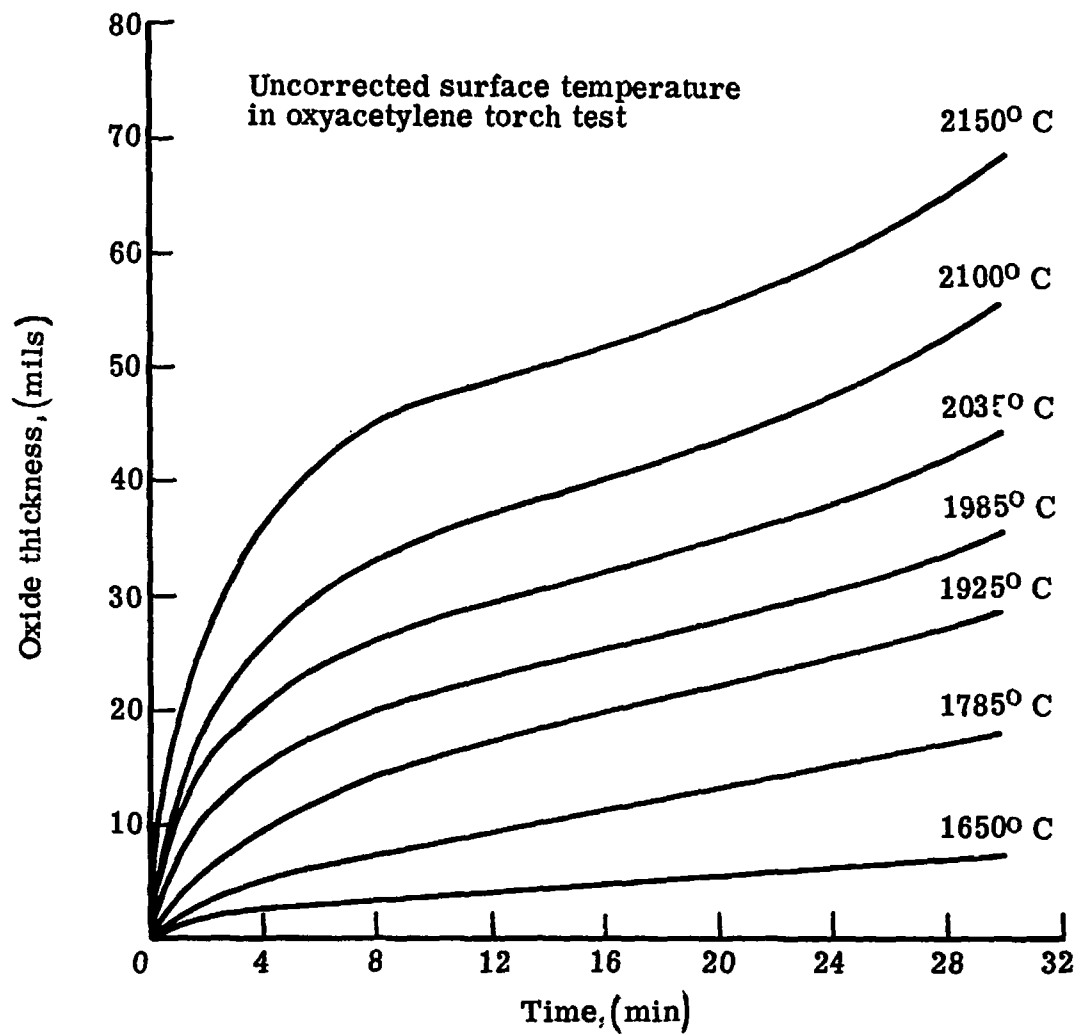


Figure 5. Oxide growth rate for hafnium-20% tantalum alloy.
Reproduced from Marnoch (1965)

The effect of preoxidation on the high temperature oxidation behavior of the alloy was studied by Hill and Rausch (1966) and Marnoch (1965). Hill found that preoxidation at 510°C and 650°C had no apparent effect on the oxidation behavior, but preoxidation at 870°C decreased the oxidation resistance of the alloy. Marnoch preoxidized at 2150°C and then oxidized the samples at 1650°C . He compared these to standard samples and found the preoxidized samples to be less oxidation resistant. The preoxidation apparently provided an access route for oxygen into the matrix.

Berkowitz-Matluck et al., (1967) looked at some oxidation kinetics of a Hf-27% Ta alloy and a Hf-20% Ta-2% Mo alloy using a gas analysis technique, in which the rate of oxygen picked up by the sample was monitored. The results obtained from this method indicated oxidation was parabolic over intended time periods at temperatures. Conversion depths were markedly different from Marnoch's earlier work. At 1815°C at 10 minutes exposure, conversion depths were approximately twice those observed in the oxyacetylene-torch experiments. At a furnace test temperatures of 2075°C a threefold difference existed. The furnace tests disclosed an increase in the oxidation rate near 1725°C which is the temperature of the monoclinic/tetragonal transition in HfO_2 . Berkowitz-Matluck attributes the different results to possible differences in the mechanism of oxygen transfer across the gas/oxide and oxide/metal interfaces. Her experiments were performed under conditions where the sample was at a higher temperature than the gas stream while the reverse was true in Marnoch's tests.

The low temperature oxidation behavior of the alloy (below 1370°C) is characterized by the formation of a glassy non-protective oxide film which spalls readily. Mash et al., (1968) reported, however, that oxygen penetration of the alloy matrix was minimal based on hardness change. Scale formation is relatively rapid because of the non-protective nature of the low temperature oxide layer.

X-Ray Diffraction

Marnoch (1965) conducted X-ray diffraction studies on the oxide layers of samples of different compositions heated at 2200°C . The results indicated that with increasing tantalum content, there was a corresponding increase in the amount of orthorhombic phase hafnia over monoclinic hafnia. Normally, the standard high temperature modification (above 1700°C) is the tetragonal form but Marnoch found changes in the (0K0) reflections indicating a shorter crystallographic axis in the b direction thus producing an orthorhombic structure. At 20 percent tantalum, the surface oxide was composed of roughly equal amounts of the two phases. The percentage of monoclinic phase increased in the direction of the reaction zone, reflecting the tantalum segregation which depleted the amount of stabilizing tantalum oxide available to the hafnium phase.

Hill and Rausch (1966) conducted a limited X-ray diffraction on the structures developed in the various zones oxidized at 1925°C . A possible complex oxide $6\text{HfO}_2 \cdot \text{Ta}_2\text{O}_5$ was found in the outer scale of in a Hf-25% Ta alloy. In Hf-20% Ta samples exposed for 10 minutes, they interpreted the scale as a mixture of monoclinic and tetragonal HfO_2

with a decrease in the tetragonal HfO_2 in the direction of propagation of the subscale. In samples exposed for 30 minutes the 20 weight percent Ta sample exhibited a monoclinic X-ray pattern which suggested that hafnium had diffused into the outer scale or that tantalum was lost from the outer oxide of the alloy. Because of the difficulty involved in the analysis of X-ray patterns of mixed oxides, this indicated that what they identified as the mixed tetragonal and monoclinic phases could be the complex oxide.

Mash et al., (1968) used X-ray diffraction to identify the alpha prime (α') phase which he formed by water quenching from 1450°C to room temperature. Using one sample he identified the structure to be a single phase hexagonal system with the c/a ratio of 1.573 and $a_0 = 3.192$, $c_0 = 5.024$. Pearson Handbook of lattice spacings shows $a_0 = 3.1946$ and $c_0 = 5.0510$ with the c/a ratio of 1.5811 for hafnium.

Elasticity Fundamentals

Introduction. All materials change in shape, volume, or both when under the influence of an applied stress or temperature change. The deformation is called elastic if the stress- or temperature-induced change in shape or volume is completely recovered when the material is allowed to return to its original temperature or state of stress. The elasticity of a body is a measure of its resistance to deformation. Elastic deformation occurs as a uniform increase or decrease in interatomic distances. Thus, the interatomic forces and structural energy exert a large influence on the elastic behavior of materials. Metals

in general belong to the large class of substances in which the elastic behavior is determined by direct separation, compression, or shear of the atoms, unlike other classes such as rubber, in which behavior is determined by the resistance to straightening out the links in the chains of atoms arising from thermal vibrations. Insight into the fundamental behavior of a material can be gained through study of its elastic properties. A knowledge of this behavior is necessary for the design of structural components. A background on some of the theoretical fundamentals used to describe the mechanical behavior of materials is presented in the following sections.

Concept of Stress-Strain. Stress is defined as the internal resistance of a body to an externally applied force per unit area. To obtain the stress at a point in a plane of a body with non-uniformly distributed forces over its cross section, one can take an area ΔA surrounding the point and note that a force ΔP acts on the area. By reducing the area ΔA continuously to zero, the limiting value of the ratio $\Delta P/\Delta A$ defines the stress at the point.

$$\lim_{\Delta A \rightarrow 0} \frac{\Delta P}{\Delta A} = \sigma = \text{Stress} \quad (1)$$

The stress will be in the direction of the resultant force P and normally inclined at an angle to ΔA . The total stress can be resolved into two components, a normal stress σ perpendicular to ΔA , and a shearing stress, τ , lying in the plane of the area.

The average linear strain can be defined as the ratio of the change in length to the original length of the same dimensions.

$$\epsilon = \frac{\delta}{L_0} = \frac{\Delta L}{L_0} = \frac{L - L_0}{L_0} \quad (2)$$

where ϵ = average linear strain

δ = deformation

By analogy with the definition of stress at a point, the strain at a point is the ratio of the deformation to the gage length as the gage length approaches zero.

Not only will the elastic deformation of a body result in a change in length of a linear element in the body, but it can also result in a change in the initial angle between any two lines in the body. The angular change in a right angle is called shear strain. This deviation caused by the application of a shear stress is given by γ in radians.

When forces applied to a body are sufficiently small, the linear relationship which exists between stress and strain within the elastic limit is given by Hooke's law which says that the average stress is proportional to the average strain,

$$\frac{\sigma}{\epsilon} = E = \text{Constant} \quad (3)$$

The constant E is defined as the modulus of elasticity, or Young's modulus. Correspondingly, the shear modulus is defined as the ratio of the shear stress to the shear strain

$$\frac{\tau}{\gamma} = G = \text{Constant} \quad (4)$$

The term elastic moduli refers to both of the above and in general is defined as the ratios of the applied stresses to the deformation resulting from these stresses.

Poisson's ratio, μ , is another elastic property of a material and is given by the ratio of transverse to axial strain as the result of a uniaxial tensile or compressive stress.

$$\mu = - \frac{\epsilon_y}{\epsilon_x} \quad (5)$$

Knowing any two of the three constants E , G , and μ , one may calculate the other by the relation

$$G = \frac{E}{2(1 + \mu)} \quad (6)$$

The preceding relationships apply for an isotropic, homogeneous body or a random polycrystalline aggregate whose individual grains are elastically anisotropic.

The stress-strain behavior of a material can be expressed diagrammatically in a graphical plot of stress versus strain as given by a typical uniaxial tensile test as shown in Figure 6. The linear portion of the curve between points 1 and 2 is the elastic region in which Hooke's law is obeyed. Point 1 is the elastic limit, defined as the greatest stress that a metal can withstand without experiencing a permanent strain with removal of the load. The proportional limit, point 2, is the stress at which the stress-strain curve deviates from linearity. The slope of the stress-strain curve within this region is the modulus of elasticity.

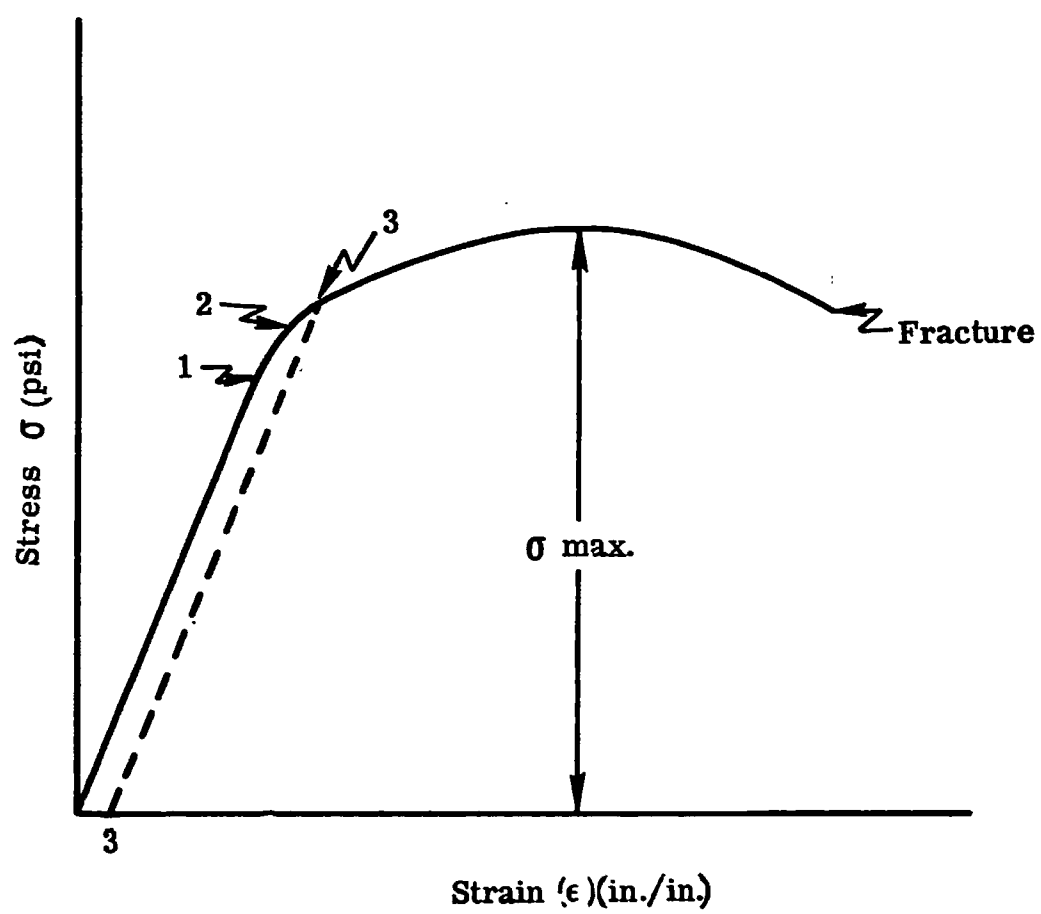


Figure 6. Typical stress-strain diagram for a ductile, elastic material

The limit of usable elastic behavior is described by point 3, the yield strength. It is defined as the stress which will produce a small amount of permanent deformation, generally about 0.2 percent of the gage length of a tensile specimen if the material does not have a definite, recognizable yield point which is evident in some materials. The ultimate tensile strength of the material is denoted as σ_{\max} and is defined as the maximum load divided by the original area of the specimen.

Dynamic Elasticity Fundamentals. The elastic moduli relations which have been described in the preceding section can be defined in terms of classical vibration theory. A review of the general development of this theory follows.

Lord Rayleigh (1877) discusses the fundamental vibration theory of thin rods and beams in the classical book on the "Theory of Sound." The vibrations of a bar can be divided into three kinds -- longitudinal, torsional, and flexural (lateral, transverse). Rayleigh investigated the effect of shape and elasticity on the resonant frequency of flexural vibration of a homogeneous, isotropic prismatic bar, making a simplifying approximation that the only contribution to the kinetic energy of the vibrating bar is the translation of its elements perpendicular to its length in the plane of flexure. He obtained the equation

$$E = \frac{48\pi^2 \rho L^4 f^2}{m^4 t^2} \quad (7)$$

where E = Young's or elastic modulus

ρ = density of material

L = bar length

f = flexural resonant frequency

m = constant dependent on the mode of vibration of the bar

t = bar thickness in the plane of flexure

Rayleigh later modified this equation by a correction factor to correct for rotary inertia of the bar.

Love (1944) modified the differential equation of motion from which equation (7) was obtained to consider lateral inertia of the bar (inertia of motion of contraction and expansion of the cross sections of the bar in proportion to Poisson's ratio, μ , when longitudinally extended or compressed). Pickett (1945) gives this correction as zero for bars of square cross section and is negligible for bars of rectangular cross section.

Timoshenko (1921, 1922) considered the influence of shearing forces exerted by the cross-sectional elements on one another and found that the shear correction was about four times the correction for rotary inertia. His equation of motion of the bar includes shear and rotary inertia terms. Pickett (1945) studied Timoshenko's differential equation and its solution by Goens (1931). He gives equations and graphical representations for computing elastic constants from flexural and torsional resonant frequencies of vibrations of prisms and cylinders.

From one-dimensional theory, Goens (1931) derived the relation between Young's modulus E and the flexural resonance frequency, f , of a cylinder of density ρ , length l , and diameter d , as

$$E = \frac{64\pi^2 \rho l^4 f_n^2}{M_n^4 d^2} \quad (8)$$

where f_n = resonance frequency of the n th mode of vibration

M_n = solutions of the equation $\cos m \cosh m = 1$

Timoshenko (1937) added his shear and rotating inertia corrections, and Goens (1931) reduced the equation to

$$E = \frac{64\pi^2 \rho l^4 f_n^2}{M_n^4 d^2} T_n \quad (9)$$

where T_n is a function of d/l and Poisson's ratio, μ . T_n approaches one as d/l approaches zero, for all values of n and μ .

Pickett (1945) made numerical computations of T_n and gave approximate equations for this computation. In another paper Pickett (1945) gave more accurate values in his solution based upon the three-dimensional differential equation of elasticity.

Tefft (1960) provided a simultaneous numerical solution of these equations. The results are presented in tabular form of correction factors to be applied to the thin rod approximation for the fundamental flexural resonance and the first two overtones. These results provide an accurate means of calculating Young's modulus from the density, dimensions, and resonance frequencies of cylindrical rods having diameter-to-length ratios as high as 0.6.

Wachtman et al., (1960) pointed out that Pickett had not given the derivation and range of applicability of his interpolation formula. Spinner et al., (1960) made a comparison of experimental and theoretical relations between Young's modulus and the flexural and longitudinal resonance frequencies of uniform bars of both cylindrical and rectangular cross section. Spinner and Tefft (1961) gave these relations and other discussions of the dynamic technique in the Proceedings of the American Society for Testing and Materials. This paper was utilized extensively in the evaluation of the elastic moduli of the hafnium-20% tantalum alloy whose data are presented in this dissertation.

For cylinders, and utilizing the fundamental mode of flexural vibration, Young's modulus can be calculated from the relation

$$E = \frac{1.261886\rho l^4}{d^2} f_1^2 T_n \quad (10)$$

where ρ = density of the material

l = length of the specimen

d = diameter of cylindrical specimen

f_1 = fundamental resonant frequency

T_n = correction factor based on specimen geometry and Poisson's ratio

The numerical factor in this equation is dimensionless, therefore, any consistent system of units can be used. For the cgs system, densities in gms/cc, lengths in cm, and frequencies in cycles per second give the moduli in dynes/cm². In the English system, density in lbs/in³, lengths in inches, and frequencies in cycles per second

give moduli in lb/in-sec². This can be converted to lbs/in² by dividing the result by the acceleration of gravity, g, 386.09 in/sec². Tables for the correction factor T_n , along with interpolation formulas are given in this paper.

For prisms of rectangular cross section and using the fundamental mode

$$E = 0.94642 \frac{\rho l^4 f^2}{t^2} T \quad (11)$$

where T is a correction factor given approximately by

$$T = 1 + 6.585(1 + 0.0752\mu + 0.8109\mu^2)\left(\frac{t}{l}\right)^2 - 0.868\left(\frac{t}{l}\right)^4 \\ - \frac{8.340(1 + 0.2023\mu + 2.173\mu^2)\left(\frac{t}{l}\right)^4}{1 + 6.338(1 + 0.14081\mu + 1.536\mu^2)\left(\frac{t}{l}\right)^2} \quad (12)$$

The longitudinal resonances of cylindrical rods or bars of square or rectangular cross sections provide the most accurate method of calculating the moduli. The equation for the computation of Young's modulus of a cylindrical specimen is:

$$E = \frac{\rho}{K_n} \left(\frac{2lf_n}{n} \right)^2 \quad (13)$$

where K_n is the correction factor for the nth mode of longitudinal vibration and can be calculated in the case of diameter/wavelength (d/l) ratio $\ll 1$ by

$$K_n \approx 1 - \frac{\pi^2 n^2 \mu^2 d^2}{8l^2} \quad (14)$$

The torsional resonance is used to calculate the shear modulus, G . The theory behind this type of vibration is simpler and more accurate for cylindrical specimens, however, experimental procedures are easier for prismatic specimens. The basic equation for torsional resonance is:

$$G = \rho \left[\frac{2lf_n}{n} \right]^2 R \quad (15)$$

where R is a complicated function of the specimen geometry. For cylinders

$$R = 1 \quad (16)$$

If the cross-sectional correction factor K_n is neglected in equation (14), then Poisson's ratio, μ , can be computed directly from the fundamental frequencies by the relation

$$\mu = \frac{1}{2} \left(\frac{f_{\text{Long.}}}{f_{\text{Tors.}}} \right)^2 - 1 \quad (17)$$

For prisms of square cross section the shape factor R can be calculated very accurately from the relations derived by Tefft et al., (1961) as

$$R = R_0 \left[1 + n^2 \left(\frac{b}{l} \right)^3 (0.01746 + 0.00148n + 0.00009n^2) \right] \quad (18)$$

where $n = 1, 2, 3$, etc. (for fundamental, 1st overtone, etc.)

R_0 = shape factor for infinitely thin, square specimens = 1.18559

For prisms of rectangular cross section, the theory becomes more complicated. Timoshenko (1951) solved the equations to give

$$R_o = \frac{1 + \left(\frac{b}{a}\right)^2}{4 - 2.521 \frac{a}{b} \left(1 - \frac{1.991}{e^{\pi b/a} + 1}\right)} \quad (19)$$

where a and b = cross-sectional dimensions.

For $a \ll b$ Pickett (1945) gives

$$R_o \approx \frac{1 + \left(\frac{b}{a}\right)^2}{4 - 2.521 \frac{a}{b}} \quad (20)$$

Spinner and Valore (1958) found that empirically for $\frac{b}{l} \approx 0.21$

and $1 \leq \frac{b}{a} \leq 10$, the value of R differed from Pickett's equation.

Tefft (1961) indicates that a better relation which is a combination of Davies' (1938) solution and Spinner's empirical results is given for the shape factor by:

$$R = \left[\frac{1 + \left(\frac{b}{a}\right)^2}{4 - 2.521 \frac{a}{b} \left(1 - \frac{1.991}{e^{\pi b/a} + 1}\right)} \right] \left[1 + \frac{0.00851}{l^2} n^2 b^2 \right] - 0.060 \left(\frac{nb}{l}\right)^{3/2} \left(\frac{b}{a} - 1\right)^2 \dots \quad (21)$$

The accuracy for the equations presented here varies to within

0.01 percent in the case of equation (18) to about 0.2 percent for

equation (21) (depending on b/l and b/a ratios). In extreme cases,

the errors involved in most of these equations do not exceed 1 percent.

Internal Friction Review

The ability or capacity of a vibrating solid to convert its mechanical energy of vibration into heat, even when it is isolated so well from its surroundings that energy losses to its surroundings are negligible, is called "internal friction." The most common manifestation of internal friction is the damping, or loss of vibration amplitude of a freely vibrating body. Interest in this subject extends back to the earliest cymbals and bells. In modern times there has been widespread interest in damping for engineering applications and is commonly reported in terms of a quantity called "damping capacity." Depending on the particular application, one may wish to obtain either a very high or a very low rate of damping. High damping materials will reduce the amplitude of vibrations and reduce stresses, thereby lengthening the fatigue life of parts in service. High temperature damping characteristics are of special interest in leading edge and hypersonic engine applications.

Another area of wide interest has been in the use of internal friction as a tool to study internal structure and atomic movements in the solid state. The method has provided information on such processes as diffusion, ordering, solubilities of interstitial elements, intergranular corrosion, and estimation of the density of dislocations.

Internal friction or damping effects correspond to a phase lag between the applied stress and the resulting strain. A perfectly elastic material will not produce damping since, under vibrating conditions, stress and strain are always in phase, and consequently no mechanical hysteresis or loss of vibrational energy can take place.

Damping is, therefore, a result of the non-elastic behavior of materials. The fact that it can be detected at stress levels far below those at which plastic flow occurs indicates that there is really no such thing as an "elastic range." This fact has opened an important division of the field of non-elastic behavior known as anelasticity.

Much of our present knowledge of this area, which is concerned with internal friction effects independent of the amplitude of vibration, is due to Clarence Zener and his co-workers (1948).

There are several measures used to describe damping, as indicated by Kolsky (1953). In structural works one often uses the ratio

$$\frac{\Delta W}{W} \quad (22)$$

where ΔW is the energy dissipated in the specimen in passing through one stress cycle and W is the elastic energy stored within the specimen at maximum strain. This ratio is known as the "specific damping capacity" or "specific loss." Measure of the decay in amplitude of a freely vibrating system is another measure of internal friction. This can be expressed in terms the "logarithmic decrement" which is defined as the natural logarithm of the ratio of successive amplitudes.

$$\log \text{ dec.} = \ln \frac{A_n}{A_{n+1}} \quad (23)$$

Another measure of internal friction is given by the relative sharpness of the resonance peak in a sample undergoing a forced constant vibration. If the sample's vibration amplitude is plotted versus frequency of vibration, a maximum in amplitude will occur at its

Resonant frequency, f_r . The sharpness of resonance is readily determined by measuring the width of the frequency curve at half maximum amplitude, and dividing by the resonant frequency. Thus

$$\frac{\Delta f}{f_r} = \frac{f_2 - f_1}{f_r} \quad (24)$$

is a measure of internal frequency where f_2 , f_1 , and f_r are indicated in Figure 7.

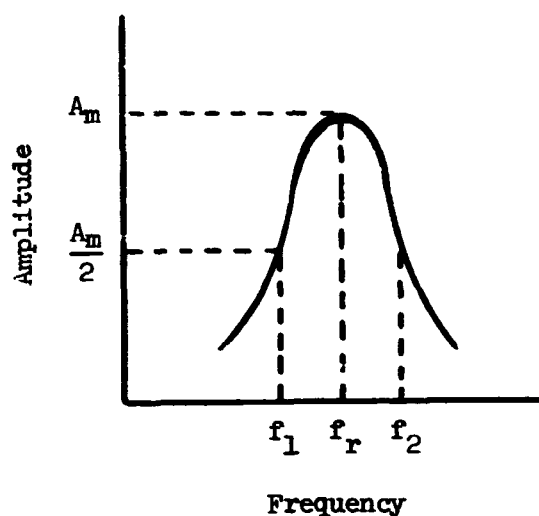


Figure 7. Typical resonance frequency curve for specimen undergoing constant forced vibration

The various measures of damping or internal friction are all simply related; which term to use is a matter of convenience. The most common measure used today is a quantity Q^{-1} derived from analogy with electrical theory and is defined as

$$1/Q = Q^{-1} = \text{elastic phase constant} = \frac{\Delta f}{\sqrt{3} f_r} \quad (25)$$

Kolsky (1953) has shown the relationship of the "log decrement" and the "specific loss" to be

$$\frac{\Delta W}{W} = 2 (\log \text{ decrement}) = 2 \ln \frac{A_n}{A_{n+1}} \quad (26)$$

Zener (1948) has shown that the sharpness of resonance is related to the "specific loss" by the relation

$$\frac{\Delta f}{f_r} = \frac{\sqrt{3}}{2\pi} (\text{specific loss}) = \frac{\sqrt{3}}{2\pi} \left(\frac{\Delta W}{W} \right) \quad (27)$$

Equations (25), (26), and (27) can be combined to show that

$$Q^{-1} = \frac{1}{\pi} (\ln \text{ dec.}) = \frac{1}{2\pi} (\text{specific loss}) \quad (28)$$

In a freely vibrating system, the time elapsed during several vibrations and the relative amplitudes of the first and last vibrations in this series is a useful measure at high frequencies and low internal friction. The relationship

$$Q^{-1} = \frac{\ln \frac{A_0}{A_t}}{\pi f t} \quad (29)$$

applies, where A_0 is the amplitude of the first vibration considered, A_t is the amplitude of a vibration occurring after an elapsed time, t , and f is the frequency of the vibration.

For large internal friction values, the peak width method is generally used to determine Q^{-1} , while for low values the decay method is preferred.

Having generally discussed internal friction and the various measures in which it is described, it is appropriate to discuss several of the internal mechanisms by which it manifests itself. Experimentally, it has been found that for many curves of internal friction as a function of temperature or of frequency of vibration, there exist peaks in the measured value of internal friction. There are many theoretical models which have been established to describe the phenomena occurring within the solid state. These anelastic effects have been attributed mainly to thermal effects, point and line defects, and grain boundaries.

An excellent discussion and bibliography have been provided by Marlowe and Wilder (1964). Some of these mechanisms are discussed briefly in the following sections. For more detailed reviews one may consult Niblett and Wilks (1960) and Norwick (1953) and Poslinkov et al., (1967).

Internal Friction Resulting from Thermal Effects. If an element of material is suddenly subjected to a stress the resulting strain is generally accompanied by a change in temperature. For homogeneous stress throughout a specimen, the temperature change occurs equally at every point, but if the stress is non-homogeneous, temperature gradients are set up in the material. As a result, there is a flow of heat accompanied by an increase of entropy and a dissipation of energy which gives rise to internal friction. For a rod or bar type specimen undergoing flexural vibration, in each half cycle, the convex side is stretched and, therefore, cooled, while the concave side is compressed

and, therefore, heated. This causes a periodic flow of heat back and forth across the sample. At very high frequencies there is insufficient time for appreciable heat flow to take place during a cycle, therefore, the process is essentially adiabatic and no damping occurs. At low frequencies, the specimen remains in thermal equilibrium. The process is isothermal and no damping occurs. At intermediate frequencies, when the frequency is such that the period of vibration is comparable with the time required for heat to flow across the sample, there is an irreversible conversion of mechanical energy into heat.

Zener (1937) has derived relationships for the internal friction of rods and bars and his theory has been verified by several investigators. For an ordinary thickness specimen, the internal friction peak would occur somewhere in the region 1 to 100 cps (Dieter, 1961). Thermoelastic damping is small for bars in longitudinal vibration. The frequency region where the peak would occur would be of the order of 10^{10} to 10^{11} cps, which is beyond the range of normal observations.

Torsional vibrations produce shearing stresses which are not accompanied by a change in temperature. Consequently, specimens in torsional vibration have very little thermoelastic damping.

For a polycrystalline material, another energy absorption mechanism can occur. Neighboring grains within the sample have different orientations with respect to the strain during flexure thus producing different stresses. This causes a variation of temperature from grain to grain within the sample. Hence, thermal currents flow across the grain boundaries, giving rise to an internal friction whose magnitude and characteristic frequency is grain size dependent.

Internal Friction Resulting from Point Defects. Berry (1961) has reviewed internal friction caused by point defects, their combinations, and their interactions. He indicates that internal friction can be expected whenever introduction of the point defect produces distortions which have a lower symmetry than the lattice.

The presence of dissolved interstitial atoms in metals with a body-centered cubic lattice often gives rise to a characteristic relaxation peak. In an unstressed crystal the interstitial atoms are randomly distributed, but an application of a tensile stress, the energy of an interstitial atom will be less in certain sites because of the distortion produced by the applied stress. Hence, the stress produces a redistribution of the interstitial atoms so that some sites are occupied preferentially. This process of redistribution gives rise to an internal friction peak first explained by Snoek (1941). The same effect is noticed under oscillating stresses as imposed by an internal friction apparatus as the interstitial atoms are in continuous motion, either tending toward or tending away from a preferred orientation.

Stress induced ordering also arises in substitutional solutions, such as brass, because the substitution of one type of atom for another leaves the lattice with the same cubic symmetry. However, a pair of solute atoms in nearest neighbor positions will produce distortion along the axis joining them, so that an applied stress will induce a preferential orientation of pairs of solute atoms as described by Zener (1947).

Wachtman (1963) has combined dielectric loss measurements and internal friction measurements in a study of preferential orientation of vacancy-impurity atom pairs in titanium oxide under the influence of electrical and mechanical stresses.

Internal Friction Resulting from Dislocations. Read (1940) was the first to recognize the contribution of the motion of dislocations to the internal friction of materials. In a study of crystalline copper, tin, lead and zinc, he found that the log decrement of an unannealed single crystal could be as large as that of the polycrystalline material, that annealing reduced the decrement, and that both Young's modulus and the decrement varied with the vibration strain amplitude at strain amplitudes as low as 10^{-6} . He suggested that the mechanism involved was a propagated dislocation with the observed internal friction being attributed to the atomic jumps and local slip of the order of one atomic distance.

Dislocation damping is often the principal source of damping in metals. There are various models which have been proposed that account for dislocation contribution to internal friction. Niblett and Wilks (1960) discuss these models in detail. Marlowe and Wilder (1964) provide a short review of several of the most important models which are discussed below.

Koehler (1950) suggested that observed damping in metals was caused by dislocations pinned by impurity atoms at various positions along its length and oscillating back and forth like a stretched string undergoing damped vibrations.

Granato and Lucke (1956, 1956) expanded Koehler's model to more adequately account for the dependence of internal friction on strain amplitude. They suggest that the dislocations are pinned by the "nodes" of the dislocation network and by impurity atoms. This model accounts for two types of damping. The first type is a frequency dependent, strain amplitude-independent loss caused by vibration of the dislocation line between impurity atoms as in Koehler's model. This loss results in a constant internal friction at low strain amplitudes.

The other loss is frequency independent but strongly strain amplitude dependent. This damping occurs when the applied stresses are large enough to cause dislocation to break away from its impurity pinning points resulting in a large increase in the dislocation strain for no increase in applied stress. Upon reversal of stress, the dislocation loop does not follow the same path back to its original position so that a hysteresis loss is generated. If the stress is sufficiently large, the dislocation continues to bow about its nodes eventually creating a new dislocation loop in the manner of the Frank-Read Source. The distances between impurity atoms along the dislocation lines vary giving rise to a distribution of loop lengths resulting in a smooth increase of internal friction with strain amplitude. Larger concentrations of impurity atoms shorten the loop lengths, lowering the stress required to bow the dislocation line, hence, increasing the internal friction.

Lucke and Granato (1956) reviewed this model and checked the agreement with experimental data.

The only relaxation process which gives an internal friction peak that is definitely ascribable to dislocations is the Bordoni peak found in FCC metals at very low temperatures in the region of 30° to 100° K (Dieter, 1961). There are indications that the Bordoni peak is due to some intrinsic property of dislocations and is not involved with the interaction of dislocations with impurity atoms and other dislocations. These peaks have been found to have a characteristic activation energy interpreted as the thermal energy required for the dislocations to overcome the energy barriers imposed by Peierls forces (those periodic forces exerted by the crystal lattice on the dislocation) (Bommel, 1956). These forces originate from the fact that a dislocation possesses some preference for certain special positions in the crystal lattice where it causes the least energetic disturbance to the surrounding atoms.

The Bordoni peak has been extensively investigated in polycrystalline and single crystal copper specimens. The height of the peak, and the temperature at which it occurs are almost independent of the amplitude of vibration. This phenomenon is not generally observed in fully annealed specimens.

Internal Friction Resulting from Grain Boundaries. An important source of internal friction in metals is stress relaxation along grain boundaries. Ke (1947) first demonstrated the strong internal friction peak due to grain-boundary relaxation by experiments on high purity aluminum wires. At the low torsional strains used in this work the strain was completely recoverable, and all internal friction effects were

independent of amplitude. In polycrystalline aluminum a broad peak occurred near 300° C, while no internal friction peak occurred in single crystal aluminum. Measurements of the elastic modulus showed a sharp drop for the polycrystalline specimen beginning at the onset of the internal friction peak. The single crystal specimen continued its linear decrease in modulus. Ke was able to discount all other sources of internal friction and proposed that the mechanism producing the internal damping was that of grain boundaries behaving in a viscous manner at elevated temperatures.

A controversy has existed since the early 1900's over the existence of amorphous grain boundaries. Jeffries and Archer (1924) indicated that the grain boundary metal possessed mechanical properties like those of a vitreous amorphous substance. Zener (1948) eliminated the need for existence of a truly amorphous material at the grain boundaries when he said that it was only necessary to assume the resistance to slipping of one grain over an adjacent grain obeys the laws commonly associated with amorphous materials rather than the laws associated with crystalline materials. Since the surface atoms of one grain cannot fit into the lattice positions of an adjacent grain, the binding across the interface of two grains may reasonably be expected to have characteristics associated with amorphous materials.

The effect of viscous grain boundaries on internal friction of materials is explained by the fact that viscous flow is always accompanied by the dissipation of mechanical energy. The energy dissipated at each grain is given by

$$\text{Energy dissipated} \sim (\text{relative displacement}) \times (\text{shear stress}) \quad (30)$$

The deformation of a viscous material obeys the relationship

$$\text{Shear stress} = \eta \times \text{shear strain rate} \quad (31)$$

where η = coefficient of viscosity which varies with temperature in the following manner:

$$\eta \sim \exp H/RT \quad (32)$$

where H = activation energy, R = gas constant, and T = absolute temperature. Thus an increase in temperature decreases the viscosity and it is, therefore, expected that the resistance to slipping across the grain boundaries will be lowered with respect to the resistance to deformation within the interior of the grains.

Consider the right side of equation (30). At low temperatures the relative displacement of neighboring grains is small because of the high viscosity of the grain boundary. At high temperatures the shear stress resisting motion becomes very small because of the low viscosity of the grain boundary. Only at temperatures intermediate to these extremes where the product of relative displacement and shear stress across the grain boundaries does not become very small is there any appreciable contribution to internal friction.

In follow-on studies Ke (1947, 1948) continued to provide evidence that grain boundary relaxation was responsible for the high internal friction peaks in polycrystalline materials. He showed that the magnitude of the internal friction peak was independent of grain size

provided the grain size was small with respect to the sample size; however, an increase in grain size would shift the position of the peak to higher temperatures. Ke also showed that an increase in frequency of vibration had the same effect as an increase in grain size, both being the result of a higher temperature required for the same degree of relaxation.

Other Sources of Internal Friction. In this brief review an attempt has been made to discuss some of the major sources of internal friction. Other sources such as the movement of twin boundaries, magnetoelastic phenomena, and phase transformations contribute to the internal friction observed in metals. Norwick (1953) discusses some of these contributions. Precipitation of a second phase in a copper-beryllium alloy phase transformation has been shown to increase the damping (Polotskii, 1967). For a transformation that does not occur by nucleation and growth, internal friction effects have been noted. The lattice is relatively unstable near the transformation temperature, and an increase in internal friction can be expected and has been demonstrated in transformations occurring in the Ag-Zn alloys (Köster, 1940) and ferronickels (Scheil, 1944).

Internal Friction Measurements

The methods of measurement of internal friction fall into three main groups:

1. Torsional pendulum method
2. Ultrasonic pulse method
3. Resonant bar method

It is to be noted that each method is usually only suitable for making measurements over a comparatively small range of frequencies and this considerably restricts the amount of information which can be obtained from a given specimen.

A brief outline of the chief features and variations of each method is given below.

Torsional Pendulum Method. The earliest measurements of internal friction were made by means of a torsional pendulum. Ke (1947) describes this method in detail. Basically, the specimen is in the form of a wire or thin rod, held in a pin-vise or lathe clench-type holder, to which an inertia member is attached to give a period of oscillation of the order of a second. Part of the inertia member may be made from ferromagnetic material, and the vibrations excited electromagnetically. The internal friction is usually measured by the damping of free vibrations, successive amplitudes being observed by a mirror, lamp and scale, or some automatic arrangement. Various modifications of this method have been used. Unless care is taken, the torsional pendulum is unsuitable for measuring specimens with very low internal friction, since the background damping of the apparatus can be of the order of 10^{-4} . It is also difficult to make measurements at low strain amplitudes, the strain usually varying from zero at the cylinder axis to about 10^{-5} at the surface.

Ultrasonic Pulse Method. Internal friction may be measured at megacycle frequencies by the ultrasonic pulse method. A short ultrasonic pulse is introduced into one end of the specimen by a piezoelectric

crystal, and the attenuation in the specimen is measured by observing the amplitude of the pulse transmitted through it to a second crystal, or reflected back to the transmitting crystal.

Roderick and Truell (1952) explain this method in detail, and obtained attenuation measurements over a frequency range of 5650 Mc/sec. They describe two methods of measuring the attenuation. In the first method, a quartz crystal is mounted directly on one face of the specimen, and the pulse is reflected from the opposite face, which is accurately parallel to the first. The specimen dimensions are such that reflections from the sides do not interfere with the main echoes. In the second method, the pulse is passed through a layer of water between the transducer and the specimen. This arrangement makes it possible to measure the reflection loss at the surface of the specimen, which cannot be done when the transmitter is cemented directly to the specimen.

The strain amplitudes used in this method are usually too small to be used in measuring amplitude-dependent effects. It has, however, proved useful for measuring the frequency dependency over a wide range of values.

Resonant Bar Method. The most frequent method used to measure internal friction has been to excite a rod or bar specimen in one of its normal modes of vibration, without using an auxiliary inertia member. The frequency is dependent on the specimen dimensions. This method is the one used for measurements of internal friction reported in this paper. A detail description is provided under the experimental discussion.

Various electrical and magnetic methods have been employed to excite the vibrations. Some have required attaching magnetic pole pieces to the specimen, with excitation provided by means of an alternating magnetic field in a coil connected to an oscillator. Förster (1937) introduced a method of exciting and detecting the vibrations through the support system. This method requires a magnetic or piezoelectric line which transmits the vibrations to the specimen by means of its supporting wires, thus eliminating the necessity for attaching pole-pieces.

The resonant bar method may be used for specimens of high or low damping by using either forced or free vibrations. Care must be taken in the method of supporting the specimens at the vibrational nodes, but the background losses due to the supports may usually be made relatively unimportant. This method may be used over a wide range of strain amplitudes, with strains greater than 10^{-3} having been obtained by Mason (1956) using a barium titanate transducer coupled to an exponential horn. A disadvantage of this method is that the frequencies at which the internal friction may be measured are normally limited to the fundamental resonant frequency or one or two harmonics.

MATERIALS

The material used in this investigation was a hafnium-20% tantalum alloy whose precise chemical composition is given in Table 1. The alloy was produced under special order by the Wah Chang Albany Corporation. A 1.75-inch-diameter hafnium crystal bar (see Table 2) was used as the base metal. To this bar, a 0.125-inch-thick, 1-inch-wide tantalum (see Table 3) strip was fusion welded in inert gas along its length to form an electrode of 2-inch diameter and weighing 50 pounds. To consolidate the two metals, the electrode was double vacuum AC arc melted to form a 4-inch-diameter ingot. The ingot was then machined to a 3.375-inch diameter with a weight of 24 pounds. After machining, the ingot was fitted in a molybdenum can of 4-inch outside diameter for protection against oxidation, induction heated to 1425° C, and extruded through a 2-inch-diameter die. Eight billets 1.475 inches in diameter × 2.5 inches long were obtained. These billets were glass coated, heated in argon to 1200° C and extruded by a "Dynapac" process through a 0.5-inch-diameter die. Four rods of the hafnium-20% alloy, each 18 inches long, were machined to a final 0.44 diameter by centerless grinding. Wah Chang pickled the rods in a concentrated acid bath to determine if the molybdenum had been removed. During this process four additional rods were dropped into the acid bath and were reduced to a 0.125-inch diameter. From the original 50-pound electrode, the yield was 5.3 pounds exclusive of the small diameter rods. In addition to the hafnium-tantalum material, one 4-inch rod of hafnium was received. Chemical analysis of this rod is indicated by Table 2.

Table 1. Hafnium-tantalum final ingot analysis

	Top	Center	Bottom
Ta	18.22%	19.16%	18.84%
Hf		Balance	
Impurity content, ppm			
Al	43	39	41
B	<0.2	<0.2	<0.2
C	< 30	< 30	< 30
Cb	<100	<100	<100
Cu	< 40	< 40	< 40
Fe	115	140	100
H	1.3		3.8
Mo	50	50	50
N	9		12
O	130		100
Si	<40	<40	<40
Ti	100	91	100
W	24	25	31
Zr	2.8%	2.8%	2.8%

Table 2. Hafnium crystal bar analysis

All values in ppm unless otherwise noted			
Al	< 58	N	< 10
B	< 0.5	Ni	< 25
C	< 10	O	< 50
Cd	< 2.5	Pb	< 10
Co	< 5	Si	< 20
Cr	< 20	Sn	< 15
Cu	< 25	Ti	< 39
Fe	< 100	V	< 10
H	26	W	< 20
Hf	97.0%	Zr	3.0%
Mg	< 10	Nb	< 35
Mn	< 10	Ta	< 100
Mo	< 5		

Table 3. Tantalum analysis

All values in ppm			
C	< 30	Al	< 20
O	60	B	< 1
H	3.2	Cb	< 1
N	30	Co	< 5
Zr	50	Mo	< 10
Cb	300	Si	< 10
Fe	47	Ti	< 10
Ni	< 10	V	< 10
Cu	3	W	75

An electron microprobe analysis was carried out on a typical rod cross section to verify the manufacturer's chemical analysis. An X-ray intensity scan for both the hafnium and the tantalum across the rod section indicated a homogeneous structure with concentrations agreeing with the Wah Chang analysis.

Density measurements were performed on the as received alloy in accordance with ASTM standard B311-58 in which the specimen is weighed in air, using an analytical balance, and then suspended by a fine wire. The specimen and wire are weighed in a beaker of water. The wire by itself is immersed into the water to the same level as before and the density is calculated by the equation

$$D = \frac{AXE}{A - B + C} \quad (33)$$

where D = density of specimen in grams per cubic centimeter

A = weight of specimen in air in grams

B = weight of specimen and wire in water

E = density of water in grams per cubic centimeter

C = weight in grams of wire immersed in water

The density obtained by this method was 13.48 gms/cm³ (0.487 lb/in³) which was verified by weighing the longer rod specimens and measuring precisely their dimensions with precision micrometers. The weight per unit volume was readily calculated and served as a check on the measured densities.

EQUIPMENT AND EXPERIMENTAL PROCEDURE

Dynamic Elasticity and Internal Friction Measurements

The measurement of the elastic properties and internal friction of the hafnium-20% tantalum alloy were conducted on three different equipment setups, each having different capabilities, but all utilizing the same basic principles. The resonant bar method previously mentioned was followed. A description of each setup and the experimental procedure followed in making these measurements are described in the following paragraphs.

Four- and five-inch long cylindrical specimens were cut from the hafnium-tantalum rods. Diameter and length of each specimen were measured to 0.001 inch using a standard bench micrometer and caliper. Weight of each specimen was determined by an analytical balance. The rods had been previously machined by Wah Chang Albany to a diameter of ≈ 0.44 inch and were concentric to within 0.001 inch along their length.

The Magnaflux Corporation Model SR-200 Elastomat shown in Figure 8 was used for measurement of the elastic properties and internal friction of the hafnium-tantalum alloy from room temperature to 1000° C in an air or oxidizing atmosphere. A block diagram schematic of this system is shown in Figure 9. The specimen, either rod or rectangular bar shape, is suspended in the furnace by a fine wire (0.008-inch-diameter, platinum-rhodium thermocouple). The wire is looped around the specimen at the precise nodal points (located at a distance from



Figure 8. Magnaflux SR-200 Elastomat for dynamic elasticity measurements up to 1000° C

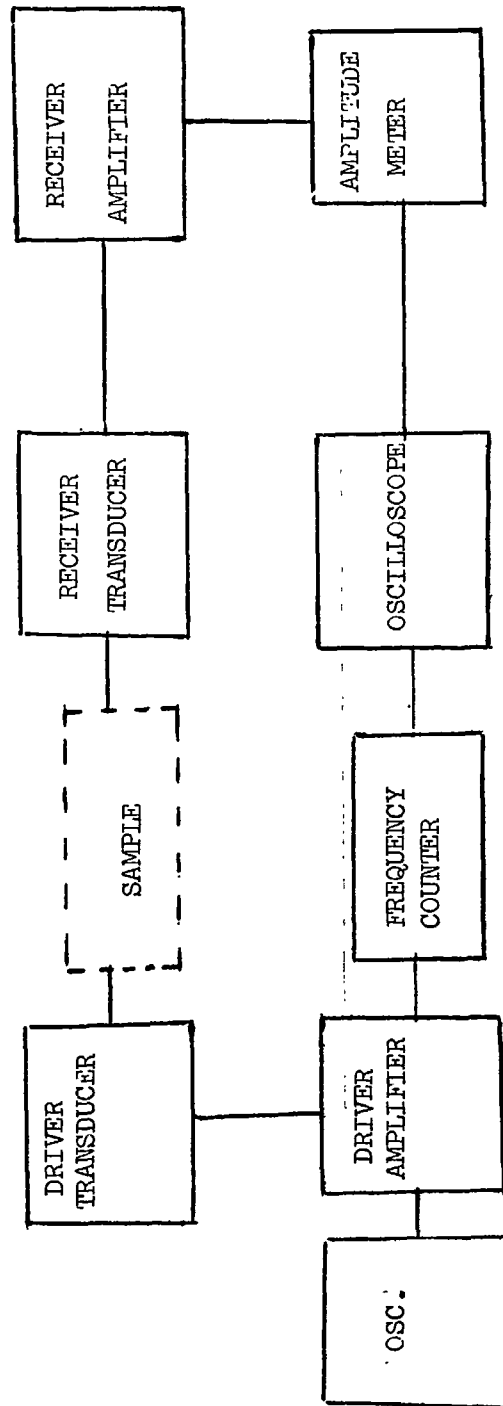


Figure 9. Block diagram of Magnaflux SR-200 dynamic elasticity equipment

the end of $0.224 \times \text{length of bar}$) and attached to the metal shell in the furnace. Rectangular specimens can be rested on the fine wire as indicated by Figure 10.

Excitation of the specimen is accomplished through the use of a Rochelle Salt piezoelectric transducer which converts the electrical drive signal to a mechanical vibration. The vibration is transmitted from the driving transducer to the specimen by means of a fine high temperature semi-flexible wire (0.010 mil tungsten-26% rhenium) which is bonded in a small indentation in the end of the specimen. A high temperature Al_2O_3 adhesive, Ceramabond 502, was used to prevent loosening of this wire at high temperatures. The wire is attached to the cross section of the rod at a location halfway between its center-line and edge.

An identical receiving or pickup transducer is bonded to the opposite end of the specimen to convert the specimen vibration back to an electrical signal which is analyzed by a frequency counter. Adjustments are made in the wire coupling to obtain a signal free of extraneous vibration. Best results are obtained with the wires slightly bowed. By virtue of the direct coupling of the transducer and specimen, excitation of all three modes of vibration, transverse, torsional and longitudinal, and their respective harmonics are possible.

Using the variable frequency oscillator, the frequency of the driving transducer may be regulated from 600 cycles/sec to 50,000 cycles/sec. The electrical signal from the driving transducer is impressed on the horizontal plates of the oscilloscope and the pickup signal on the vertical plates. As the frequency of vibration is varied

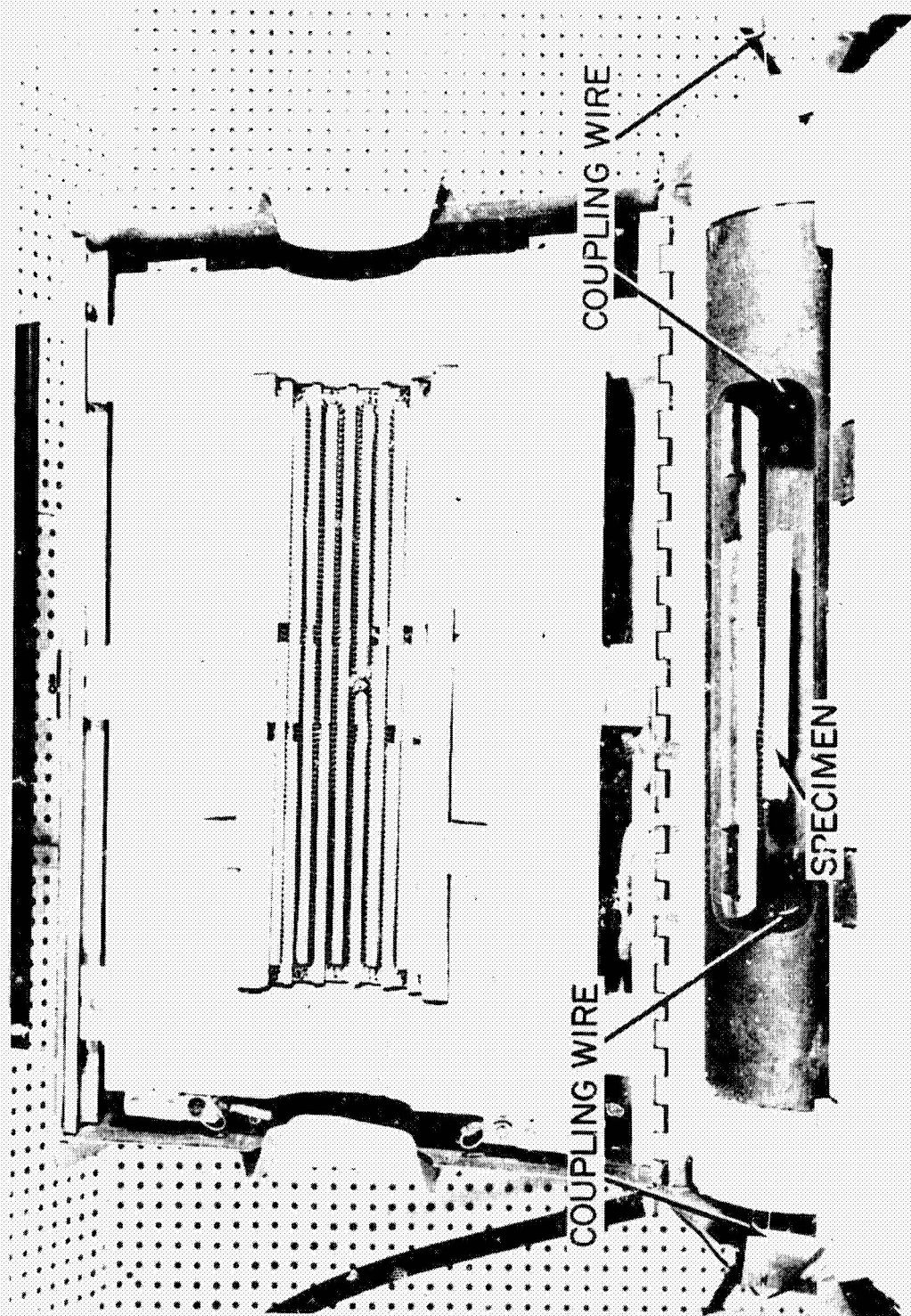


Figure 10. Rectangular specimen test setup for Elastomat Furnace

and approaches the mechanical resonance frequency of the specimen, the amplitude of vibration increases rapidly. The increased amplitude is detected by the formation of a Lissajous figure (one of elliptical shape) on the oscilloscope screen and also by a built-in amplitude meter. The oscillator frequency setting at which the Lissajous pattern has its maximum, and as indicated by the maximum deflection of the amplitude meter, denotes a resonance frequency of the specimen. The frequency is analyzed by the Hewlett-Packard model 5512 A electronic frequency counter, and visually displayed to an accuracy of 0.01 cycle/sec when allowed a 10-second measurement period.

Free damping or internal friction measurements were made on the Elastomat by adjusting the amplitude of the resonance frequency so that the deflection on the amplitude meter is larger than 90 divisions. The electrical signal to the driving transducer is interrupted by the damping switch. The vibration of the specimens decays exponentially and the number of cycles for the specimen amplitude to decay to 36.6 percent or $1/e$ of its value are counted on the frequency counter. The reciprocal of this number represents the logarithmic decrement.

Based on resonant frequency data for a 0.22-inch-diameter, 6-inch-long pure hafnium rod as provided by Washburn (1966), an approximate transverse resonant frequency of a 0.444-inch-diameter, 4-inch rod of as received, hafnium-20% was estimated to be 2460 cycles/sec. This was based on the fact that the frequency of the two rods could be related by

$$F_{res} \propto \frac{\text{Dia.}}{\text{Length}^2} \quad (34)$$

This figure provided a working base around which the scan of the frequency spectrum could begin.

Using the variable frequency oscillator the frequency spectrum was scanned slowly between 1300 and 5700 cycles/sec. All frequencies at which Lissajous figures appear on the screen were recorded. One of the most difficult tasks was eliminating the many fictitious Lissajous that appeared in the spectrum and defining the true resonant frequencies of the specimen. In the first sample a strong resonance appeared at 2700 cycles/sec. In a similar manner and using the relationship

$$F_{\text{Long.}} \propto \frac{1}{L^2} \quad (35)$$

the longitudinal frequency of both the 4- and 5-inch-long specimen was identified as being 14,409 and 11,430 cycles/sec, respectively. These two frequencies when used in equation (13) for elastic modulus based on longitudinal vibration gave a similar value of the elastic modulus based on transverse vibration as provided by equation (10). Having identified both the transverse and longitudinal resonant frequencies an approximation of the torsional resonant frequency was made based on equation (17) which defines Poisson's ratio by

$$\mu = \frac{1}{2} \left(\frac{F_L}{F_{\text{Tor.}}} \right)^2 - 1 \quad (36)$$

or rearranged

$$F_{\text{Tor.}} = \sqrt{\frac{0.5 F_L^2}{\mu + 1}} \quad (37)$$

Assuming that μ could be between a realistic value of 0.2 and 0.4 which encompasses the values for the majority of metals and alloys, it was determined that the torsional resonant frequency should lie between 8600 and 9300 cycles/sec for a 4-inch specimen and between 6830 and 7380 for a 5-inch specimen. Each specimen was then carefully scanned in this frequency range, and a strong resonance was detected at 9224 and 7310, respectively. The room temperature resonant frequencies having been identified, the temperature of the specimen was raised in small increments of 5 to 15 degrees up to 1000° C, and the change in resonant frequencies was recorded. The transverse frequency was primarily monitored, however, both the torsional and longitudinal frequencies were measured a sufficient number of times to determine their temperature dependence. Damping data was monitored only for transverse frequency as the suspension system provided minimum contribution in this mode of vibration as the wire loops were located at the transverse nodal points.

The specimen temperature was measured by a chromel-alumel thermocouple located 0.0625 inch below the specimen and was recorded continuously on a Honeywell Brown Recorder.

The specimen was allowed to come to an equilibrium temperature as verified by a constant thermocouple reading and a constant sample frequency count for a period of 5 minutes. The time between temperature increments varied. At low temperatures a longer time was required for equilibrium of the sample.

At least five damping measurements were made at each temperature increment. If the number of cycles counted varied appreciably, more

readings were obtained and an average value was calculated based on the most consistent readings. From 8 to 10 hours were required per specimen to make the necessary measurements in heating up to 1000°C . Measurements were taken as the specimen cooled at periodic intervals as conditions permitted.

An attempt was made to fill the Elastomat furnace with an inert atmosphere to obtain measurements without oxidation of the sample. However, because of the holes in the furnace ends necessary for the coupling wires to be attached to the sample, the hot argon gas escaped and melted the transducer crystals. Because the transducers had to be continuously adjusted to regulate the force in the coupling wires as they thermally expanded, the whole furnace system could not be enclosed in a vacuum. A glove-box assembly was built to house the furnace system. The whole system was purged with argon in an attempt to provide an inert atmosphere. However, this again proved unsuccessful as the hafnium-tantalum continued to oxidize.

One sample of the as received hafnium-tantalum rod was vacuum annealed to 1200°C . The sample was heated slowly from 20°C to 1200°C in 1.5 hours, and held at temperature for 1.5 hours. The sample was allowed to cool slowly in vacuum back to room temperature over a 6-hour period. The elasticity and internal friction measurements were made on this specimen as well as the pure hafnium specimen provided by Wah Chang Albany as a reference material.

In order to facilitate the identification of the fundamental resonant frequencies, a room temperature measuring system as shown in

Figure 11 was developed. This system as discussed by Spinner and Tefft (1962) provides a means of positive identification of the resonant frequencies of the specimen. Excitation of the sample is provided by an audio speaker (Electro-Voice, Inc., Model TW-35 VHF Driver) and detection of the sample vibration is accomplished by a phonograph cartridge (Astatic Type 445).

As the specimen is vibrating, it is probed by the phonograph pickup. The pickup is held lightly against the specimen and is moved horizontally along its length. The phase relationships of the corresponding Lissajous figures are noted on the oscilloscope. For transverse vibration, the ends of the specimen vibrate out of phase from the middle and there is no vibration amplitude at the nodal points. For longitudinal vibration, the ends of the specimen are out of phase with each other with a nodal point at the middle of the specimen. For torsional vibration, one must move across the specimen end cross section noting that opposite edges are out of phase with each other with a nodal point at the middle of the cross section.

These phase relationships as seen on the oscilloscope are shown in Figure 12.

Using the room temperature setup as described, the three fundamental modes of vibration were positively identified for all later dynamic elasticity measurements.

Elasticity and damping characteristics of the alloy were run in a vacuum environment and up to 2000° C in different test setup which is shown in Figures 13 and 14. A block diagram schematic of this system is shown in Figure 15. The basic difference in this system and the

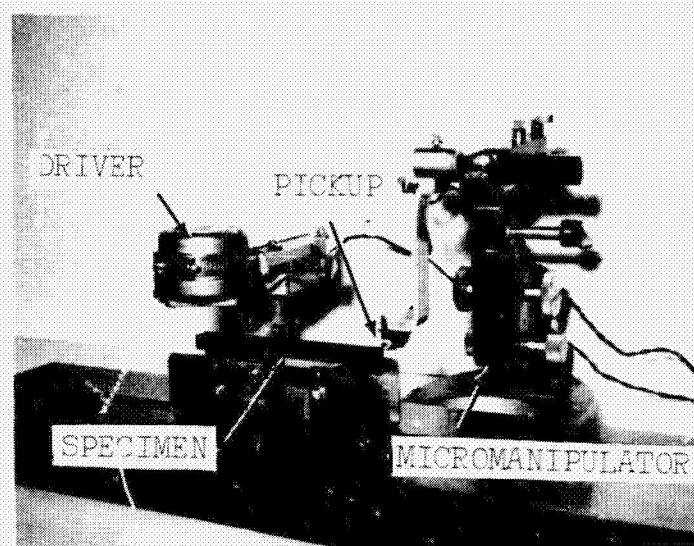


Figure 11. Room temperature sonic resonant frequency system

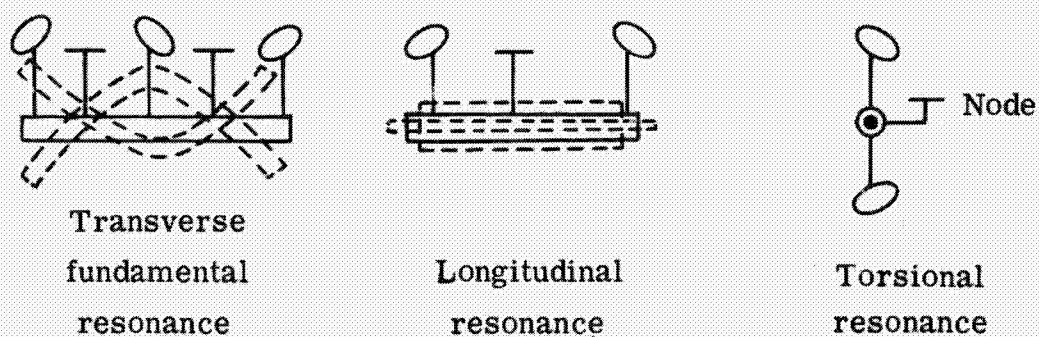


Figure 12. Lissajous figure phase relationships for various modes of vibration

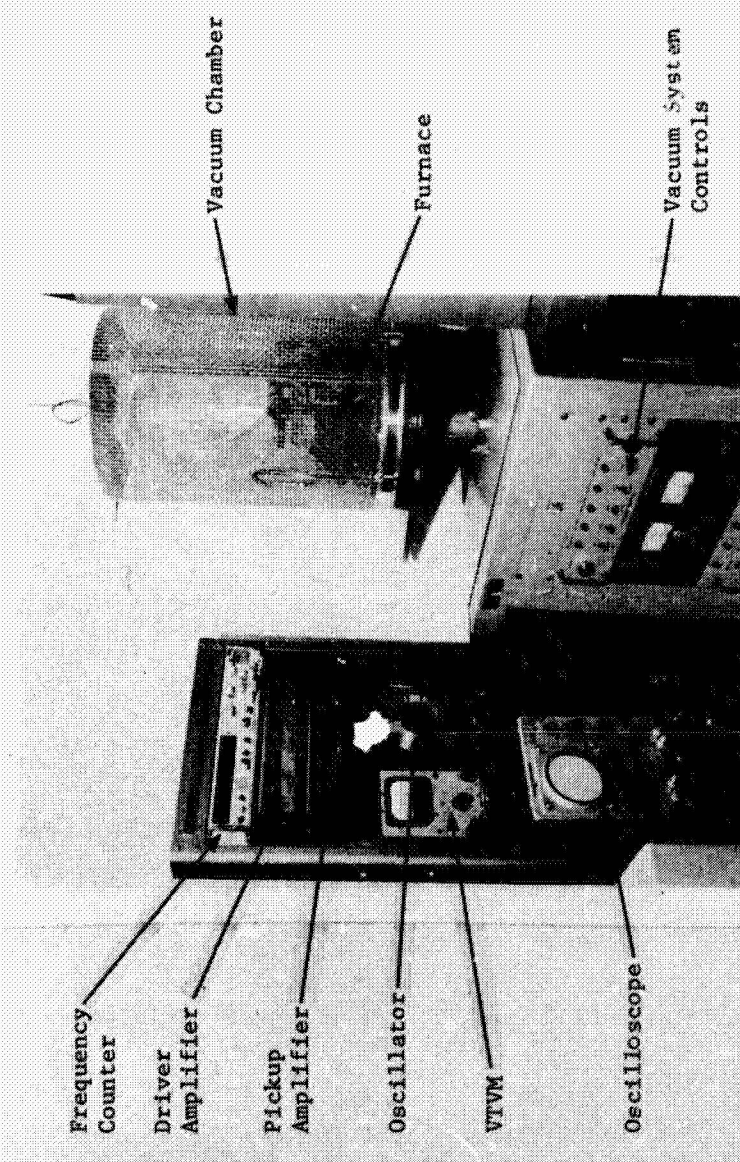


Figure 13. Vacuum high-temperature dynamic elasticity apparatus

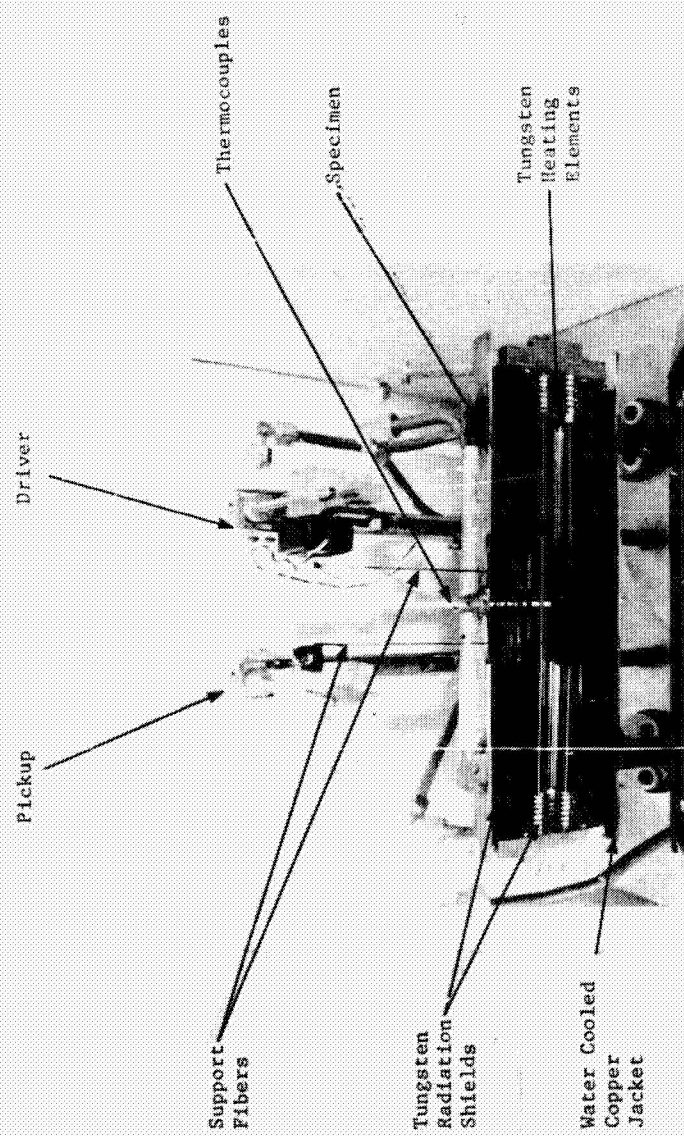


Figure 14. Furnace and suspension system for dynamic elasticity apparatus

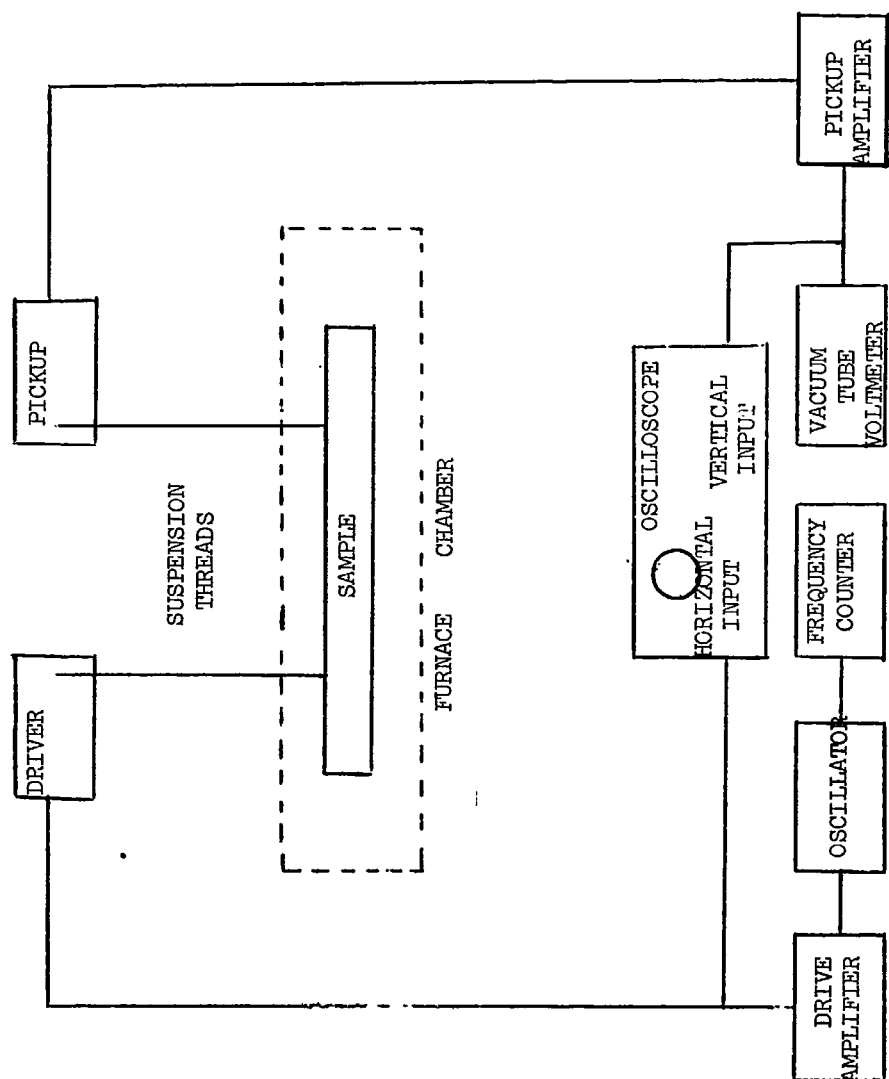


Figure 15. Block diagram schematic of vacuum high-temperature dynamic elasticity equipment

Elastomat, in addition to the vacuum and higher temperature capability, is in the manner in which the sample vibration is excited. The method used is known as the Förster (1937) method. Using this setup, the electrical driving signal is converted to a mechanical vibration by a magnetic record-cutting head (Astatic type M41-8).

The vibration of the driver is transmitted to the specimen through one of the two threads which are located near the transverse nodal points and which suspend the specimen in the high temperature furnace. The vibration of the specimen is transmitted through the other thread which is attached directly to a ceramic crystal phonograph cartridge pickup as indicated in Figure 16. This suspension system is discussed by Dickson and Spinner (1968) and enables one to excite transverse and torsional vibration.

The rest of the control system consists of a variable frequency oscillator, electronic frequency counter, oscilloscope, voltmeter (amplitude meter), and amplifiers, which all perform the same functions as previously discussed for the Elastomat.

The high temperature furnace shown by Figure 14 is a split shell design with tungsten heating elements. Temperature measurements are made on the specimen with a 95 percent tungsten/5 percent rhenium/74 percent tungsten/26 percent rhenium thermocouple encased by a thorium oxide tube. The thermocouple is located adjacent to the specimen and near its middle.

Damping measurements can be made on this equipment by either the free decay method or measurement of the half-width of the resonance peak. In the free decay method, the specimen is tuned at the resonant

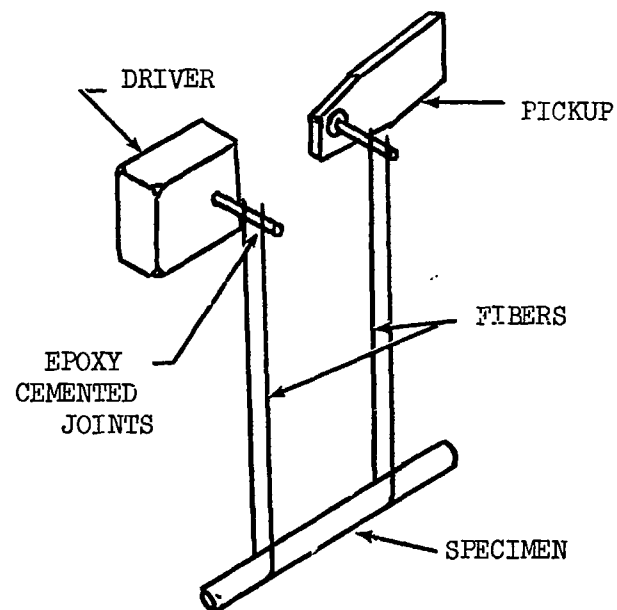


Figure 16. Detail of suspension system for round specimen

frequency and the trigger circuit is connected to the horizontal input of the oscilloscope in place of the driver signal. The oscilloscope is adjusted so the horizontal sweep is triggered by opening the trigger circuit which also shuts off the signal to the driver. The decay curve is then displayed on the oscilloscope and recorded photographically on ASA 3000 speed Polaroid film. From measurements of the amplitude of the envelope of the sine wave describing the decay of free vibrations of the sample, and knowing the time interval between amplitude measurements from the oscilloscope trace sweep rate, the value of the internal friction can be calculated by equation (29).

The method utilizing measurement of the half-width of the resonance peak is carried out by detuning the oscillator on either side of the peak to give a deflection of the vacuum tube voltmeter equal to half that observed at the position of the peak. The frequencies are determined with the electronic frequency counter.

Room temperature identification of the transverse and torsional resonant frequencies having been determined by previous measurements and calculations, specimens of the hafnium-20% tantalum were suspended with Pluton, type 10A carbon fiber, obtained from a Minnesota Mining and Manufacturing Co. fabric. The fiber was looped around the specimen as close to the transverse nodal points as possible.

It was not possible to excite transverse resonance at the precise nodal points, however, by very slightly displacing the suspension threads, a strong signal was possible. Smaller size specimens were required with the Pluton thread suspension as it would not support the heavier specimens used on the Elastomat. The 0.44-inch-diameter

specimens were machined to a smaller diameter and the 0.125-inch rod material was used to accommodate the carbon fiber. Attempts were made to use 0.005-inch-diameter molybdenum wire, however, the pickup signal was too distorted to be of value, probably due to a spring effect from the specimen vibration.

Room and elevated temperature damping and elasticity measurements were made in a vacuum of 1×10^{-5} torr. The temperature of the specimen was raised in 25° - 50° C increments with the specimen remaining at temperature until equilibrium was obtained. Here again, the specimen was deemed at equilibrium when a constant thermocouple output and resonant frequency count was achieved for 5 minutes. The measurements of the transverse and torsional frequencies at each temperature were recorded. Free decay and forced resonance damping measurements were made on the transverse resonant frequency. Specimens of as received, vacuum annealed, and oxidized material were run at elevated temperatures up to 2000° C. It was not always possible to make every run to this temperature due to the high noise level which always developed around 1000° C and the fact that the suspension thread broke on occasion during the run.

An annealing study of the alloy was performed by heating an as received specimen from room temperature to 500° C in 15 minutes, then to 1112° C in an additional 15 minutes, and then holding at this equilibrium temperature and recording the transverse resonant frequency change as a function of time at the annealing temperature. An indication of the internal friction change with time was obtained from the change in output voltage of the crystal pickup.

A more detailed study of the room temperature damping characteristics of the hafnium-20% tantalum alloy was performed using the equipment shown in Figures 17 and 18. A rectangular annealed bar specimen was suspended precisely at the nodal points with cotton thread. A semiconductor strain-gage pickup was bonded directly to the sample near its middle. Excitation of sample vibration was provided by striking the specimen with a steel rod with the force being actuated by a solenoid. Force imparted to the specimen and thus amplitude of vibration was controlled by varying the voltage of the solenoid signal. Decay of the sample vibration was visually displayed on the Tektronix oscilloscope and recorded photographically by Polaroid film.

Stress-Strain Behavior

The room temperature stress-strain behavior of the hafnium-20% tantalum alloy was investigated using a 20,000-pound capacity Instron Universal Testing System shown in Figure 19. Tensile tests were conducted under guidelines provided by ASTM Standard E8-68, "Tensile Testing of Metallic Materials." The number of test specimens run was necessarily small due to the cost per sample and the small amount of material received.

Wah Chang Albany conducted tensile tests at their laboratory on pure hafnium rod and made the data available to this author to provide a comparison with the hafnium-20% tantalum alloy data.

Four tensile specimens were machined from the as received material. These rod specimens were machined with reduced cross sections and had standard 2-inch gage lengths. One specimen was oxidized for 5 hours

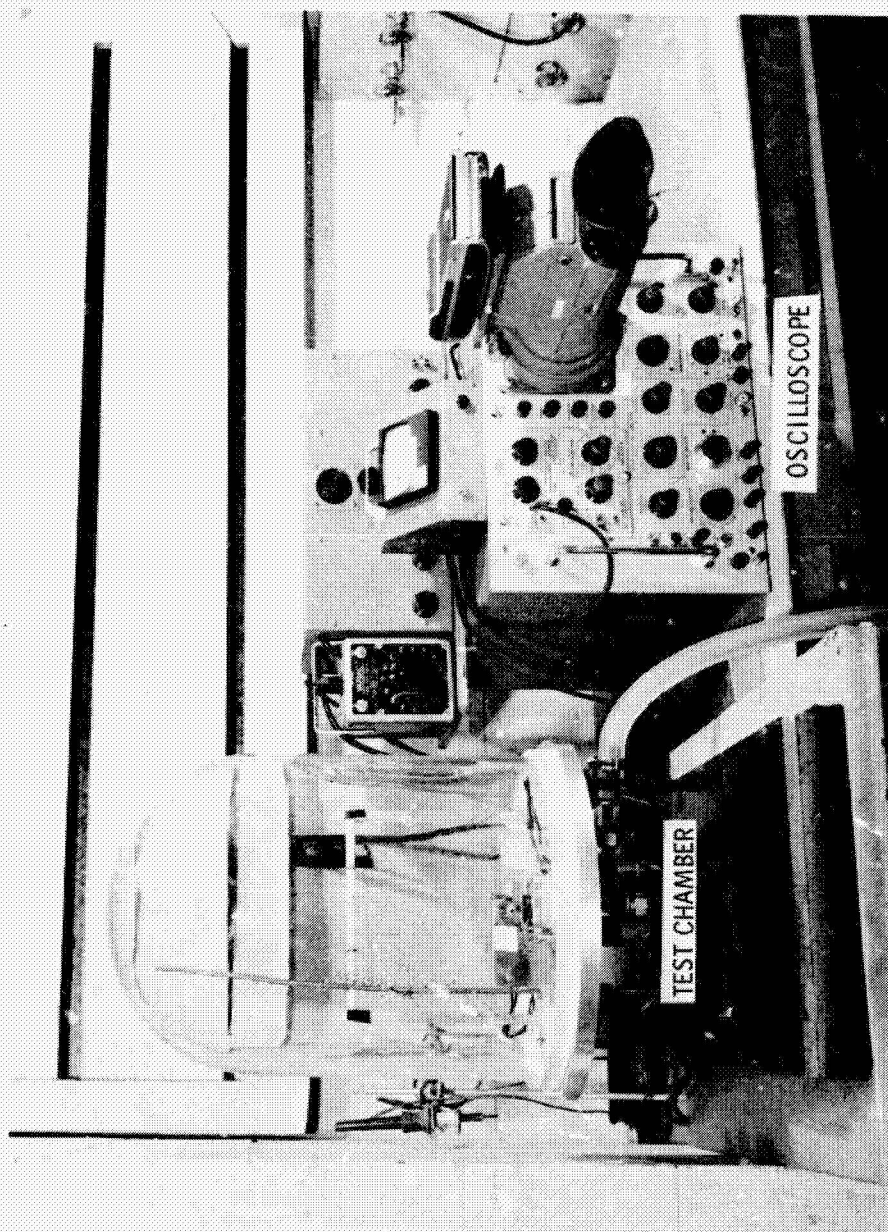


Figure 17. Room temperature damping apparatus

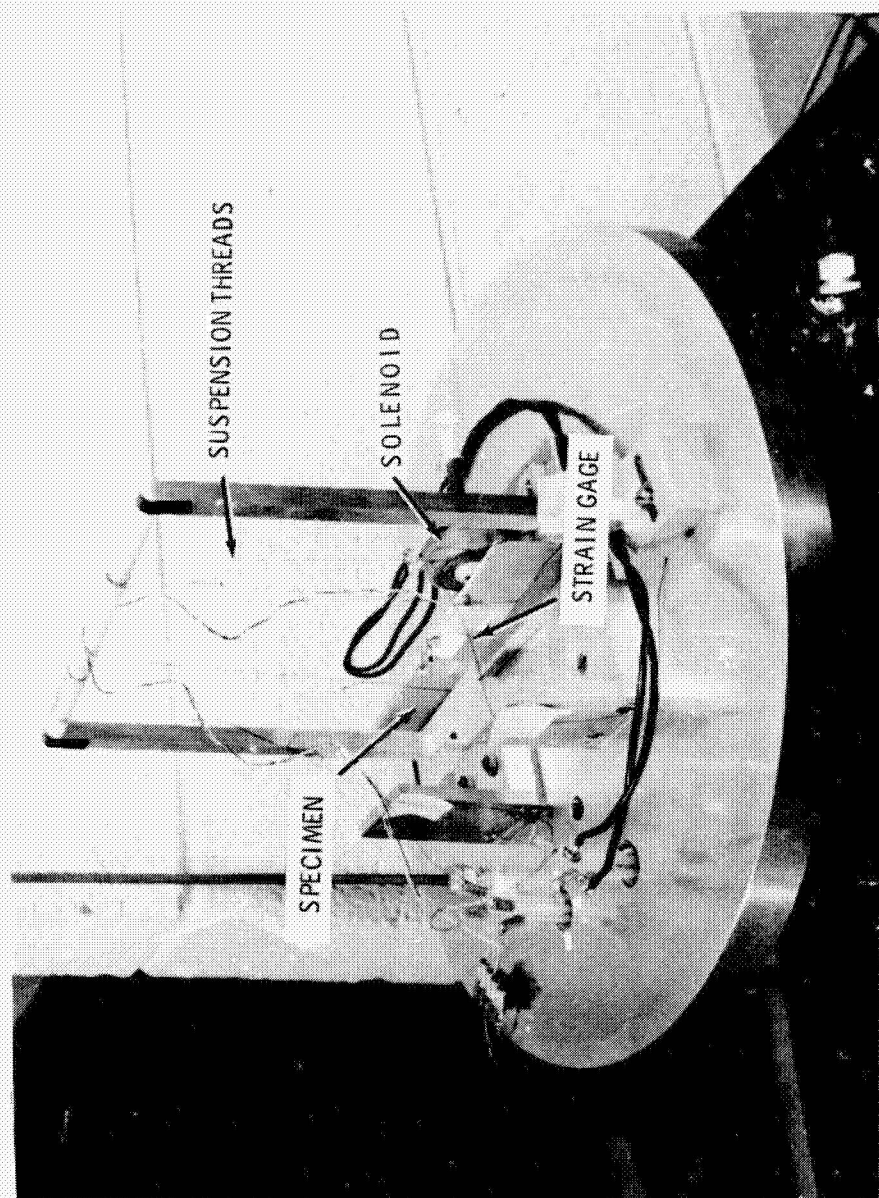


Figure 18. Detail view of room temperature damping test setup

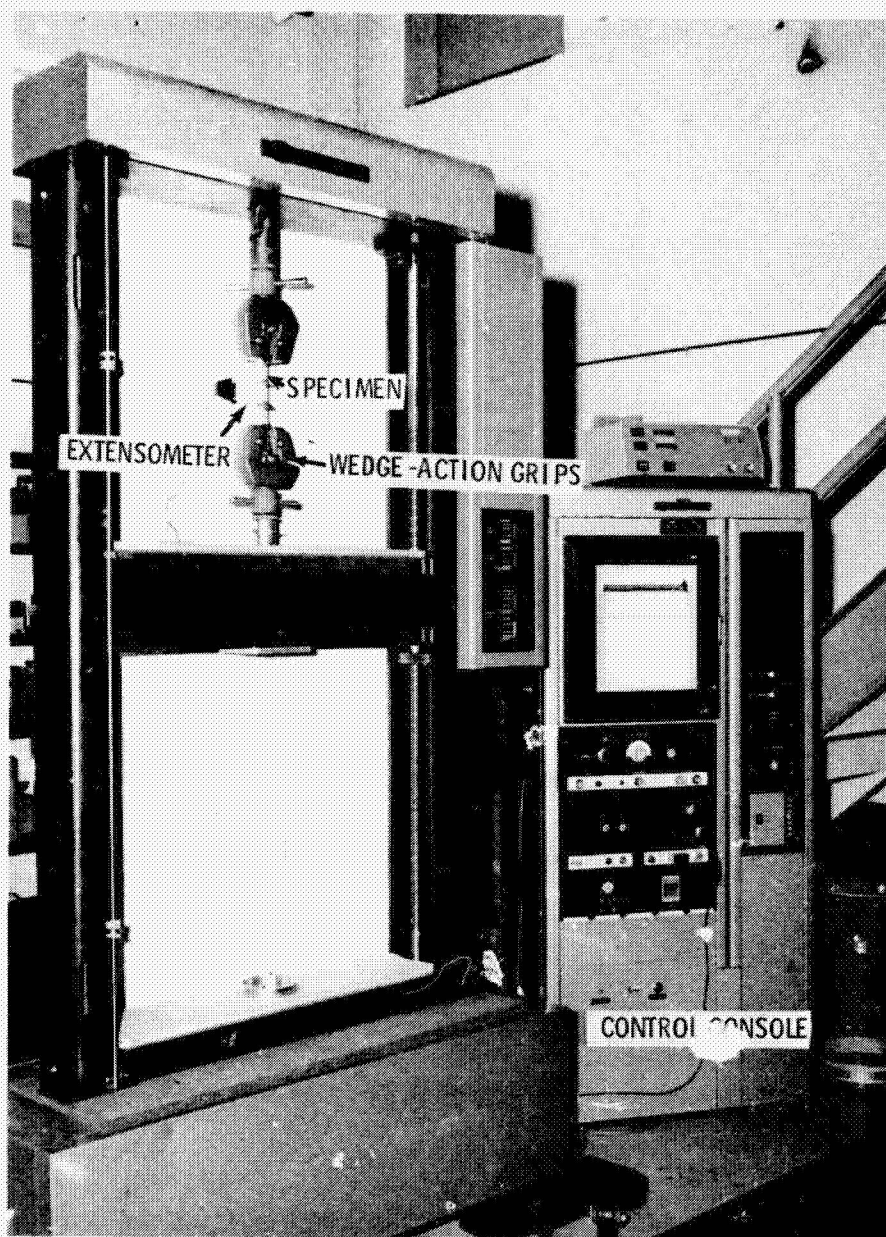


Figure 19. Instron static tensile test setup

at 1000° C, one specimen was fully annealed at 1200° C for 2 hours, and two were not heat treated, but tested as received. The specimens were held using standard wedge-action grips and the load was applied using a crosshead speed of 0.1 in/min. Strain was measured with a standard 2-inch Instron extensometer which measured elongation between 2-inch gage marks on the specimen cross section.

Phase Transformation Study

Earlier work by Svechnikov (1964) and Mash (1968) indicated the existence of a metastable phase α' which could be formed by heat treatment of the hafnium-tantalum alloys followed by rapid cooling. Further insight into this phase transformation was investigated through hot stage metallographic observation, X-ray diffraction analyses, and microhardness measurements.

Cylindrical wafer specimens of 0.136-inch diameter and 0.01-inch thickness were cut from the as received hafnium-20% tantalum rod material. These specimens were hand polished with microcloth and 0.3 micron Al_2O_3 powder and simultaneously etched with a diluted solution of HF and HNO_3 acid to enhance grain boundary details in the sample. An X-ray diffraction pattern was established on the as received material using the General Electric XRD-6 X-ray equipment shown in Figure 20. A complete scan of the specimen through a diffraction angle, 2θ , ranging from 20°-148°, was carried out at room temperature using a scanning speed of 0.2°, $2\theta/\text{min}$ in order to obtain an accurate pattern. A copper target X-ray tube was utilized with a power setting of 45 KVP and 15 milliamperes. The SPG-4 scintillation counter tube was used to detect the diffracted X-rays.

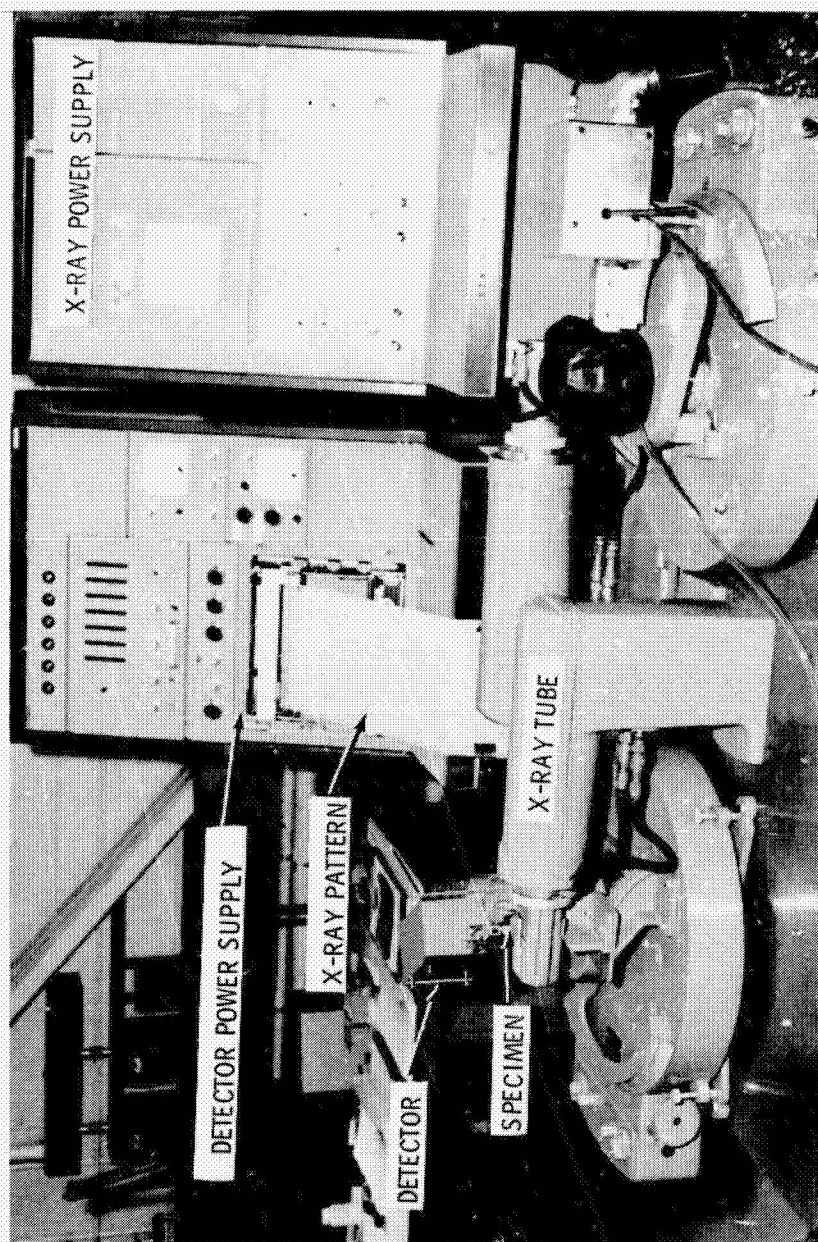


Figure 20. X-ray diffraction test setup

Further characterization of the alloy prior to heat treatment was carried out using the Wilson Tukon hardness tester shown in Figure 21. Knoop hardness measurements were made across the surface of the sample and an average value was calculated.

Photomicrographs of the etched specimen were made at room temperature on a Bausch and Lomb Research II metallograph prior to insertion in the hot stage metallograph.

The phase transformation in the hafnium-20% tantalum alloy was observed at high temperature using the Leitz Metallux microscope and accompanying vacuum heating stage setup shown in Figures 22 and 23. The thin wafer specimen was placed directly on top of the pure tungsten resistance heating element. Temperature measurements on the sample were made concurrently by a Pyro optical pyrometer and a chromel-alumel thermocouple in contact with the heating element. Temperature of the hot stage was varied by controlling the amperage of the input power supply.

In order to correct the optical pyrometer temperature measurements, the emissivity of the specimen must be known. The emissivity of the hafnium-20% tantalum was unknown, therefore an alternate measurement was used. A thin tungsten specimen of the same size as the hafnium-tantalum wafer was placed on the tungsten heating element. The hot stage was heated to 1400°C and optical pyrometer readings were taken on both the heating element and the tungsten sample. The readings were identical as the color of tungsten specimen was at all times identical to the heating element. This indicated no thermal gradient existed in the specimen and it indeed was at the same temperature as



Figure 21. Knoop microhardness measurements test setup

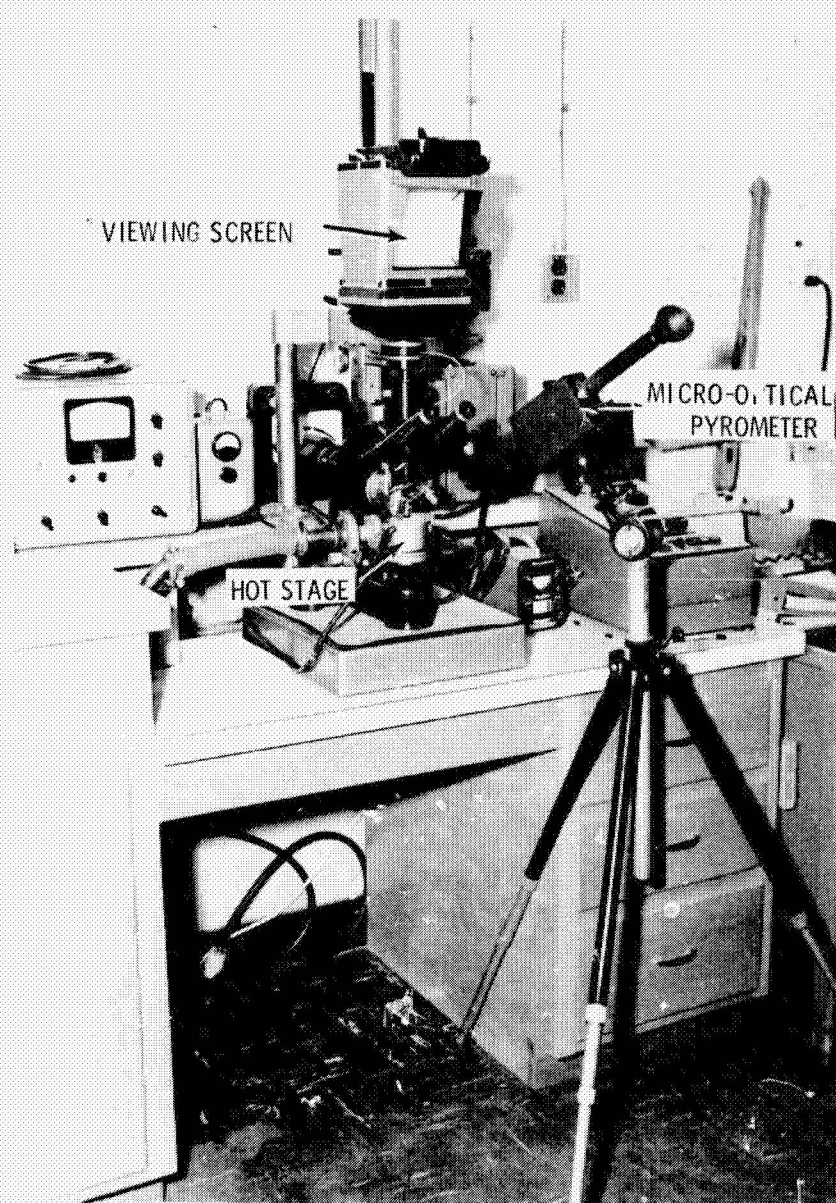


Figure 22. Hot stage metallograph for phase transformation study

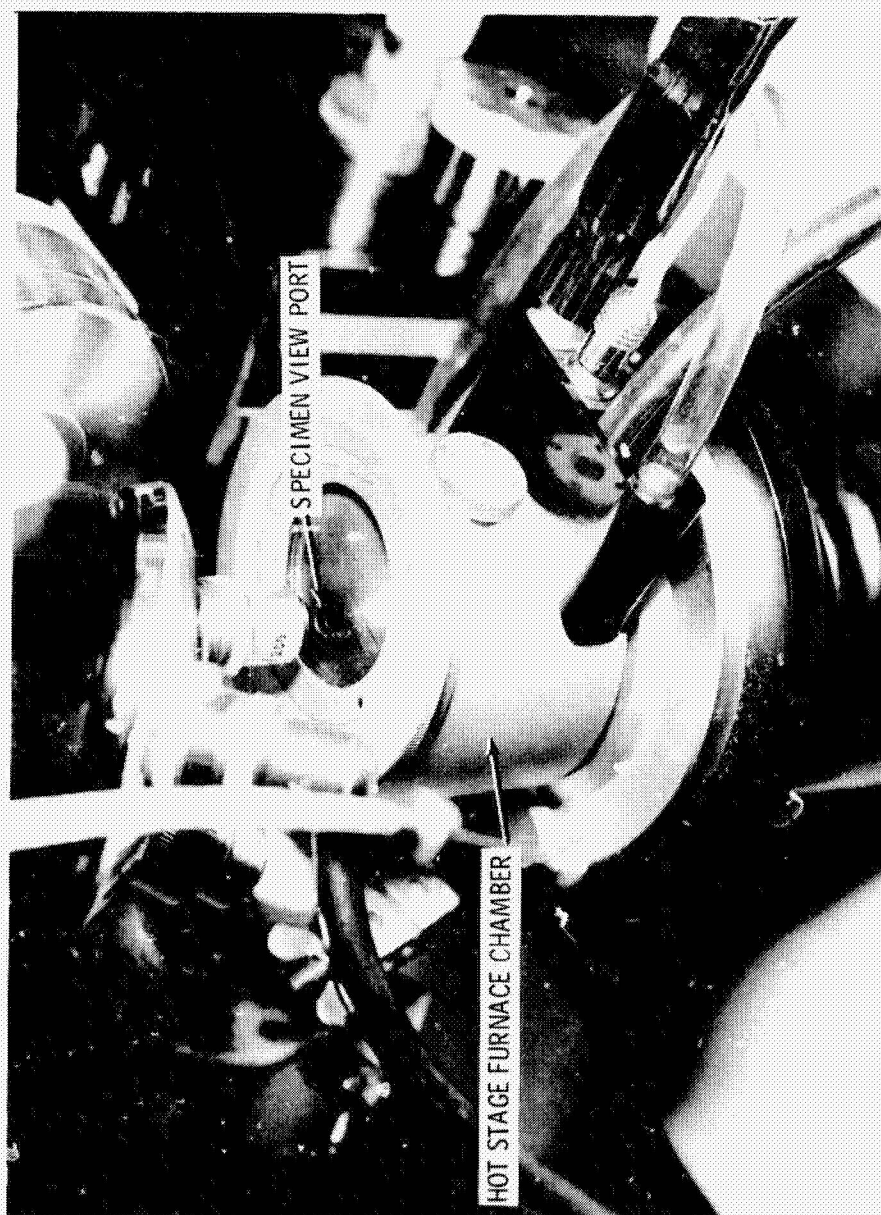


Figure 23. Vacuum hot stage chamber

the heating element. Therefore temperature measurements could be made during the phase transformation study by measuring the temperature of the tungsten heating element in contact with the hafnium-tantalum specimen and making the temperature corrections based on known emissivity data for the tungsten. Having established a guideline for the temperature measurements, the hafnium-20% tantalum specimen was placed in the hot stage and under a vacuum of 5×10^{-5} torr, and the temperature was gradually raised in increments varying from 50° - 150° C.

Photomicrographs were made at 500X magnification using a Leica 35-mm camera at each equilibrium temperature up to above 1400° C. Having reached a maximum temperature which placed the specimen well within the single β phase region indicated by the phase diagram of Figure 1, the power input was decreased by 5 amperes causing a rapid cooling of the specimen to approximately 1287° C where additional photomicrographs were taken. The temperature of the sample was reduced in 50° increments down to 385° C, visually observing and photographing at each increment. At this point, the power was secured allowing the sample to cool to room temperature. After removal from the hot stage, an X-ray diffraction pattern of the heat-treated alloy was run, along with Knoop microhardness measurements. Using the Cambridge scanning electron microscope, shown in Figure 24, micrographs of the heat-treated specimen were taken. For comparison purposes carbon replicas of the specimen surface were prepared and conventional electron micrographs were made on a Hitachi model HU-11A electron microscope. For additional verification, a second specimen was tested in the hot stage

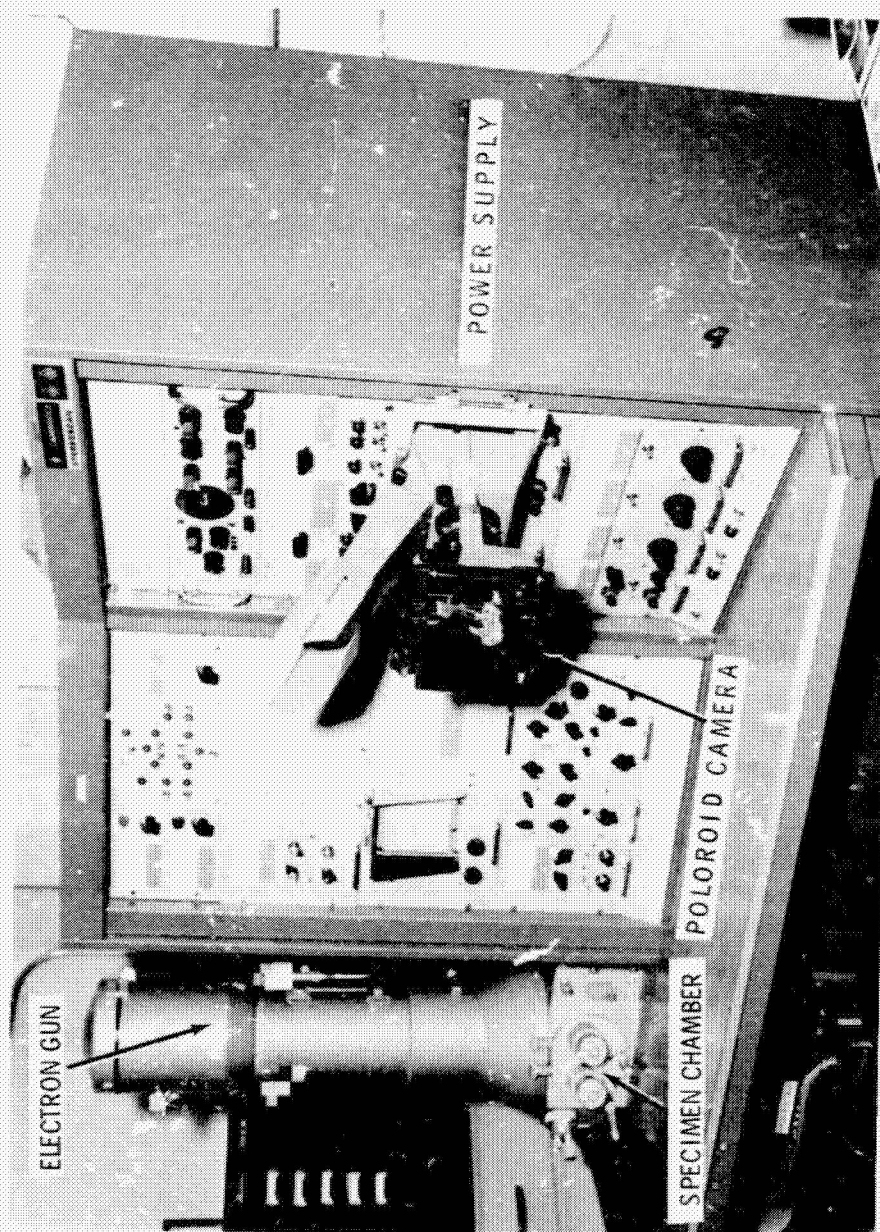


Figure 24. Cambridge scanning electron microscope

using a similar procedure. Photomicrographs for this test were made using the Polaroid cassette and ASA 3000 film.

Static Oxidation Behavior

A series of oxidation tests were conducted on the hafnium-tantalum alloy to assess qualitatively and quantitatively its oxidation behavior in a static air environment at five temperatures ranging from 1000° C to 1700° C. Disk-shaped specimens of 0.44-inch diameter and 0.3- to 0.4-inch thickness were machined from the extruded rod material. The specimens were hand polished using 600 grit silicon carbide paper followed by 0.3 micron Al_2O_3 powder to give a smooth external surface. Tests were conducted in a Centorr Series 10 tungsten rod heating element shown in Figure 25. The furnace was equipped with a high temperature Al_2O_3 muffle tube which enabled temperatures up to 1700° C to be obtained in a static oxidizing environment. Specimen dimensions were measured exactly with precision micrometers. From these dimensions the exposed surface area was computed. Each specimen was weighed to four place accuracy using a Sartorius analytical balance.

The specimen was suspended in the heat zone in a platinum wire basket as shown in Figure 26. Specimen temperature was read directly by a Pyro optical pyrometer. Corrections for sample emissivity were based on a value of $\epsilon = 0.65$ for HfO_2 as indicated by Marnoch (1967). Using a dummy oxidized specimen suspended in the middle of the heat zone, the furnace temperature was slowly raised to the desired level to prevent cracking of the Al_2O_3 muffle tube. Once at the desired temperature, the dummy specimen was removed and the test specimen inserted into the furnace. Optical pyrometer temperature readings were again

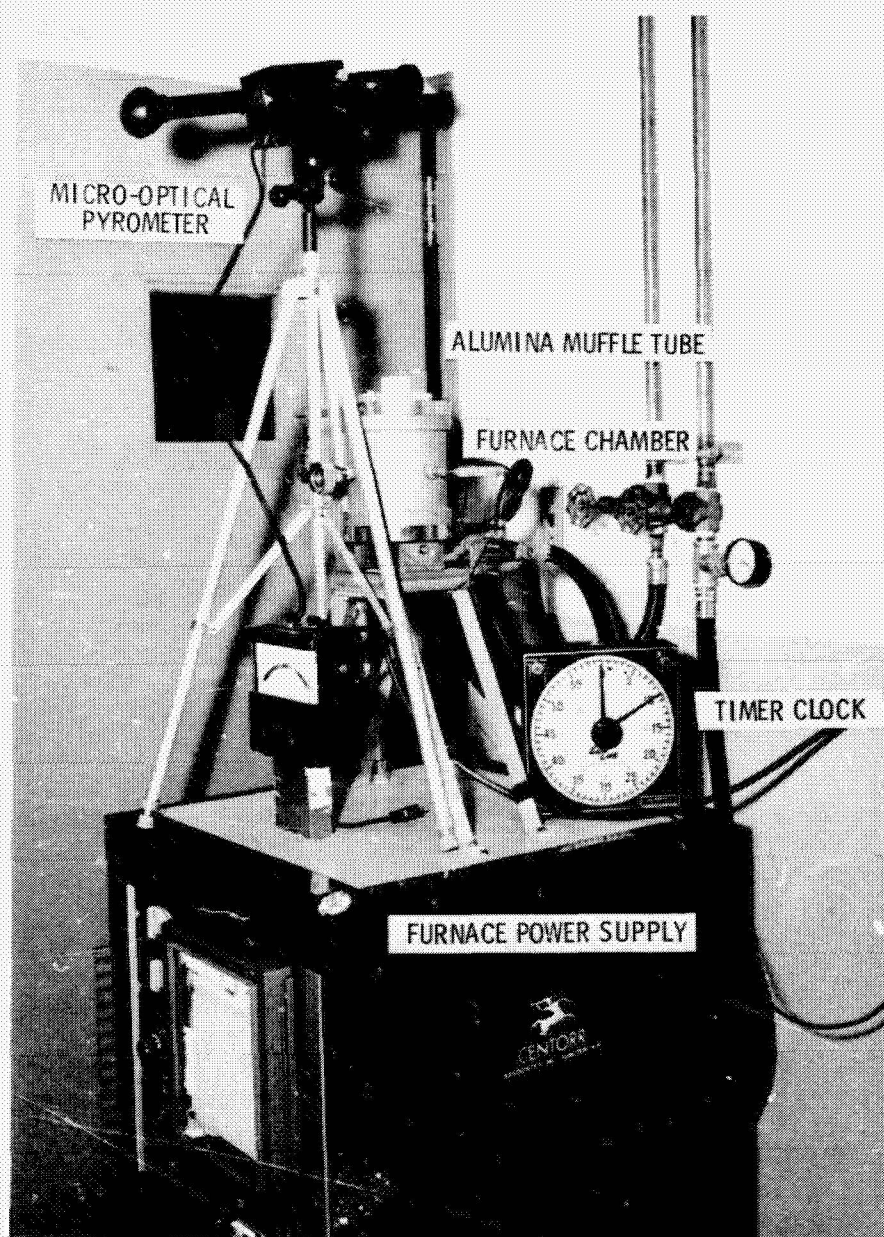


Figure 25. Overall test set-up for static oxidation tests

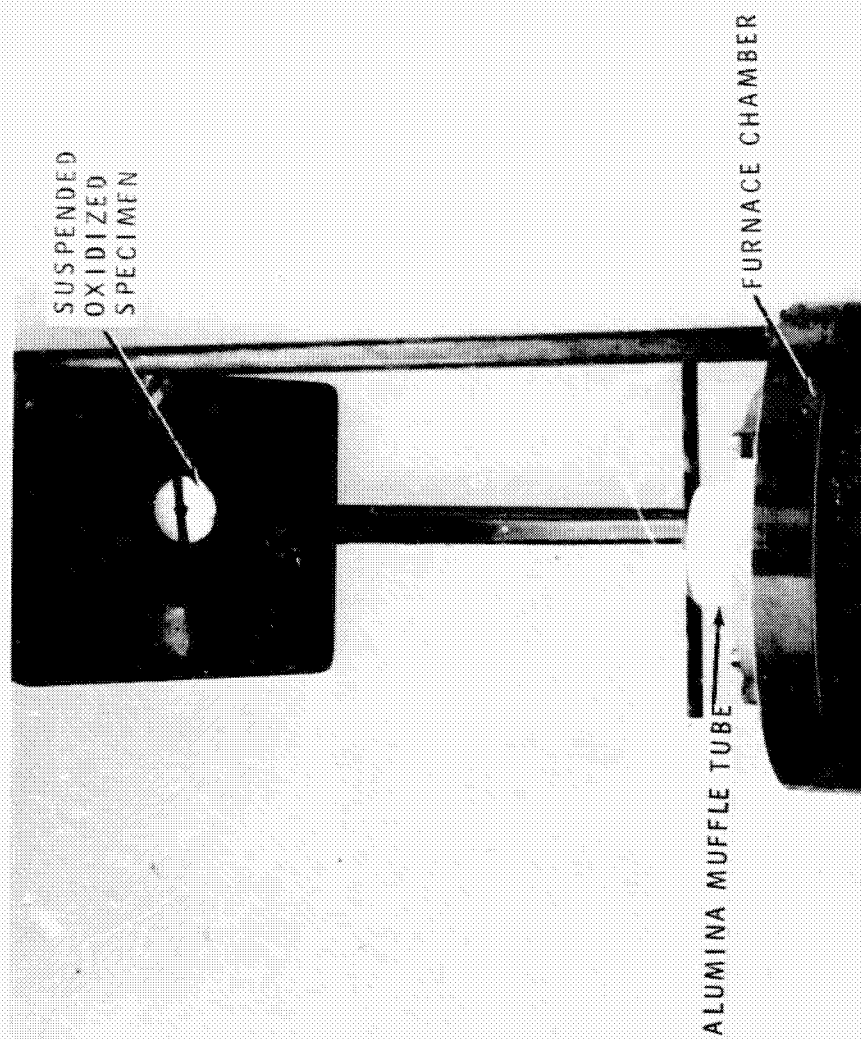


Figure 26. Specimen suspension system for static oxidation tests

made on the test specimen. A timer clock was used to regulate time at temperature. The specimen was removed from the furnace at 2-minute intervals for the first 20 minutes and immediately weighed on the analytical balance. Photomacrographs at 4X magnification were taken of the top surface to show surface oxidation formation at each time increment.

After photographing the specimen it was immediately returned to the furnace for re-exposure. Twenty-minute exposure increments were used for the completion of the first hour after which time weight change measurements and photomacrographs were taken every hour for times up to 8 hours maximum exposure. Several of the specimens were cross-sectioned and photomicrographs taken to qualitatively show oxide penetration into the material. Color 3X magnification photographs were taken of the specimen surface after the final exposure to show the difference between the low and high temperature oxide.

Scanning electron microscopy was used to study the surface morphology of the low and high temperature oxide. Using the Centorr furnace and a similar setup to that previously described, a second series of static oxidation tests were carried out. Specimens of the hafnium-tantalum were exposed for 3-, 10-, and 30-minute intervals at five temperatures from 1000° C to 1700° C. After each interval of exposure, the specimen was photographed at magnifications up to 17,500X using the S.E.M. After the final thermal exposure, it was necessary to coat the specimen with an anti-static solution prior to insertion into the scanning electron microscope.

One test specimen was exposed for 30 minutes at 1700° C. Using the General Electric diffractometer as previously described, X-ray diffraction patterns were established on the surface oxide. Knoop microhardness measurements were made across the specimen. The specimen was then hand polished to remove a 0.004-inch layer using silicon carbide paper with final polishing done with 0.03 micron Al_2O_3 powder. After each layer was removed, an X-ray diffraction pattern was established along with corresponding microhardness measurements.

Additional X-ray diffraction analyses were conducted on the low temperature (1000° C) unprotective oxide. Oxide scale which readily spalled was ground by mortar and pestle into 200 mesh powder. This powder was lightly pressed into a powder sample holder and X-ray patterns established for comparison with the tightly adherent high temperature oxide.

Angular location of X-ray peaks was determined by measurement of the midpoint of the half peak height line. From the angular locations, the "d" spacings for the hkl planes responsible for the peaks, were determined from tables for copper K_α radiation.

Using this information along with the ASTM Powder Diffraction file crystal system classifications were determined.

Metallographic Techniques

The basic microstructure of the hafnium-tantalum alloy was studied using conventional reflecting light microscopy, electron microscopy, and scanning electron microscopy as have been previously described.

Standard metallographic procedures were employed with the specimen being polished with silicon carbide pressure sensitive abrasive paper starting with 240 grit and working through the finer grits 320, 400, and 600 successively. Final polish was carried out using from 0.03 to 0.05 micron Al_2O_3 powder on a microcloth covered polishing wheel or Buehler Vibromet polisher. Several combinations of hydrofluoric and nitric acid etchant solutions were tried, however, the solution giving the best results had the following composition:

45 milliliters HNO_3 acid

10 milliliters HF acid

5000 milliliters water

The best results using this etchant were obtained by dispersing a few drops of the solution on the polishing wheel along with the Al_2O_3 powder, thus polishing and etching simultaneously for 2 to 3 minutes after which examination was carried out on the metallograph.

RESULTS AND DISCUSSION

Room Temperature Dynamic Elasticity Measurements

The elastic or Young's modulus, shear modulus, and Poisson's ratio of the hafnium-20% tantalum alloy were calculated from the measured room temperature transverse, longitudinal, and torsional frequencies using the appropriate relationships as given by equations (10), (13), and (15). The correction factors applied to these equations to correct for individual specimen geometry and Poisson's ratio were obtained from the tables in Spinner and Tefft (1962), based on an assume Poisson's ratio of 0.25. A typical correction factor for E based on transverse vibration for a 4-inch-long specimen, 0.4445-inch diameter, was found to be $T_n = 1.063$ of 6.3 percent. The results of these calculations are shown in Table 4. The extruded rod in the as received condition, with no heat treatment, had a calculated average value of the elastic modulus of 16.98×10^6 psi and a shear modulus of 6.86×10^6 psi. Poisson's ratio, based on equation (6), was found to be 0.24. The average value of the elastic modulus of the two specimens annealed at 1200°C for 4 hours increased to 18.63×10^6 psi or 9.7 percent. The shear modulus for the annealed specimen increased to 7.36×10^6 psi or 7.3 percent for specimen number 6. The torsional resonant frequencies were not detected in sample 7. Poisson's ratio for the specimens annealed for 4 hours was found to be 0.27 or an increase of 12.5 percent. Similar calculations for the annealed pure hafnium rod specimen yielded a modulus of $E = 20.52 \times 10^6$ psi and shear modulus of 8.02×10^6 psi with a corresponding Poisson's ratio of 0.28.

Table 4.-- Room temperature elastic moduli of hafnium-20% tantalum alloy.

SPECIMEN No.	DIMENSIONS		TRANSVERSE RESONANT FREQUENCY (cycles/sec)	ELASTIC MODULUS E (10^6 psi)	LONGITUDINAL RESONANT FREQUENCY (cycles/sec)	ELASTIC MODULUS E (10^6 psi)	TORSIONAL RESONANT FREQUENCY (cycles/sec)	SHEAR MODULUS G (10^6 psi)	POISSON'S RATIO	COMMENTS:
	Length	Dia.								
1	4.008	0.4445	2770	16.96	14417	16.87	9168	6.81	.244	Elastomat (air) as received material
2	4.000	0.4445	2780	16.94	14553		9225	6.87	.233	Elastomat (air) as received
3	3.991	0.441	2788	17.15	14522	16.98	9208	6.81	.258	Elastomat (air) as received
4	4.956	0.445	1826	16.88	11687	16.93	7488	6.95	.214	Elastomat (air) as received
5	3.55	0.2447	1973.2	16.95						Top suspension Vacuum = 1 x 10^{-5} torr
6	3.656	0.257	2051.2	18.59			10444	7.36		Vacuum annealed 2200°F for 4 hrs.
7	3.262	0.249	2506.1	18.68						Vacuum annealed 2200°F for 4 hrs.
8	4.016	0.486	3364	20.52	16200	20.61	10119	8.023	.279	Pure Hafnium Rod Annealed condi- tion

The increase in elastic and shear moduli on the order of 10 percent on annealing has been noted in polycrystalline materials, such as copper, which exhibited a high degree of anisotropy as reported by McLean (1962), and Bradfield and Pursey (1953). The lower moduli of the as received hafnium-tantalum can likely be attributed to the preferred orientation of crystals caused by the extrusion process in the production of the rod material. Stress and strain vary from crystal to crystal and even across individual crystals within a polycrystal. In single crystals of zinc, Young's modulus has been shown to vary with orientation by a factor of 4:1. X-ray diffraction patterns established on the as received and annealed alloy showed a considerable difference in peak intensities, thereby indicating a lack of randomness in the as received specimens. The subsequent annealing process on the alloy produced a sufficient random distribution of the orientations to permit the polycrystalline hafnium-tantalum to behave in a more isotropic manner.

There is no existing elastic modulus or shear modulus data for the hafnium-20% tantalum alloy system. However, Marnoch (1967) reported that tensile test data for the hafnium-27% tantalum indicated a static elastic modulus of 25.6×10^6 psi. Thus it is seen that in reducing the tantalum content by 7 percent to improve the oxidation resistance, the modulus of the material was reduced to 18.6×10^6 psi, or a reduction of 27 percent. It is to be noted that the hafnium-20% used in this investigation was a two-phase substitutional solid solution alloy and showed a negative deviation from a rule of mixtures for estimating the modulus of elasticity based on the modulus and composition of the base alloys. The elastic modulus of 18.6×10^6 psi is less than the

modulus of either base component. On the other hand, Marnoch tests indicated a modulus of elasticity which was somewhat higher than that of hafnium and that predicted by a rule of mixtures. This different behavior can be attributed to two possible reasons:

1. The degree of preferred orientation differences in the specimens.
2. The hafnium-20% tantalum is of hypomonotectoid composition whereas the hafnium-27% tantalum is hypermonotectoid.

Even though test results were based on annealed specimens, a certain amount of preferred orientation likely existed in each. Marnoch's specimens were machined from rolled sheet material whereas those used in this investigation were machined from extruded rod material. From the phase diagram (shown in Fig. 1), it can be seen that during the formation of the two-phase $\alpha + \beta$ equilibrium solid solution of the hypomonotectoid composition from the melt, the β hafnium solid solution transforms through the two-phase $\alpha + \beta$ Hf solid solutions down to the equilibrium two-phase solid solution of $\alpha + \beta$ Ta. Likewise, the hypermonotectoid composition of the alloy transforms through a two-phase solid solution; however, this is seen to consist of β Hf + β Ta phases. It is, therefore, likely that the final equilibrium state of $\alpha + \beta$ Ta may be sufficiently different on a microstructural level to account for the difference in the mechanical behavior of the material at room temperature.

Room Temperature Stress-Strain Behavior

The results of the static tensile tests conducted on the hafnium-20% tantalum alloy are summarized in Table 5 and a stress-strain diagram for the alloy system is shown in Figure 27. The ultimate tensile strength of the alloy in the as extruded condition averaged 151,000 psi with a yield strength measured at 0.2 percent offset of 119,600 psi. The specimen vacuum annealed for 2 hours at 1200° C had an ultimate tensile strength of 120,400 psi with a corresponding yield strength of 104,000 psi. The static elastic modulus as calculated from the stress versus strain output data yielded a value of slightly over 18×10^6 psi. This method of calculation is not nearly as accurate as the more sensitive resonant frequency data, however, it does agree within experimental error with that value obtained dynamically. This data again substantiates the fact that the extrusion process used to fabricate the alloy, aligned the polycrystals in a preferred orientation which was partially recovered during the annealing process. Fracture of the as received material as indicated by Figure 28 was a typical ductile cup-cone type. However, as expected, oxygen interstitial contamination, as shown by a cross section of the tensile specimen oxidized for 5 hours at 1000° C, caused the failure mode to become a typical brittle fracture. The stress-strain behavior of the oxidized alloy was similar to unoxidized material during the elastic portion; however, strain-to-failure was typically decreased by 75 percent.

Tensile tests conducted by Wah Chang on the hafnium crystal bar indicated a modulus of elasticity between 24 and 27×10^6 psi which is 20 percent higher than that reported elsewhere in the literature. From

Table 5. Summary of static tensile test data for hafnium-20% tantalum alloy

Test No.	Heat treatment	Modulus of elasticity (psi $\times 10^{-6}$)	Yield strength (0.2% offset) (psi)	Ultimate tensile strength (psi)	Percent elongation	Reduction in cross-sectional area (percent)
1	As received	18.34	119,600	149,750	13	55
2	As received	---	---	152,134	11.11	48
3	Vacuum annealed	18.18	104,000	120,400	10.85	38
4	Oxidized 1850° C 5 hr	19.43	102,000	121,250	2.95	2.38
5	Annealed Hf	27.8	25,400	73,500	28	
6	Annealed Hf	24.1	27,800	73,400	29	

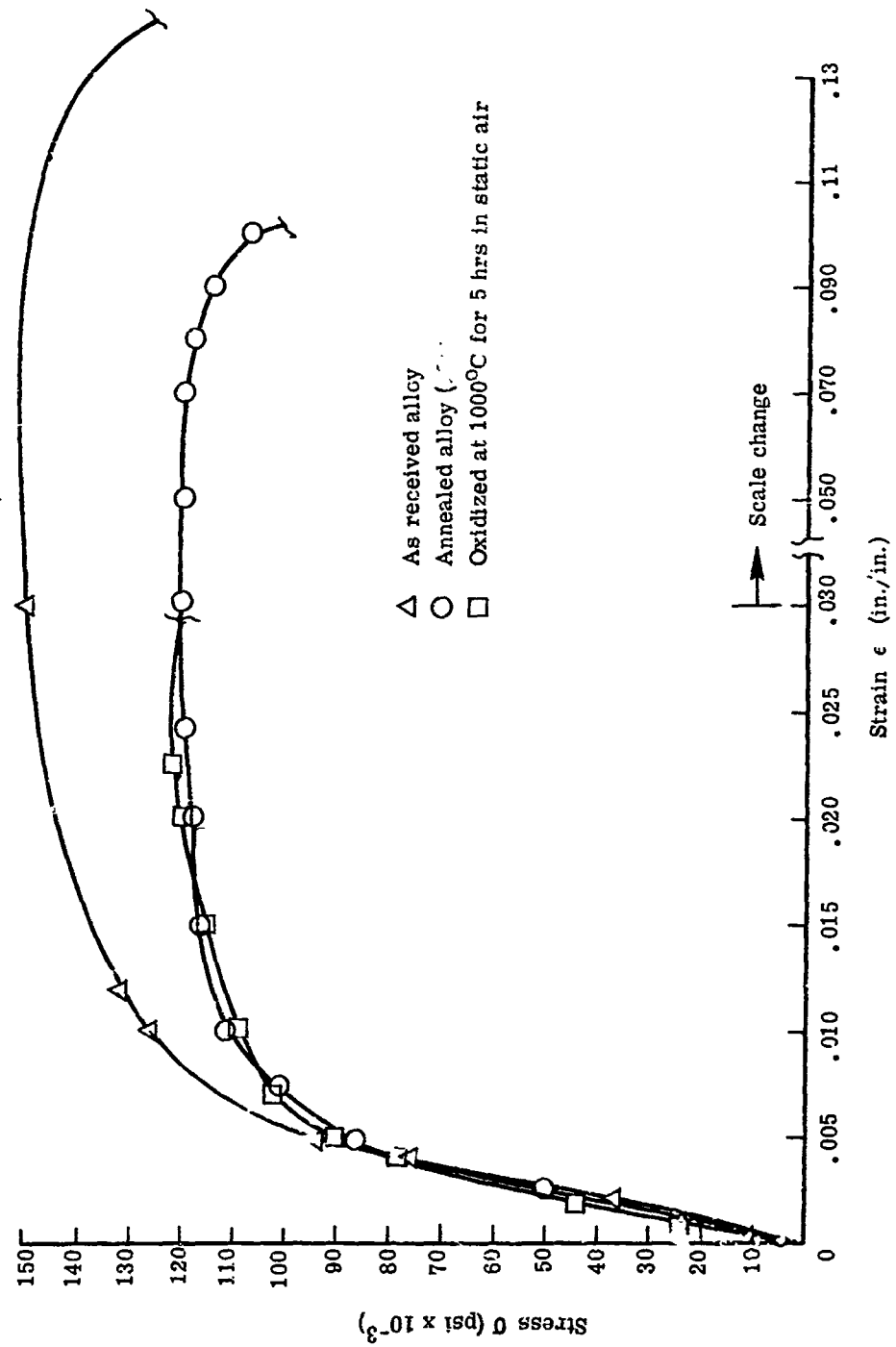
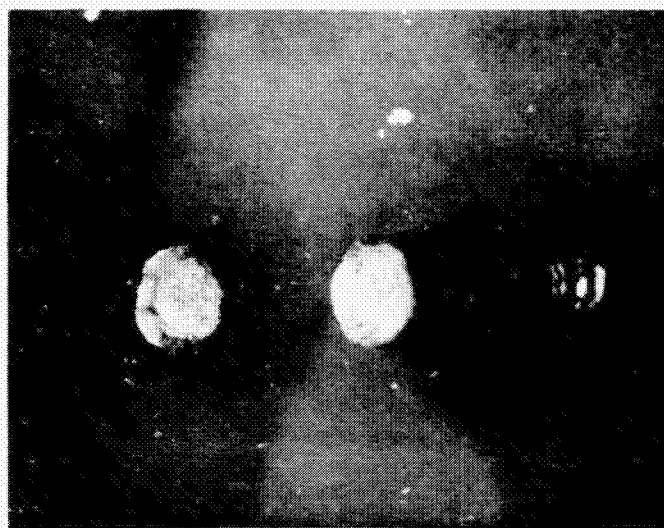
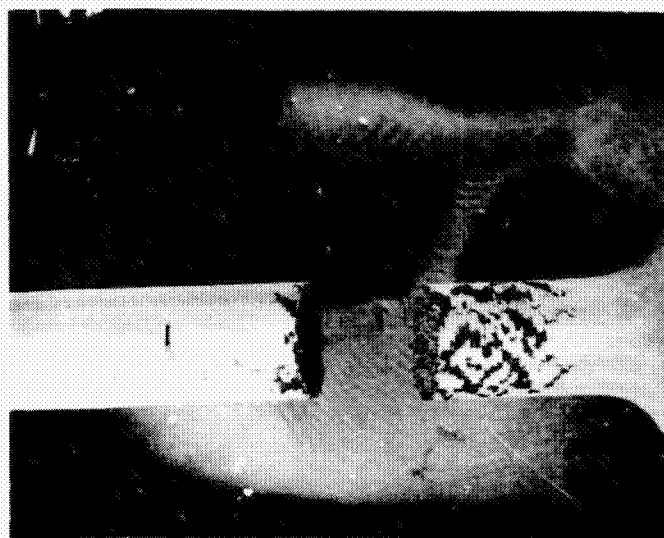


Figure 27. Hafnium-20% tantalum stress-strain diagram



AS RECEIVED



OXIDIZED

Figure 28. Typical ductile and brittle fractures for as-received and oxidized hafnium-20% tantalum alloy

this data one can see that by adding 20 percent tantalum to hafnium one can increase the ultimate strength of hafnium by 60 percent and the yield strength by a factor of 4.

Test results by Marnoch have shown the hafnium-27% tantalum sheet specimens in the annealed condition to have an ultimate strength of 156,000 psi with a corresponding yield strength of 147,100 psi at 0.2 percent offset which are higher than the hafnium-20% tantalum as would be expected from an increase in the tantalum content in the hafnium-27% tantalum.

Room Temperature Internal Friction

Using the room temperature damping setup previously described and shown in Figures 17 and 18, the room temperature damping characteristics of the annealed hafnium-20% tantalum alloy were studied in detail. With the sample suspended at the nodal points, inside the bell jar at 1-atmosphere pressure, excitation of the sample vibration was induced by the solenoid actuated steel rod striking the center of the bar. A typical free decay envelope of the sample vibration is shown in Figure 29. Knowing the oscilloscope sweep rate and by taking physical measurements and counting the number of full cycles of vibration from the polaroid picture, the frequency of vibration is computed from the equation

$$\text{Frequency} = \frac{\text{No. of cycles}}{(\text{Distance between 2 points})(\text{Sweep rate})} \quad (38)$$

Results indicated a resonant frequency of transverse vibration of 1831 cycles/sec for the annealed rectangular bar specimen. The

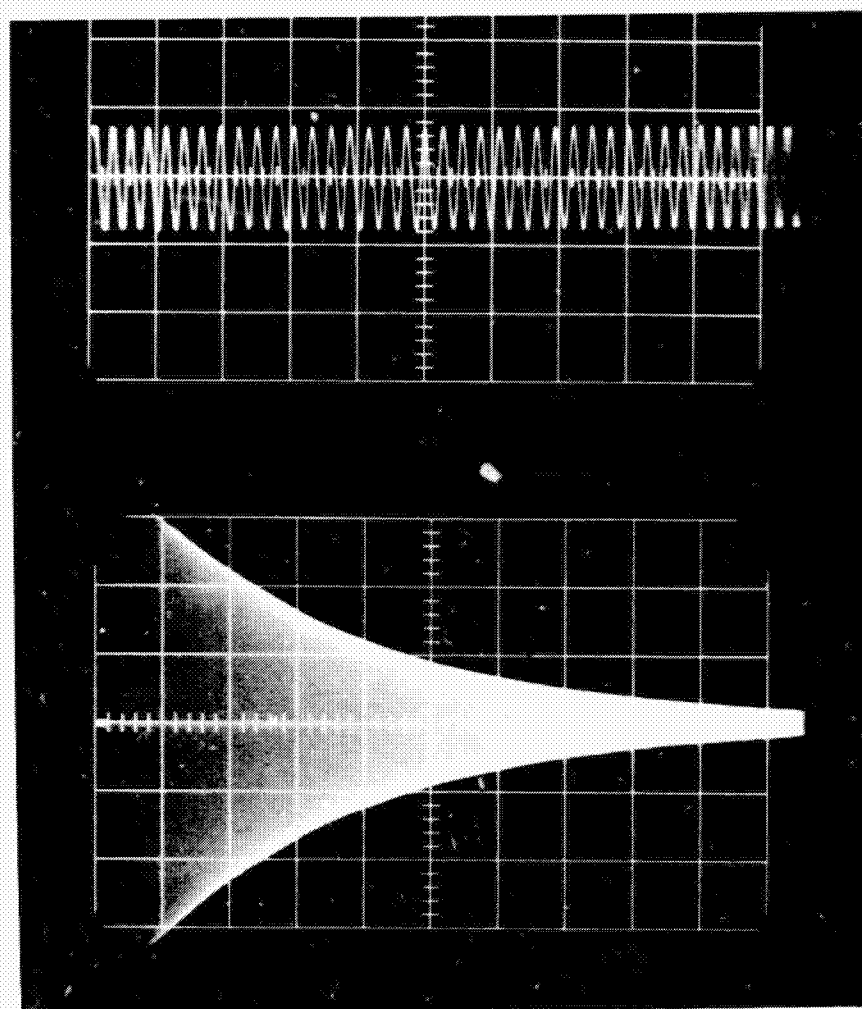


Figure 29. Typical room temperature damping curve for the hafnium-20% tantalum alloy

amplitude of vibration at two different times was measured directly from the photograph of the decay of the specimen vibration. The internal friction was then calculated from

$$Q^{-1} = \frac{\ln \frac{A_0}{A_t}}{\pi f t} \quad (39)$$

as previously described. Force of the solenoid actuated steel rod striking the sample was varied by increasing the power to the solenoid. Three different power levels were utilized to see if there was any amplitude dependency of the internal friction. The average value of the room temperature internal friction, Q^{-1} , was found to be 1.74×10^{-4} . Results were consistent on all measurements and the internal friction was not found to be amplitude dependent for forces involved in these measurements.

In order to study the effect of the suspension system on the damping of the alloy, another series of measurements were made with the sample suspended 0.125 inch inside its nodal points, and also with the suspension system located 0.125 inch outside the nodal points.

As predicted by Wachtman and Tefft (1958), the apparent internal friction was found to vary with the position of the support fibers. The amplitude of vibration of a bar vibrating in a free-free mode of transverse vibration can be predicted from the equation of motion describing this vibration. Rayleigh (1877) has solved this equation to yield the amplitude at any point on the bar. Using this information with the theory developed by Wachtman and Tefft, an actual value of

internal friction was calculated which accounts for energy losses in the specimen. These calculations were made by solving two simultaneous equations of the form

$$Q_m^{-1} = Q_s^{-1} + S (y/y_0)^2 \quad (40)$$

where Q_s^{-1} = actual internal friction

Q_m^{-1} = measure internal friction

S = constant for a given specimen and suspension system

which accounts for energy losses

y/y_0 = ratio of $\frac{\text{amplitude at a given } X/L \text{ location on bar}}{\text{amplitude of end of bar}}$

The measured internal friction at a suspension location of 0.125 inch inside the nodal points ($X/L = 0.2552$) yielded a value of $Q^{-1} = 1.046 \times 10^{-4}$. For a suspension location of 0.125 inch outside the nodal points ($X/L = 0.1928$), $Q^{-1} = 1.023 \times 10^{-4}$. Using these two measured values of internal friction and the respective y/y_0 data obtained from Rayleigh's solution of the equation of motion for a vibrating bar, equation (40) was solved to yield a corrected value of the internal friction at room temperature of $Q^{-1} = 9.104 \times 10^{-5}$. Thus it can be seen that energy losses in this system are significant, but are much less than the order of magnitude differences which have been reported by Wachtman and Tefft for other suspension systems.

Typical values of internal friction of other metals and alloys are reported by Smithells (1962) to be of the order of 10^{-5} . For example, sintered molybdenum has a value of $Q^{-1} = 16 \times 10^{-5}$.

Room temperature damping measurements were also made using the Elastomat system. Typical values of $Q^{-1} = 1.04 \times 10^{-4}$ were obtained;

however, because of the particular driving and receiving wire setup used, these damping data were very inconsistent and non-repeatable from specimen to specimen, and, therefore, could not be used for absolute values of Q^{-1} . A change in the compression loading of the coupling wires would change the damping appreciably. Damping data obtained through this method were used only in showing the temperature dependence of the internal friction on a relative basis.

Table 6 represents a summary of the room temperature damping data obtained on the annealed hafnium-20% tantalum alloy.

Elevated Temperature Dynamic Elasticity and Internal Friction

The elastic and shear moduli were measured as a function of temperature as have been described using both the Elastomat in an oxidizing atmosphere and the high temperature vacuum elasticity setup. The transverse and torsional resonance frequencies at some temperature ΔT above room temperature were converted to elastic and shear moduli using the relationship

$$M_T = M_0 \left(\frac{f_T^2}{f_0^2} \right) \left(\frac{1}{1 + \alpha \Delta T} \right) \quad (41)$$

where M_T = elevated temperature modulus

M_0 = room temperature modulus

f_T = elevated temperature resonant frequency

f_0 = room temperature resonant frequency

α = linear coefficient of thermal expansion of specimen

Table 6. Summary of room temperature measured internal friction data for a hafnium-20% tantalum alloy

Measurement No.	Suspension location (X/L)	Frequency, (cycles/sec)	Variac power setting	Q^{-1} measured ($\times 10^4$)
1	0.224 (nodal points)	1831	50	1.74
2		1831	50	1.74
3		1831	50	1.74
4		1825	60	1.74
5		1831	60	1.74
6		1821	60	1.75
7		1831	70	1.74
8		1831	70	1.45
9	0.2552 (1/8 in. inside nodes)	1831	50	1.02
10		1831	50	9.79×10^{-5}
14		1831	60	1.022
15		1831	60	1.028
16		1831	70	1.022
17	0.1928 (1/8 in. outside nodes)	1831	50	1.023
18		1831	50	9.9×10^{-5}
19		1831	60	1.087×10^{-4}
20		1831	60	1.038
21		1831	60	1.054
22		1831	60	1.054
23		1831	70	1.054
24		1831	70	1.054
25		1831	70	1.054

The thermal expansion data of Marnoch (1967) was reduced from a graphical representation by a least squares fit of his data to the equation

$$\frac{\Delta L}{L} = -1.03266 \times 10^{-4} + 3.2109 \times 10^{-6} T_c + 2.80584 \times 10^{-9} T_c^2 \quad (42)$$

where $\frac{\Delta L}{L} = \alpha \Delta T = \frac{\text{change in length of specimen}}{\text{original length}}$

T_c = temperature in degrees centigrade

This correction was less than 2 percent at 1000° C.

Calculations of the elevated temperature elastic and shear moduli of the hafnium-20% tantalum alloy in the as received and annealed condition and those properties for a pure hafnium rod are summarized in Tables 7-16. These tests were all conducted on the Elastomat in both air and attempted inert argon atmosphere. Tests on specimens 3 and 4 were conducted in what was thought to be an inert atmosphere after having purged the system for over 30 minutes under positive pressure of pure argon, however, specimen 3 oxidized the same as in air. After modifications to the furnace to allow argon to pass directly over the sample, limited oxidation occurred on specimen 4, however, a small amount of oxide scale did form. The Elastomat furnace had the capability to heat specimens to 1000° C, however, difficulty of test measurements increased exponentially at higher temperatures. At higher temperatures, due to the increase of internal friction of the specimen to be discussed later, the amplitude of vibration had to be increased greatly. In several instances the coupling wires became unbonded from

Table 7. Elevated temperature elastic and shear moduli of hafnium-20% tantalum alloy

SPECIMEN 1 - As received condition, L = 4.00 in., Dia = 0.445 in.
TEST CONDITIONS: Oxidizing atmosphere

Temperature (°C)	Transverse resonant frequency (cycles/sec)	Elastic modulus E(10 ⁶ psi)	Torsional resonant frequency (cycles/sec)	Shear modulus G(10 ⁶ psi)
25	2780	16.94	9225	6.87
70	2760	16.70		
76			9152	6.76
82	2755	16.64		
132	2740	16.46		
207	2715	16.16		
218			8968	6.49
229	2701	15.99		
290	2676	15.70		
299			8843	6.31
368	2634	15.21		
420	2615	14.99	8641	6.03
478	2588	14.68	8559	5.91
530	2565	14.42	8479	5.80
571	2549	14.24	8413	5.71
623	2530	14.03		
629			8341	5.61
655	2521	13.93	8311	5.56
710	2510	13.81		
766			8165	5.38
982	2469	13.36	7988	5.15
Cooling			Lost torsional signal	
963	2538	14.12		
893	2583	14.62		
760	2649	15.38		
648	2703	16.08		
575	2748	16.55		
443	2828	17.53		
288	2982	19.49		
25	3000	19.72		

Table 8. Elevated temperature elastic and shear moduli of hafnium-20% tantalum alloy

SPECIMEN 8 - Vacuum annealed for 4 hr at 1200° C, L = 4.000 in.
Dia = 0.4415 in.

TEST CONDITIONS: Oxidizing atmosphere

Temperature (°C)	Transverse resonant frequency (cycles/sec)	Elastic modulus E (10 ⁶ psi)	Torsional resonant frequency (cycles/sec)	Shear modulus G (10 ⁶ psi)
24	2888	18.45	9489	7.27
50	2871	18.23		
80	2860	18.09	9401	7.13
124	2846	17.91		
135			8324	7.018
208	2805	17.4	9196	6.83
256	2780	17.09	9110	6.7
290	2762	16.88	9033	6.59
348	2751	16.57	8945	6.46
375	2726	16.43	8921	6.42
443	2693	16.04	8783	6.23
511	2660	15.65	8670	6.07
561	2637	15.38	8595	5.95
621	2605	15.01	8498	5.83
673	2578	14.70		
701	2569	14.60	8371	5.66
754	2548	14.36		
813	2545	14.32		
860	2534	14.2	8164	5.38
882	2544	14.3		
912	2514	13.98		
949	2587	14.8		
1010	2603	14.99		

Table 9. Elevated temperature elastic and shear moduli of hafnium-20% tantalum alloy

SPECIMEN 3 - As received condition, L = 3.991 in., Dia = 0.441 in.
TEST CONDITIONS: Argon atmosphere

Temperature (°C)	Transverse resonant frequency (cycles/sec)	Elastic modulus E(10 ⁶ psi)	Torsional resonant frequency (cycles/sec)	Shear modulus G(10 ⁶ psi)
26	2788	17.15	9208	6.81
135	2750	16.68	9069	6.61
227	2704	16.13	8921	6.40
321	2661	15.55	8710	6.10
382	2639	15.36		
399	2623	15.18		
407			8552	5.88
449	2606	14.98		
460			8481	5.781
477	2599	14.90		5.78
521	2581	14.77	8412	5.69
579	2555	14.47	8333	5.50
615	2551	14.36		
621	2546	14.30		
649	2539	14.22	8237	5.46
695	2522	14.03		
26	2866	18.12	9487	7.23

Table 10. Elevated temperature elastic and shear moduli
of hafnium-20% tantalum alloy

SPECIMEN 4 - As received condition, L = 4.956 in., Dia = 0.445 in.
TEST CONDITIONS: Argon atmosphere

Temperature (°C)	Transverse resonant frequency (cycles/sec)	Elastic modulus E(10 ⁶ psi)	Torsional resonant frequency (cycles/sec)	Shear modulus G(10 ⁶ psi)
27	1826	16.88	7488	6.95
82	1810	16.58		
129	1797	16.35	7366	6.73
190	1780	16.07	7297	
254	1765	15.77	7222	6.47
321	1746	15.43	7160	6.35
385	1722	15.01	7063	6.18
440	1708	14.77	7014	6.10
485	1695	14.54	6977	6.03
516	1687	14.41	6876	5.86
580	16.73	14.17	6813	5.75
627	1663	14.00	6764	5.67

Table 11. Elevated temperature elastic and shear moduli of pure hafnium metal

SPECIMEN 9 - Annealed, L = 4.016 in., Dia = 0.486 in.
TEST CONDITIONS: Oxidizing atmosphere

Temperature (°C)	Transverse resonant frequency (cycles/sec)	Elastic modulus E(10 ⁶ psi)	Torsional resonant frequency (cycles/sec)	Shear modulus G(10 ⁶ psi)
26	3364	20.52	10119	8.023
63	3346	20.30		
96	3337	20.19		
127			9915	7.703
196	3267	19.36		
232	3238	19.01	9714	7.39
304	3179	18.33		
323	3156	18.06	9461	7.01
371	3127	17.73		
376			9354	6.86
421	3097	17.39	9280	6.75
449	3087	17.28		
482			9105	6.50
560	2994	16.26	8913	6.22
588	2988	16.17	8862	6.15
649	2927	15.54	8735	5.98
682			8653	5.86
743	2869	14.93	8535	5.71
777			8460	5.61
843	2801	14.23		
882	2762	13.83		
916	2728	13.50		
960	2724	13.46		
26	3377	20.68	10141	8.06

Table 12. Elevated temperature elastic and shear moduli
of hafnium-20% tantalum alloy

SPECIMEN 6 - Vacuum annealed for 4 hr at 1200° C, L = 3.656 in.,
Dia = 0.257 in.
TEST CONDITIONS: 1×10^{-5} torr

Temperature (°C)	Transverse resonant frequency (cycles/sec)	Elastic modulus E(10^6 psi)	Torsional resonant frequency (cycles/sec)	Shear modulus G(10^6 psi)
29	2051	18.59	10444	7.36
187	1956	16.89	9888	6.59
231	1939	16.60	9824	6.50
273	1925	16.37	9740	6.39
333	1908	16.06	9661	6.29
434	1882	15.62	9510	6.09
481	1870	15.42	9448	6.01
526	1855	15.17	9366	5.90
586	1839	14.90	9280	5.79
640	1824	14.65		
705	1809	14.40		
732	1798	14.23	9063	5.52
838	1769	13.76		
886	1756	13.56		
943	1738	13.27		
1012	1713	12.89	8609	4.37
1068	1693	12.58	8502	4.84
1101	1648	11.92	8441	4.77
1212	1444	9.14		
1255	1403	8.62	Lost signal	
1335	1278	7.15		
1397	1244	6.77		

Table 13. Elevated temperature elastic and shear moduli of hafnium-20% tantalum alloy

SPECIMEN 6 - Vacuum annealed for 4 hr at 1200° C and heated to 1450° C for an additional 4 hr. Grains large and visible to the eye, L = 3.656 in., Dia = 0.257 in.
TEST CONDITIONS: 1×10^{-5} torr

Temperature (°C)	Transverse resonant frequency (cycles/sec)	Elastic modulus E(10^6 psi)	Torsional resonant frequency (cycles/sec)	Shear modulus G(10^6 psi)
25	2012	17.90	10325	7.19
88	1962	17.00	10071	6.84
157	1925	16.36		
203	1905	16.03	9772	6.44
271	1886	15.71		
319	1872	15.46		
438	1845	15.01		
616	1799	14.26	9229	5.73
711	1777	13.90	9112	5.58
814	1753	13.52	9025	5.47
908	1738	13.28	8900	5.33
961	1723	13.04	8852	5.25
1015	1709	12.82	8756	5.14
1067	1695	12.61		
1074	1675	12.31		
1099			8614	4.97
1105	1613	11.42		
1159	1509	9.99	7813	4.09
1211	1423	8.88	7404	3.67
1307	1283	7.21	6719	3.02

Table 14. Elevated temperature elastic modulus of
hafnium-20% tantalum alloy

SPECIMEN 5 - As received condition, L = 3.55 in., Dia = 0.2447 in.
TEST CONDITIONS: 1×10^{-5} torr

Temperature (°C)	Transverse resonant frequency (cycles/sec)	Elastic modulus E(10^6 psi)
32	1973	16.95
530	1799	14.05
1112	1612	11.23
1144	1595	10.99
1168	1559	10.49
1182	1538	10.22
1194	1520	9.98
1205	1509	9.83
1217	1443	9.62
1242	1466	9.28
1261	1442	8.97
1302	1391	8.35
1348	1321	7.52
1391	1235	6.57
1456	1142	5.62
1469	1114	5.34
1552	1052	4.76
1613	1016	4.44
1660	1006	4.35
1711	1000	4.29
1745	997	4.27
1979	905	3.50
31	2040	18.11

Table 15. Elevated temperature elastic and shear moduli of hafnium-20% tantalum alloy

SPECIMEN 5 - Vacuum annealed for 3 hr at 1112° C and 2 hr up to 2000° C, L = 3.55 in., Dia = 0.2447 in.

TEST CONDITIONS: 1×10^{-5} torr

Temperature (°C)	Transverse resonant frequency (cycles/sec)	Elastic modulus E(10^6 psi)	Torsional resonant frequency (cycles/sec)	Shear modulus G(10^6 psi)
31	2040	18.11	10482	6.99
128	1975	16.97	10129	6.52
360	1896	15.62	9749	6.03
418	1881	15.37	9682	5.95
507	1860	15.02		
573	1844	14.76		
638	1826	14.47		
713	1809	14.19		
790	1793	13.93		
930	1766	13.50		
972	1758	13.37	9232	5.34
1013	1745	13.17	9160	5.30
1052	1732	12.98	9094	5.23
1144	1609	11.19	8360	4.41
1208	1482	9.48	7695	3.74
1238	1443	8.99	7449	3.50
1303	1356	7.93		
1405	1232	6.54	6548	2.70
1473	1153	5.72		
1564	1075	4.97		
263	1923	16.08		
24.5	2050	18.31		

Table 16. Elevated temperature dependency ratio of the elastic and shear moduli ratio of a preoxidized hafnium-20% tantalum alloy

SPECIMEN 9 - Oxidized for 2 hr at 1200° C,
 L = 4.001 in., Dia = 0.139 in. (before oxidation)
 L = 4.044 in., Dia = 0.144 in. (after oxidation)
 Weight gain from oxidation = 1.2%
 TEST CONDITIONS: 1×10^{-5} torr

Temperature (°C)	Transverse resonant frequency (cycles/sec)	Elastic modulus ratio (E_T/E_0)	Torsional resonant frequency (cycles/sec)	Shear modulus ratio (G_T/G_0)
35	919	1.0	9614	1.0
165	885	.927	9326	.941
225	880	.916	9273	.93
338	871	.897	9168	.908
416	866	.886		
575	857	.867	8941	.863
714	847	.845		
906	845	.84	8684	.811
963	843	.838	8600	.795
1025	840	.83		
1067	837	.824	8524	.781
1117	834	.817		
1162	822	.794	8418	.761
1221	805	.761		
1321	787	.726	8010	.688
1404	762	.681	7776	.648
1740	685	.548	6325	.427

the specimen before the run could be completed. When this happened, the test had to be terminated.

Figures 30 and 31 provide a graphical representation of the temperature dependency of the elastic and shear moduli of the as received and vacuum annealed hafnium-20% tantalum alloy. The plot is based on average values at each temperature increment of all the specimens tested up to 1000° C using the Elastomat. As can be seen, the general curves for elastic and shear moduli of the annealed pure hafnium and the annealed hafnium-tantalum show a relatively linear decrease in values over the temperature range. In the neighborhood of 675° C, the slope of the moduli curve for the annealed Hf-Ta decreased indicating a smaller decrease of modulus per degree temperature change. It is felt that annealing effects were beginning to become prominent and even though this sample had been annealed previously for 2 hours, it did not have complete random orientation of the crystal structure. It was in this temperature range that oxidation of the specimen began increasing rapidly causing interstitial contamination of the specimen. Further evidence of the annealing process becoming a dominant factor in affecting the temperature dependency of the moduli can be seen from the curve representing the as received material. The slope of the average values of the specimens which had no previous heat treatment and exhibited the most preferred orientation decreased faster in the elevated temperature region than the material which had previous annealing treatment. The moduli of the pure hafnium material were both higher initially than the hafnium-20% tantalum, however, they decreased at a faster rate until

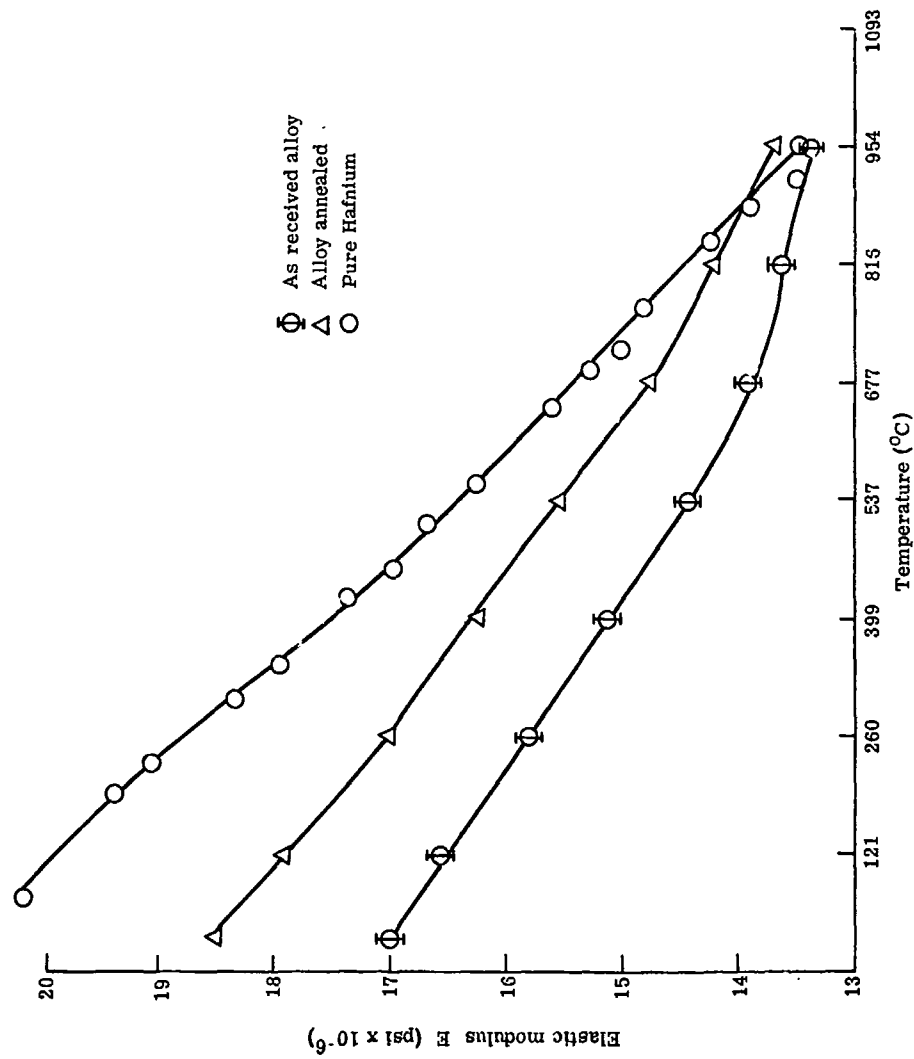


Figure 30. Temperature dependency of the elastic modulus of hafnium-20% tantalum up to 1000° C in air

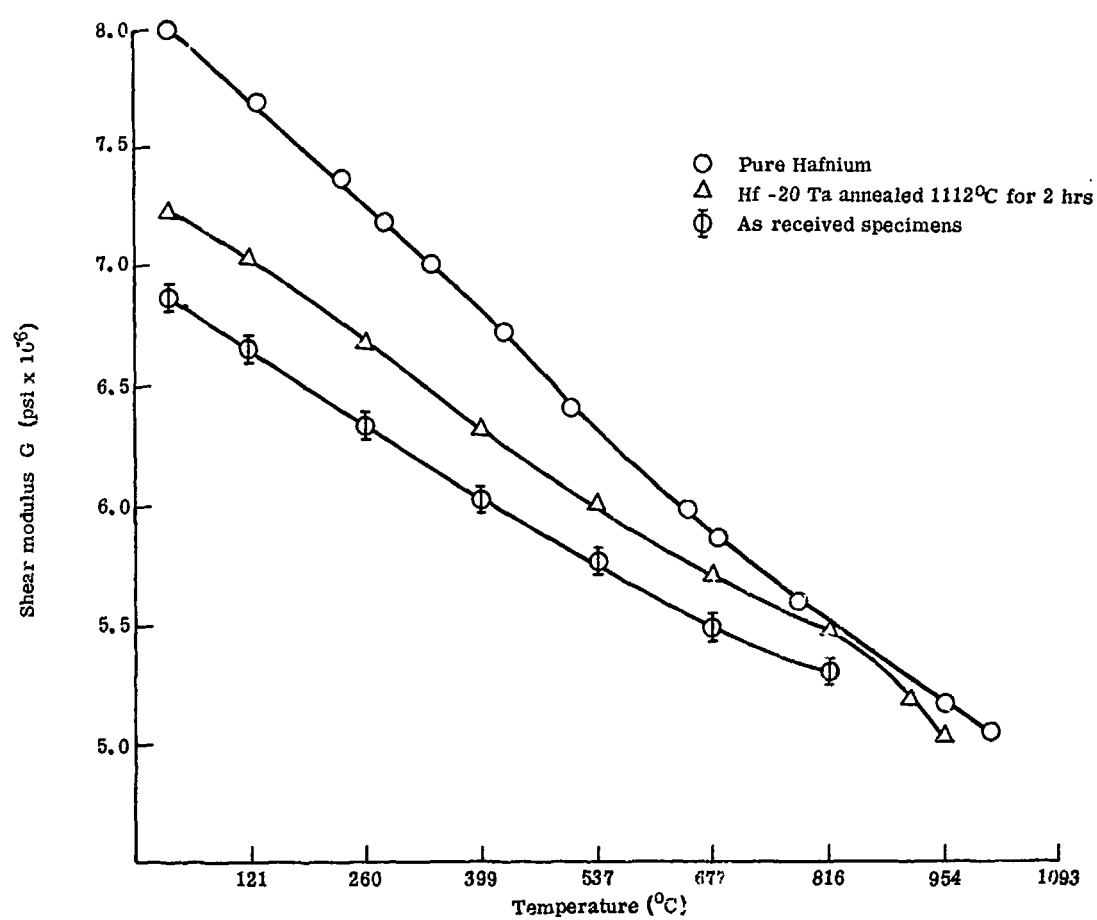


Figure 31. Temperature dependency of the shear modulus of hafnium-20% tantalum up to 1000°C in air

about 875° C at which time the hafnium moduli dropped below those of the hafnium-20% tantalum alloy.

Oxidation of the sample became a problem in all cases at elevated temperatures. As can be seen from Figure 32, the HfO₂ coating formed on the specimen very rapidly at elevated temperatures, causing the sample to become out of round and distorting the signal. On cooling slowly, an outer scale of unprotective oxide in all cases could be scraped off readily or simply fell off. In contrast, the pure hafnium rod oxidized very little on the surface after one run as shown by Figure 33. Even after four runs to 1000° C and holding at this temperature for a total of 12 hours with cooling to room temperature in between, the oxide coating did not spall on cooling. Calculations for Poisson's ratio given by the relation

$$\mu = \frac{E}{2G} - 1 \quad (6)$$

are only valid for an isotropic, homogeneous material. These calculations were made for the as received material, however, this material was highly anisotropic due to the preferred orientation of the extruded rod. Figure 34 shows the average values of these calculations for all the samples tested at elevated temperatures in air. Poisson's ratio calculations for the vacuum annealed specimen 8 are more valid, as the specimen had a more random distribution of the polycrystals. This specimen showed an increase of Poisson's ratio from 0.27 to 0.32 from room temperature to 860° C. Having conducted the series of tests up to 1000° in air, it was obvious that oxidation effects were causing a problem in obtaining true properties. In addition, the

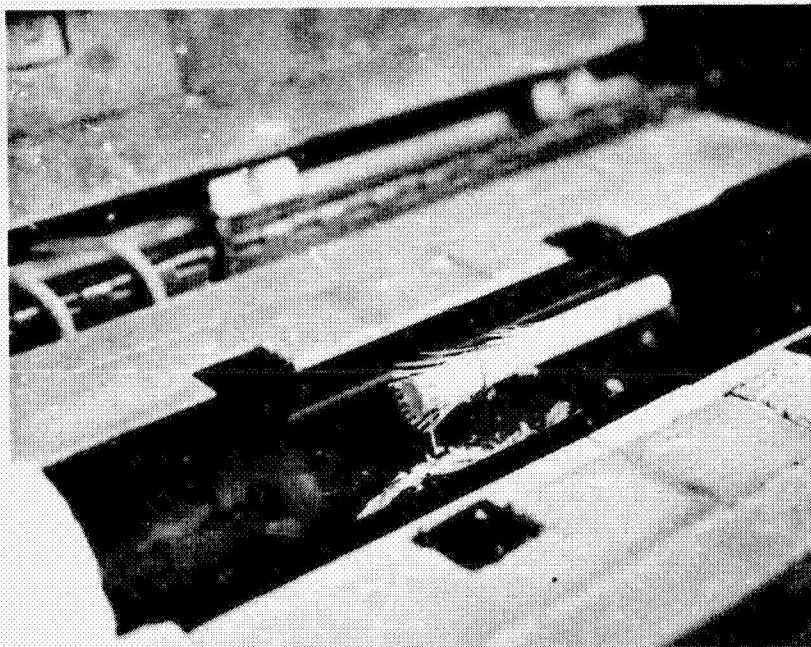
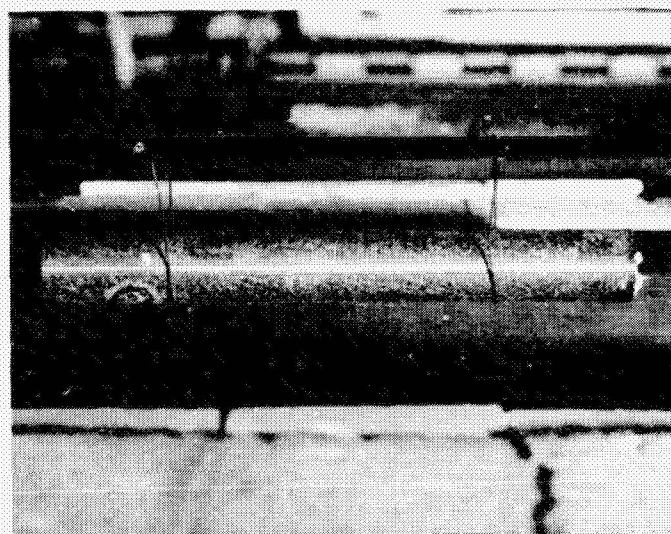
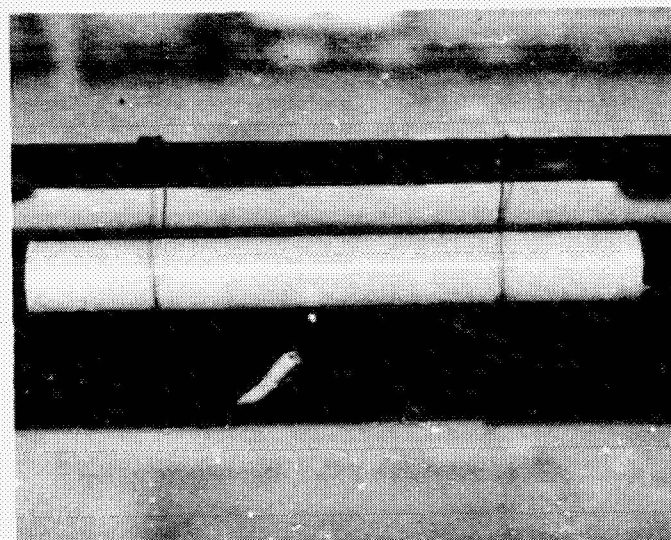


Figure 32. Oxidized hafnium-20% tantalum dynamic elasticity test specimen after cooling from 1000°C



1 CYCLE



4 CYCLES

Figure 33. Oxidized pure hafnium dynamic elasticity test specimen after cooling for one and four cycles from 1000°C

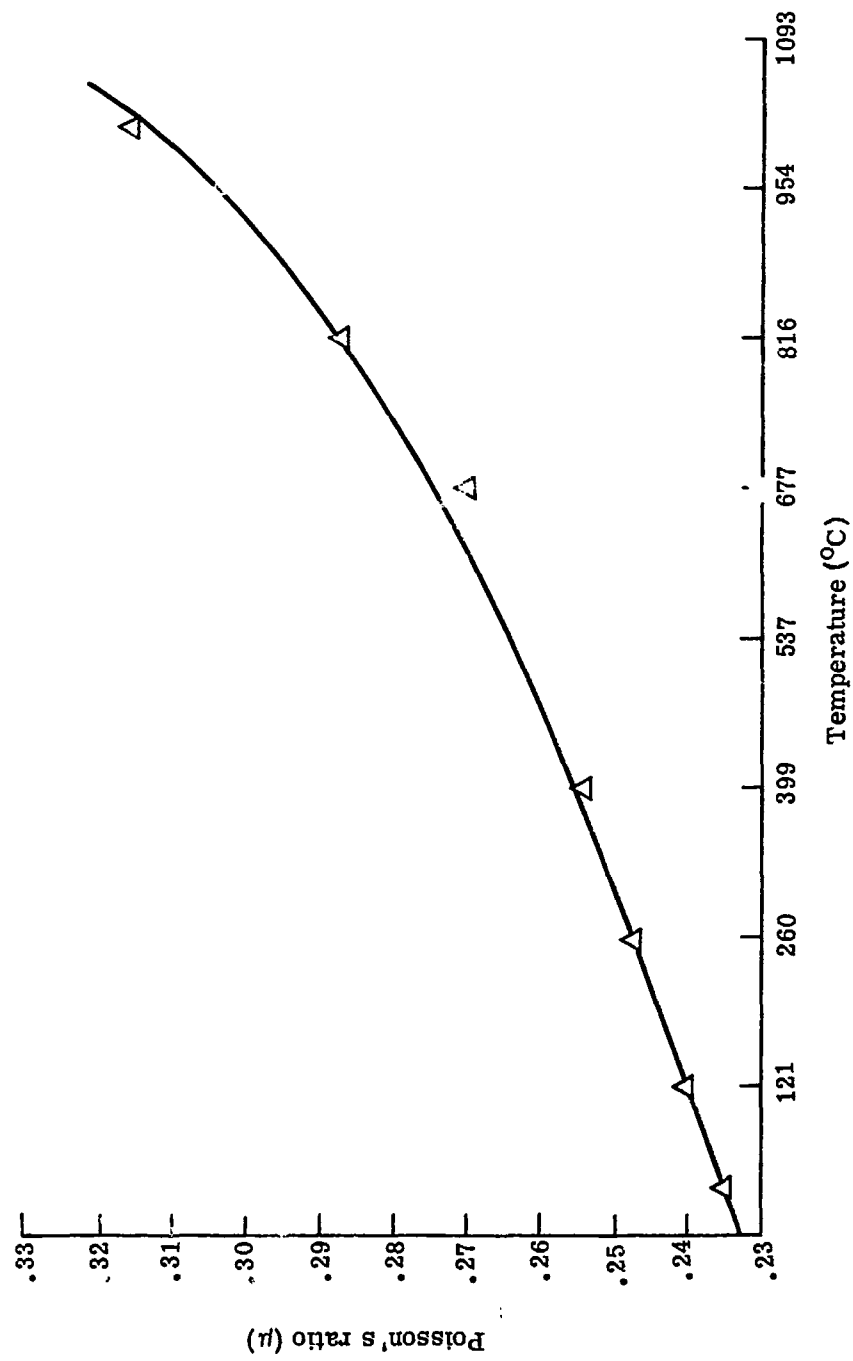


Figure 34. Average values of Poisson's ratio versus temperature up to 1000° C in air for hafnium-20% tantalum alloy

Elastomat did not have the temperature capability to allow for characterization in the temperature region where it demonstrated its greatest potential. It was therefore necessary to make use of the equipment shown by Figure 13. This equipment was made available by the General Electric Company's Vallecitos Nuclear Center. Under the guidance of Dr. M. O. Marlowe, a noted authority in the area of dynamic elasticity measurements, this writer completed the vacuum high temperature elasticity and internal friction measurements in the California laboratory.

Results of the series of vacuum high temperature tests are shown in Tables 12-16. A graphical representation of the temperature dependency of the elastic and shear moduli of the hafnium-20% tantalum alloy is given by Figures 35 and 36. This represents shear moduli data from Table 13 and elastic moduli data from Table 15. All specimens behaved similarly with temperature, these plots being typically representative of a fully annealed alloy. The elastic and shear moduli each show a relatively linear decrease with temperature up to about 1020° C at which time there was a sharp deviation in the slope of the moduli curves.

One of the major interests of this study was to determine if this test could detect structural phase changes such as occurs slightly over 1000° C. This temperature range covers the $\alpha + \beta$ Ta transformation temperature as shown by the phase diagram. The specimens were cycled through this temperature range several times and in each case the sharp transition was noted and could be followed. This indicates the potential of studying elevated temperature phase transformation not readily available by other methods. The elastic modulus dropped

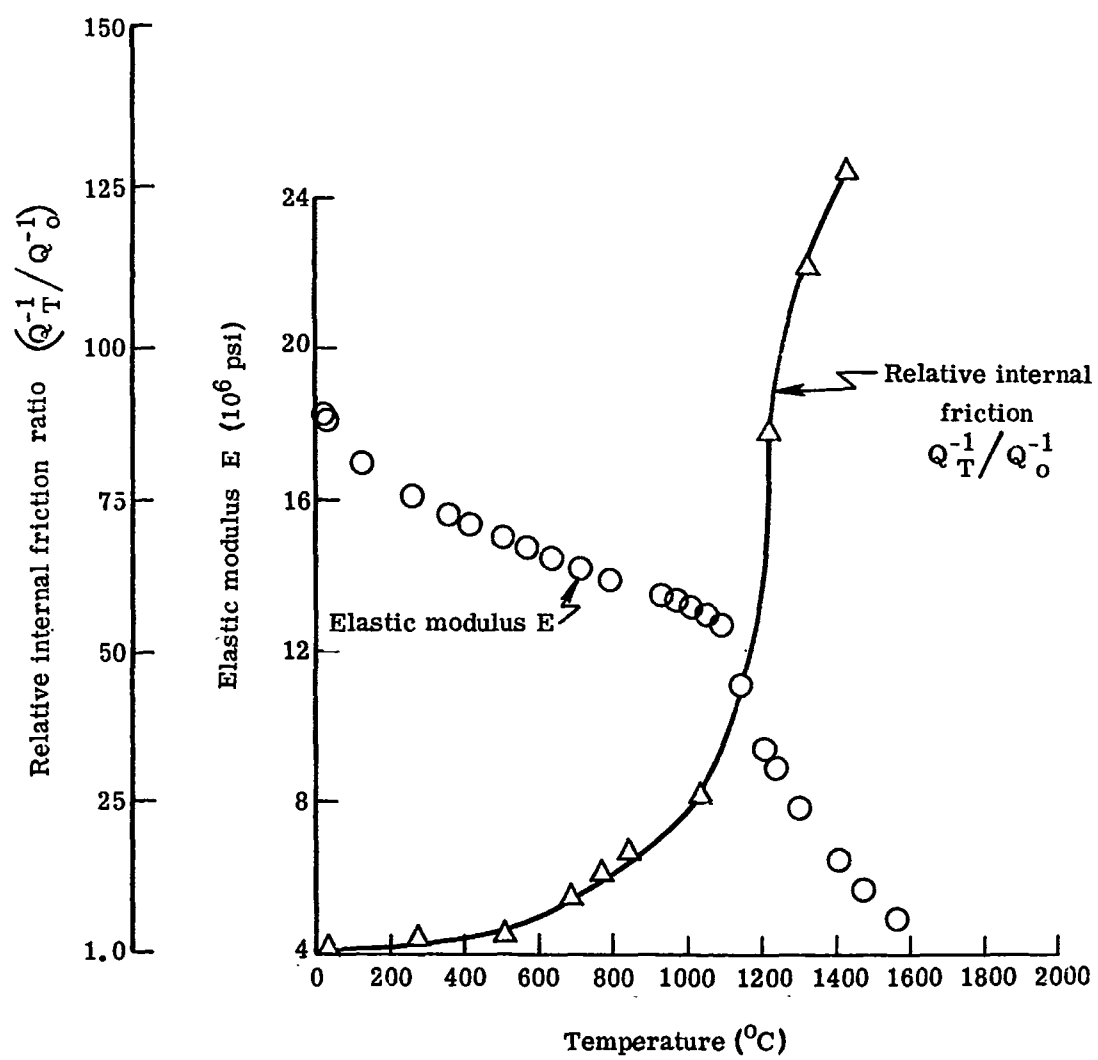


Figure 35. Elevated temperature elastic modulus and internal friction ratio of an annealed hafnium-20% tantalum alloy

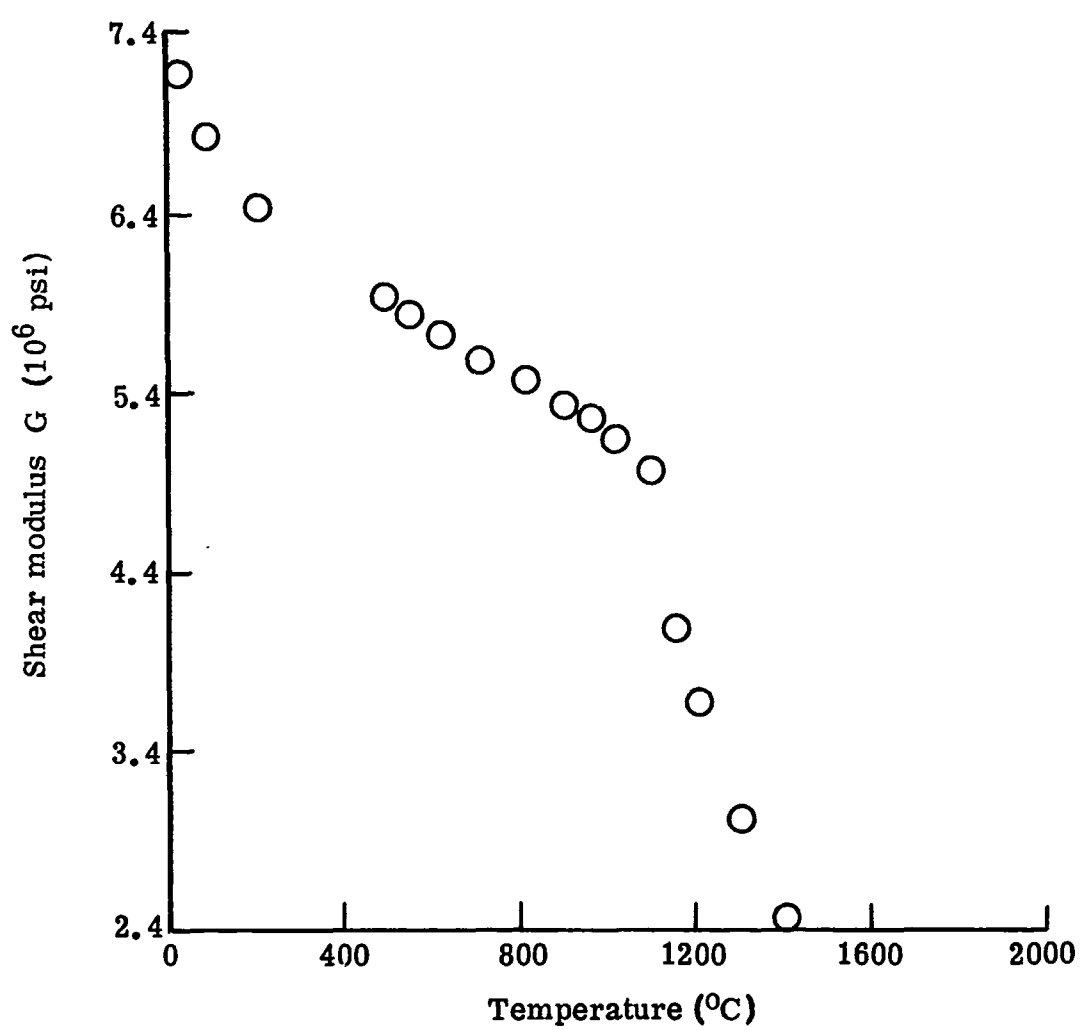


Figure 36. Elevated temperature shear modulus of an annealed hafnium-20% tantalum alloy

rapidly down to about 4.5×10^6 psi at 1600° C, however, results of Table 14 indicated a slower decrease in modulus beyond this point down to 3.5×10^6 psi at close to 2000° C. The torsional signal always became extremely weak at elevated temperatures and was lost completely at times, however, the shear modulus was found to decrease to about 2.5×10^6 psi at 1400° C. Data beyond that point is sketchy.

The relative change of the elastic and shear moduli ratio with temperature for the preoxidized specimen is shown compared to the annealed hafnium-20% tantalum alloy in Figures 37 and 38. It can be seen that the moduli do not decrease as fast throughout the temperature range, nor is their change of slope as sharp at the 1020° C range. This could be the result of some stabilization of the α Hf phase due to oxygen contamination which also contributed to lower internal friction at elevated temperatures to be discussed later.

The elevated temperature internal friction was determined in vacuum using the forced resonance technique on the transverse resonant frequency as previously described. The sample support system could not be changed during the temperature measurement, therefore, a relative internal friction parameter (Q_T^{-1}/Q_0^{-1}) , the ratio of elevated internal friction to room temperature internal friction, was plotted to show its temperature dependency. This result is tabulated in Table 17 and is shown superimposed on the elastic modulus curve of Figure 35. At the lower temperatures the internal friction remained relatively constant increasing slightly up to around 800° C at which time it began a rise upward. At around 1050° C a very rapid increase was noted. At 1400° C the ratio of elevated temperature internal friction to room temperature

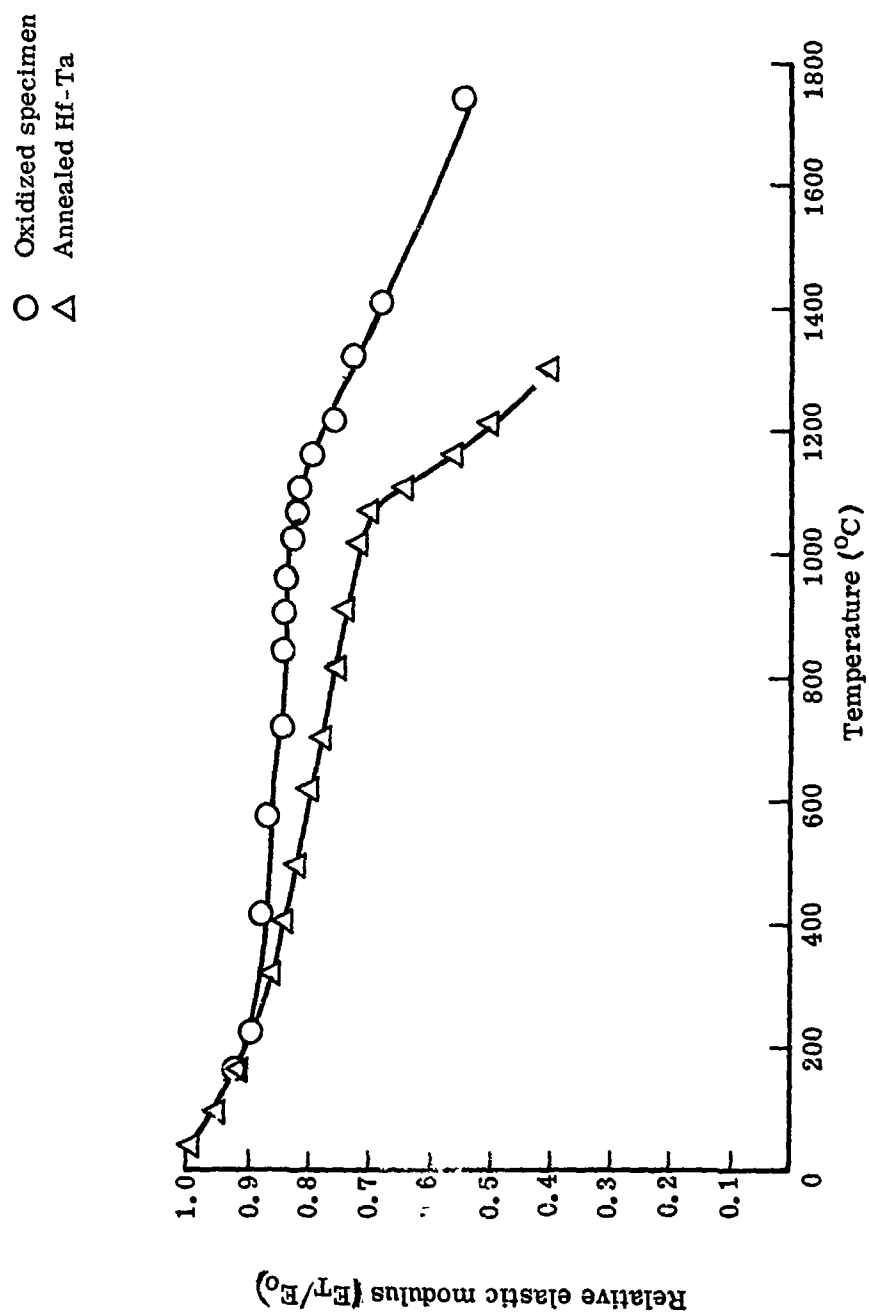


Figure 37. Elevated temperature elastic modulus ratio for an oxidized and annealed hafnium-20% tantalum alloy

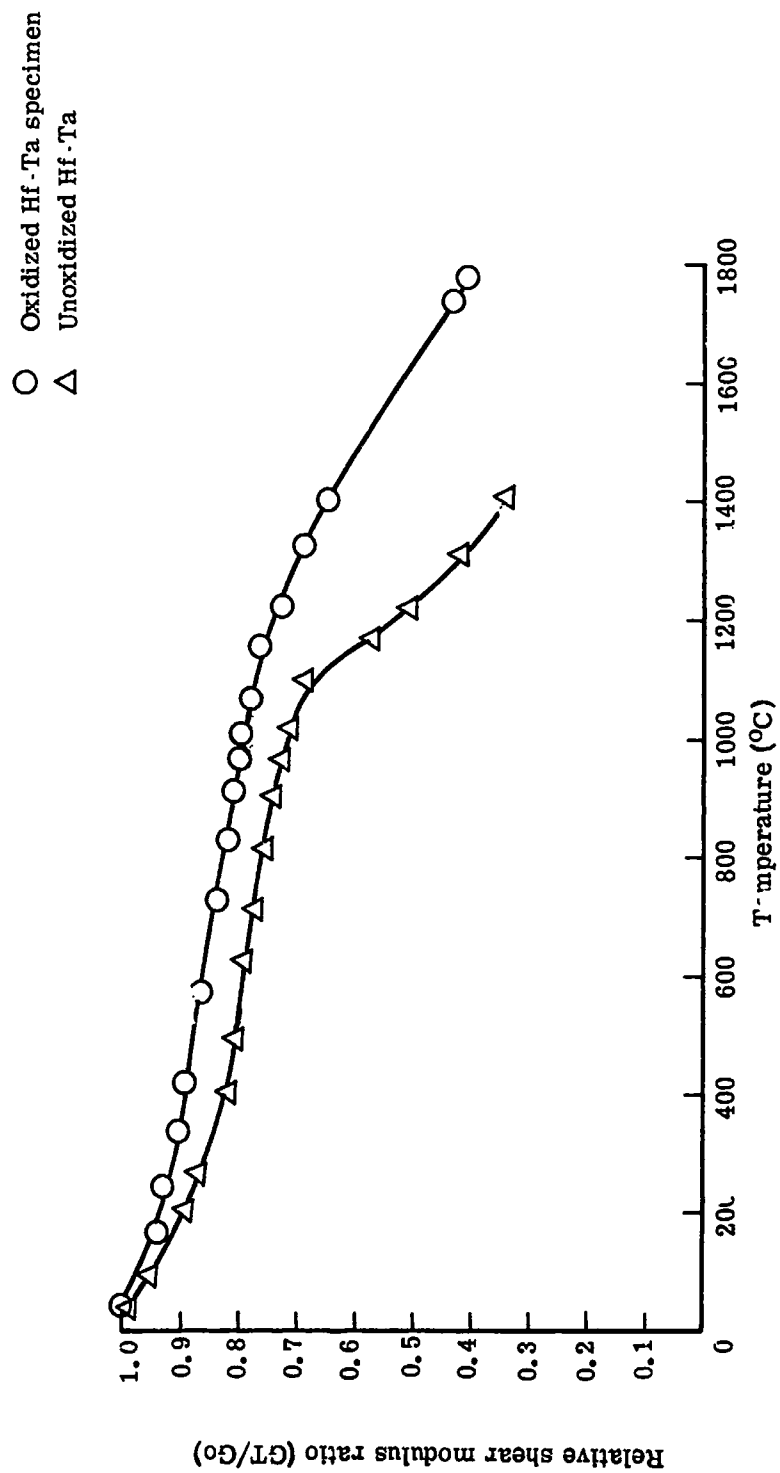


Figure 38. Elevated temperature shear modulus ratio for an oxidized and annealed hafnium-20% tantalum alloy

Table 17. Elevated temperature internal friction ratio
for hafnium-20% tantalum alloy

SPECIMEN 5 - Vacuum annealed for 3 hr at 1112° C and 2 hr up
to 2000° C

TEST CONDITIONS: 1×10^{-5} torr

Temperature (°C)	Transverse resonant frequency (cycles/sec)	Frequency at 1/2 amplitude below	Frequency at 1/2 amplitude above	Q_T^{-1}/Q_O^{-1}
31	2039.8	2039.5	2040.1	1
715				
793	1809	1808.2	1813.7	10.33
793	1794	1792	1799	13.26
859	1784	1781.8	1789.6	14.86
930	1767.1	1764.1	1772.9	16.93
980	1758.3	1752.8	1762.8	19.34
1013	1745	1740.5	1750.7	19.87
1052	1732.8	1726.9	1738.7	23.15
1091	1715.6	1710.7	1721.0	20.10
1144	1609	1597	1624	57.05
1237	1442	1425	1461	84.87
1304	1356	1333	1379	115.18
1403	1232	1211	1256	133.37

was 133 to 1. In all cases the noise level coupled with the high internal friction distorted the signal and made absolute measurements impossible. Up to 1400°C , no peak was reached, however, on monitoring the pickup voltage output it was noted that around 1500°C - 1600°C , the output voltage began increasing slightly and in some cases the Lissajous figure became less distorted. This coupled with the smaller rate of change of elastic modulus above 1600°C could be an indication that the relaxation peak reaches a maximum in this temperature range.

The high internal friction noted in this temperature range is likely due to the grain boundaries behaving in a viscous manner with the viscous behavior causing a dissipation of mechanical energy. Some contribution at around 1050°C can be attributed to the phase transformation occurring in the alloy, however, the viscous behavior is probably the dominant factor in causing the sharp decrease in elastic and shear moduli which is similar to polycrystalline aluminum at elevated temperatures demonstrated by Ke (1947).

Figure 39 shows internal friction measurements made on the Elastomat in air as a function of temperature up to about 900°C . A plot of the internal friction of an annealed alloy and one as received shows a similar temperature dependency with the onset of the internal friction peak occurring at a slightly lower temperature for the annealed material.

The internal friction measurements for the preoxidized specimen are shown in Figure 40. It is seen to increase above 1050°C but much slower than the unoxidized specimen. At 1400°C the ratio is less than 50 percent that of the corresponding unoxidized alloy ratio indicating

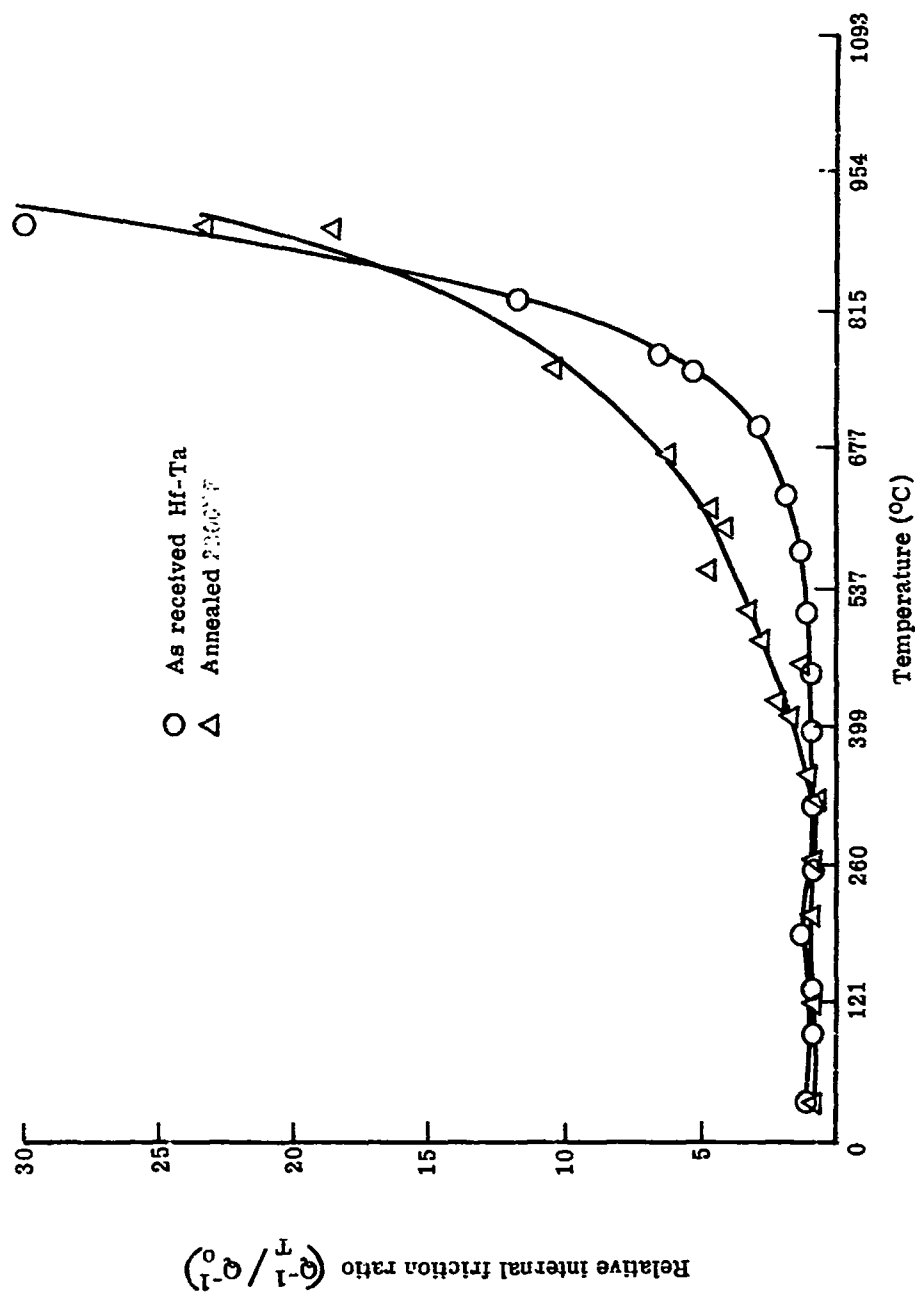


Figure 39. Relative internal friction ratio versus temperature for a hafnium-20% tantalum alloy in air

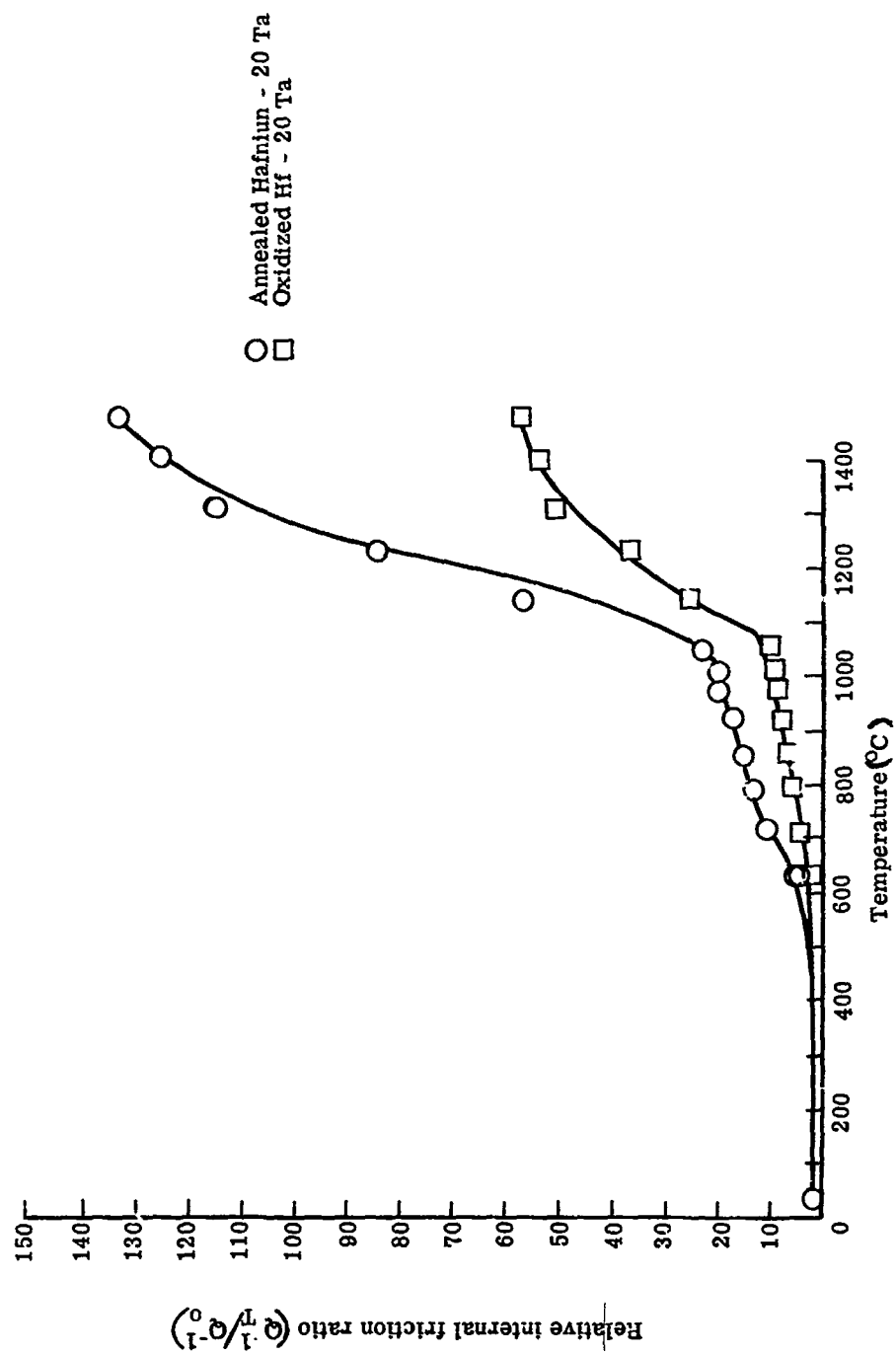


Figure 40. Elevated temperature relative internal friction ratio of an annealed and preoxidized hafnium-20% tantalum alloy

that oxide contamination at the grain boundaries is retarding the viscous behavior to a large extent. This lower internal friction ratio is manifested in a more linear temperature dependency of the elastic modulus as has been previously discussed.

Annealing Behavior

As room temperature dynamic elasticity measurements indicated an increase in the elastic and shear moduli values of the annealed hafnium-20% tantalum alloy, an individual experiment was conducted to determine the effect of time at the annealing temperature of 1112°C . The sample was brought to the annealing temperatures in two increments and held to insure an equilibrium temperature was reached. On reaching temperature of 1112°C within a 30-minute time span, the temperature was held constant and the change in resonant transverse frequency was monitored as a function of time. Likewise the output voltage of the pickup transducer, which is a relative indication of the internal friction, was monitored. Results of these measurements are shown in Figures 41 and 42. It can be seen from the plot of elastic modulus ratio versus time that the annealing process causes a parabolic type increase with time with a leveling off occurring from 2.5 to 3 hours at this temperature. This resulted in a greater than 6 percent overall increase in the elastic modulus. Correspondingly, the internal friction decreased rapidly during the annealing process to about 50 percent of its original value at the annealing temperature with a leveling off at 2.5 to 3 hours, similar to the modulus change.

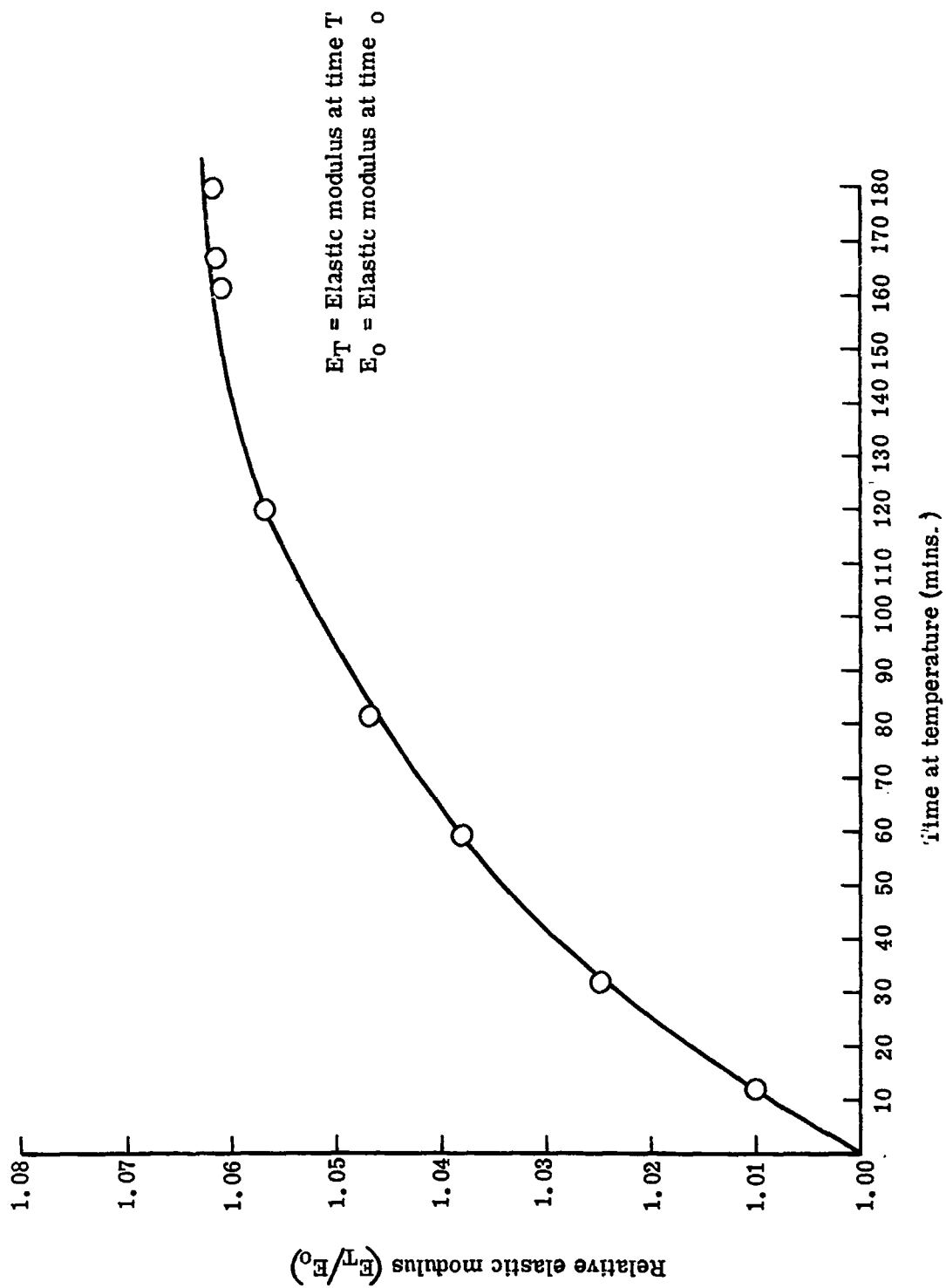


Figure 41. Change in elastic modulus with time at a constant annealing temperature of 1112° C

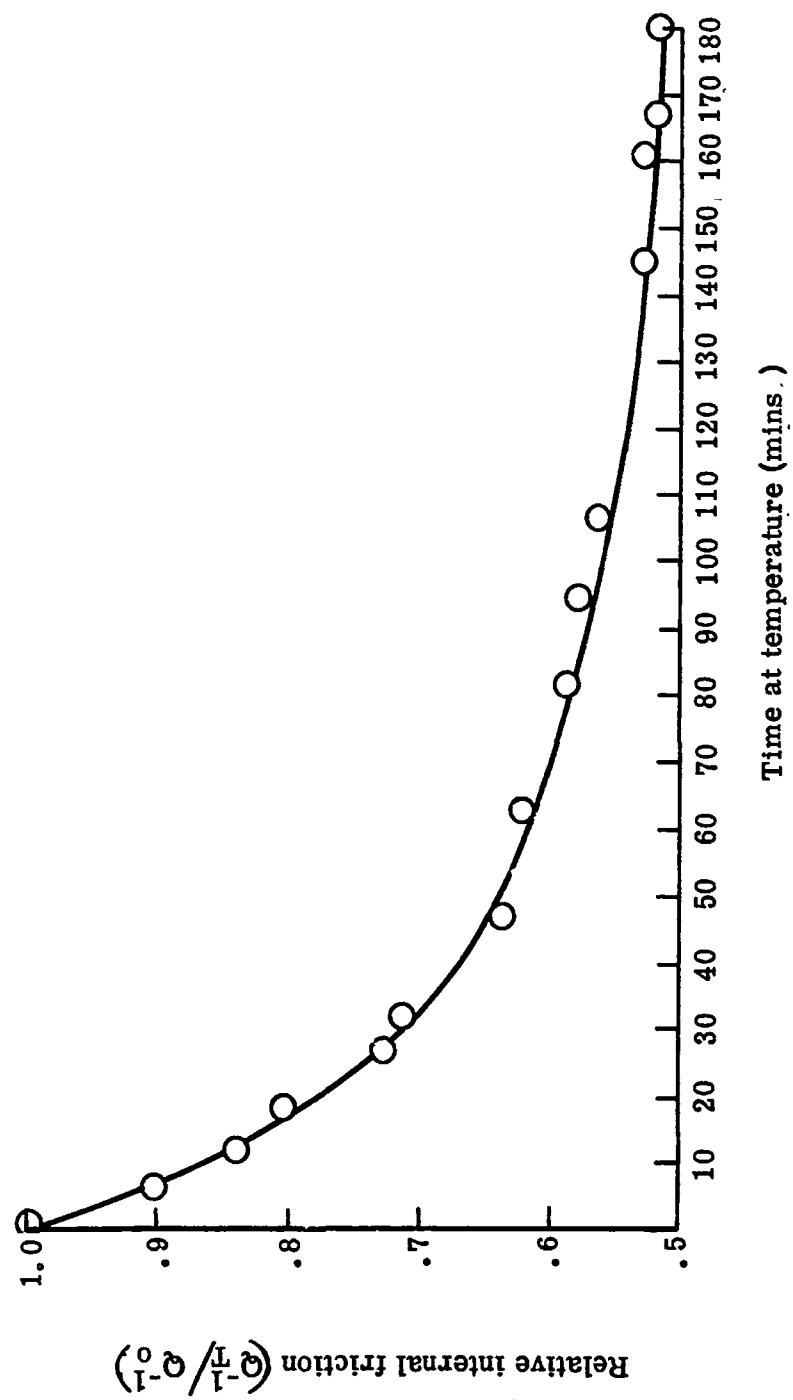
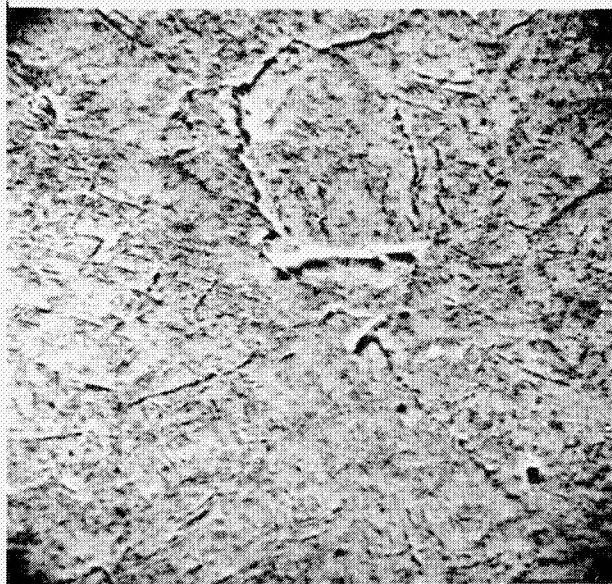


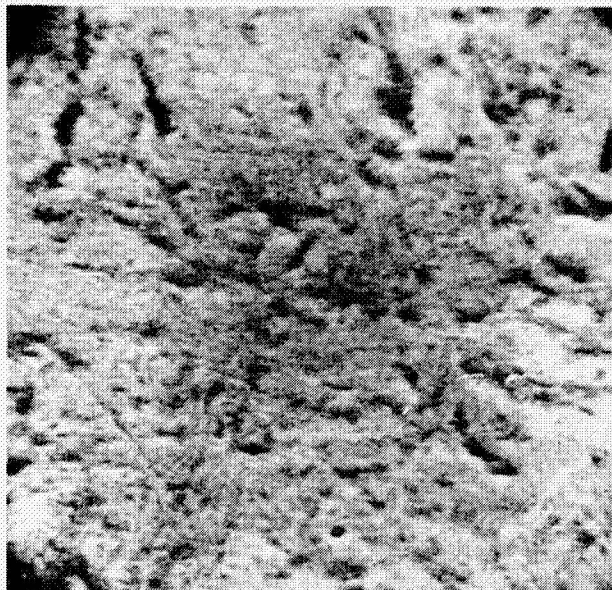
Figure 42. Change in relative internal friction ratio with time at a constant annealing temperature of 11120° C

Phase Transformation Study

Svechnikov (1964) and Mash (1968) each reported the existence of a metastable non-equilibrium phase, alpha prime (α'), which could result from the rapid cooling from the β elevated temperature equilibrium phase. Mash indicated formation of this phase by quenching from 1450° C down to room temperature. The scanning electron microscope, conventional electron microscope, X-ray diffractometer, and hot stage metallograph were used to qualitatively access this transformation behavior. The as received material as seen by Figure 43 was polished and etched with a diluted solution of HF-HNO₃ acids to bring out grain boundary and surface details. The micrographs indicated a typically two phase material. X-ray diffraction analyses on the extruded rod material indicated a structure primarily identifiable as an alpha (α) HCP structure. However, several of the β tantalum peaks overlapped, therefore, it cannot be conclusively said that the sample was not the two phase equilibrium $\alpha + \beta$ tantalum structure. There were, however, no peaks which could absolutely be identified and indexed as being of a BCC structure. Lattice parameter calculations based on (100) and (101) HCP reflections yielded $a_0 = 3.181 \text{ \AA}$, $c_0 = 5.051$, with a c/a ratio = 1.588. In order to obtain an X-ray pattern based on random orientation of the material and thus a more accurate angular representation of the diffraction peaks, -200 mesh hafnium-20% tantalum powder obtained by grinding up the extension ends left over from production of the rod material was used. The X-ray diffraction pattern on this material contained symmetrical peaks and was positively identified as a two phase $\alpha + \beta$ tantalum material. Lattice parameter calculations



2000x



10,000x

Figure 43. Scanning electron micrographs of an as-received hafnium-20% tantalum alloy. HF-HNO₂ etch

for the solid solution phase of tantalum in the α hafnium lattice based on the (200) Hf and (101) Hf diffraction peaks yielded lattice dimensions of $a_0 = 3.1968 \text{ \AA}$ and $c_0 = 5.0614 \text{ \AA}$ with the c/a ratio of 1.583; this compares to Pearsons handbook of lattice spacings of $a_0 = 3.1946$ and $c_0 = 5.0510 \text{ \AA}$ for pure hafnium whose c/a ratio = 1.5811. The only strong β tantalum peak identified was the (110) peak which gave a lattice parameter for this solid substitution phase of about 5.5 percent longer than the corresponding peak for pure β tantalum which has a lattice parameter of $a_0 = 3.3058 \text{ \AA}$ as given by the ASTM powder diffraction card.

Knoop microhardness measurements were taken across the surface of the as received specimen. Using a 100-gm load, the Knoop hardness based on average random readings on the specimen was found to be 464. Similar readings on an annealed specimen yielded a Knoop hardness of 238.

The specimen was heated on the hot stage metallograph and photographed at 500X magnification at each temperature interval. On heating the specimen up to well within the single phase β hafnium region, there was no surface change noted up to 1417° C . Radiation of the sample at this temperature proved somewhat a problem as surface details began to fade. Once at this temperature the specimen was allowed to soak for about 10 minutes, at which time the power was reduced 5 amps with the temperature being reduced to 1287° C . The surface appearance of the specimen obviously changed but at this magnification in the hot stage it was not clearly evident what the surface actually looked like. This 130° sudden decrease in temperature produced a rippled surface

appearance with the grain boundary detail no longer clearly defined. Figure 44 shows the change of appearance of the hafnium-20% tantalum specimen as it went through the heating and cooling cycle on the hot stage. It was not until reexamination of the specimen using the scanning electron microscope that a real clear observation of the phase transformation could be recorded. Figure 45 shows a 4900X magnification micrograph of the specimen surface after going through the heat treating and quenching process in the hot stage. The surface distortion is typical of a martensitic diffusionless phase transformation in which there is a shearing mechanism involved in the crystal phase change. This shearing mechanism causes a rapid platelet formation in which the smooth surface becomes distorted. Carbon replicas were made of the specimen and electron micrographs of 10,000X magnification were taken. Figure 46 shows the surface distortion. Knoop microhardness measurements were made on the quenched hot stage specimen and the average Knoop hardness increased 2 percent to a reading of 474. This likely represents a greater than 2 percent increase as annealing effects would likely have caused hardness values to drop. Verification of the structural change was attempted through analysis of the X-ray diffraction pattern. The crystal structure of the heat treated hafnium-tantalum specimen could be classified only as single phase hexagonal solid solution. No peak reflections could be attributed to the β tantalum solid solution structure. Lattice parameter calculations based on peaks at 32.45° , 2θ , attributed to planes (100) of a HCP lattice, and at 37.2° , 2θ , from (101) planes, yielded lattice dimensions of $a_0 = 3.183 \text{ \AA}$ and $c_0 = 5.007 \text{ \AA}$ with the corresponding c/a ratio of 1.573. This

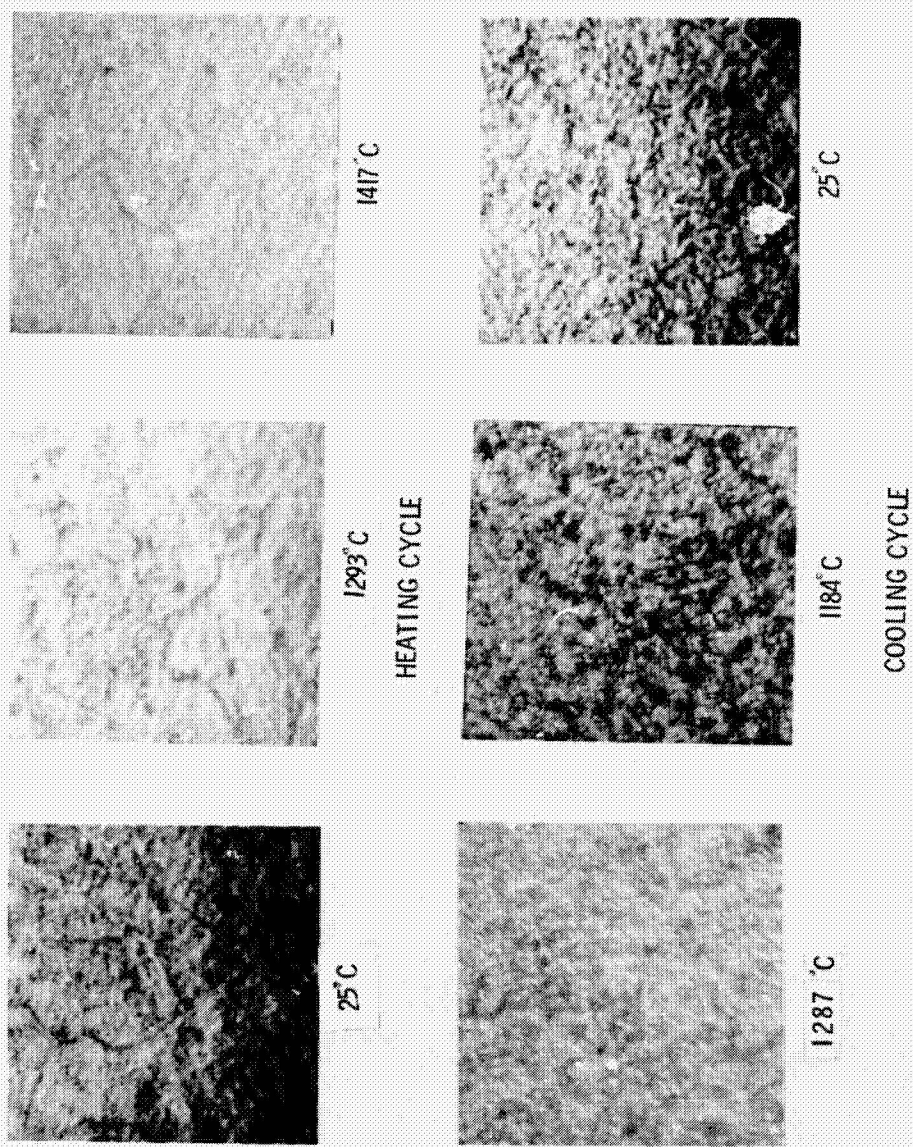
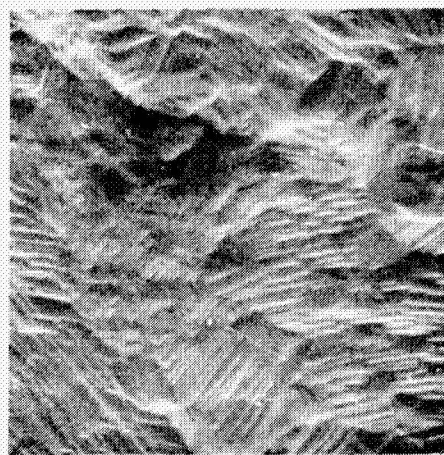
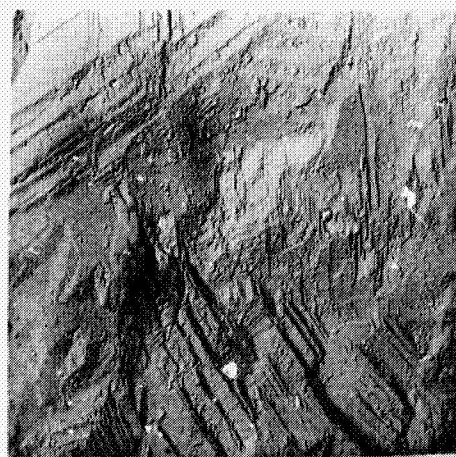


Figure 44. Hot stage metallography showing hafnium-20% tantalum phase transformation. 500 X magnification



4,900x

Figure 45. Scanning electron micrograph of hafnium-20% tantalum specimen after diffusionless transformation



10,000x

Figure 46. Replica electron micrograph showing surface distortions after diffusionless transformation

indicates a shrinkage of the unit cell volume from the as received rod specimen. This c/a ratio is identical to the ratio reported by Mash (1968) for the α' phase, however, this phase was obtained by solution treatment at 1450°C , followed by quench to 315°C in helium, isothermal treatment for 1000 seconds and water quenching to room temperature.

A verification of this phase transformation was made with another specimen. A similar surface morphology and X-ray diffraction pattern were obtained. As a result of the visual observations made during the heat treatment of the hafnium-20% tantalum alloy in the hot stage metallograph, one may conclude that no transformations are visible during the heating process, however, on rapid cooling from the β hafnium high temperature phase into the $\alpha + \beta$ hafnium region, a HCP phase is formed which is characterized by surface distortions typical of those caused by a martensitic diffusionless transformation.

Static Oxidation Tests

The results of static oxidation tests as a function of time at five temperatures ranging from 1000°C to 1700°C is presented in Figure 47. The weight gained per unit exposed surface area and the corresponding percent weight gained gives some insight into the manner in which the hafnium-20% tantalum alloy oxidizes. Previous studies have reported a linear behavior with time at temperatures below 900°C characterized by a non-protective oxide which readily spalls. At 1000°C , the oxidation tests conducted in this program show an initial parabolic behavior which is indicative of a diffusion controlled process in which the oxygen diffuses through the oxide scale as a function

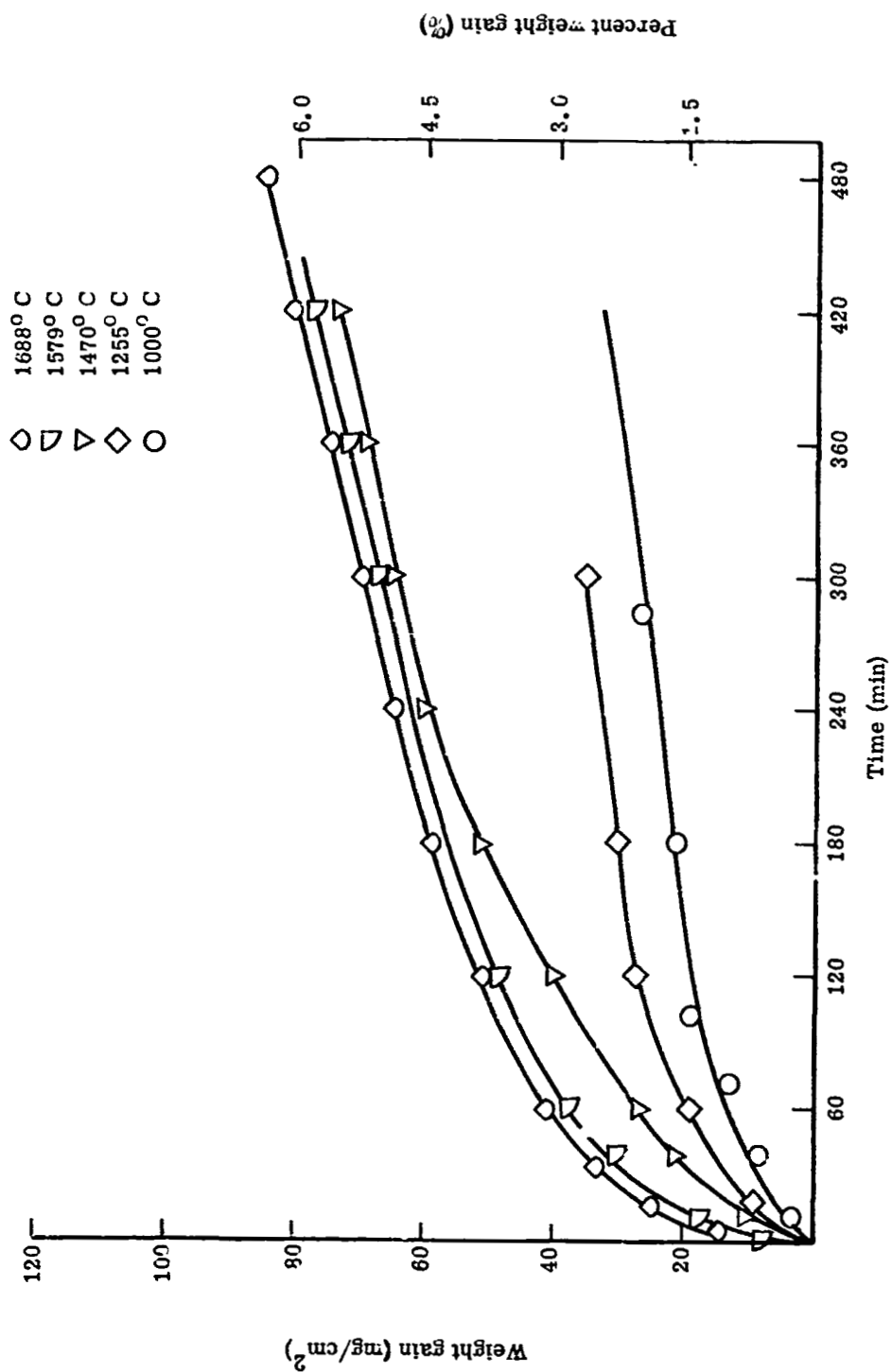


Figure 47. Oxidation behavior of a hafnium-20% tantalum alloy in static air.

of the square root of the time. Similar parabolic behavior was noted in all high temperature tests, the amount of oxide formed on the surface increasing for a given time as the temperature increased. Oxidation rates appeared to become linear after the initial 3 hours. There appeared to be a transition in the rate of oxidation from the 1255° C and the 1470° C tests. The oxide formed at the temperatures of 1000° and 1255° C was typically white in nature at the surface, whereas all specimens oxidized above 1470° C had surface oxides which were predominately blue/gray. The higher temperature oxidized specimens showed a cracking of the surface in patterns resembling grain boundaries. This cracking of the surface oxide is probably a result of stresses set in the oxide on formation and the thermal shock of removing the specimen from the furnace to ambient conditions for weighing and photomacrographing. Preferential oxidation of the sample at the edges was common with the exception of the 1688° C specimen. Oxidation on this specimen was uniform over the sample, however, it also experienced cracking of the surface. Figures 48 through 51 qualitatively show the surface oxide formation as a function of time and temperature for each of the test specimens. As the oxidation at the edges proceeded at a faster rate, the volume of oxide produced there soon expanded to the point that it would flake off readily.

A cross section of the specimen whose oxide was formed at 1688° C is shown by Figure 52. The different distinct zones of oxidation can be seen from the scanning electron micrograph. The outer scale after the 480-minute exposure was approximately 0.0006 inch thick followed by a subscale of about 0.001 inch thick. Oxygen contamination of the

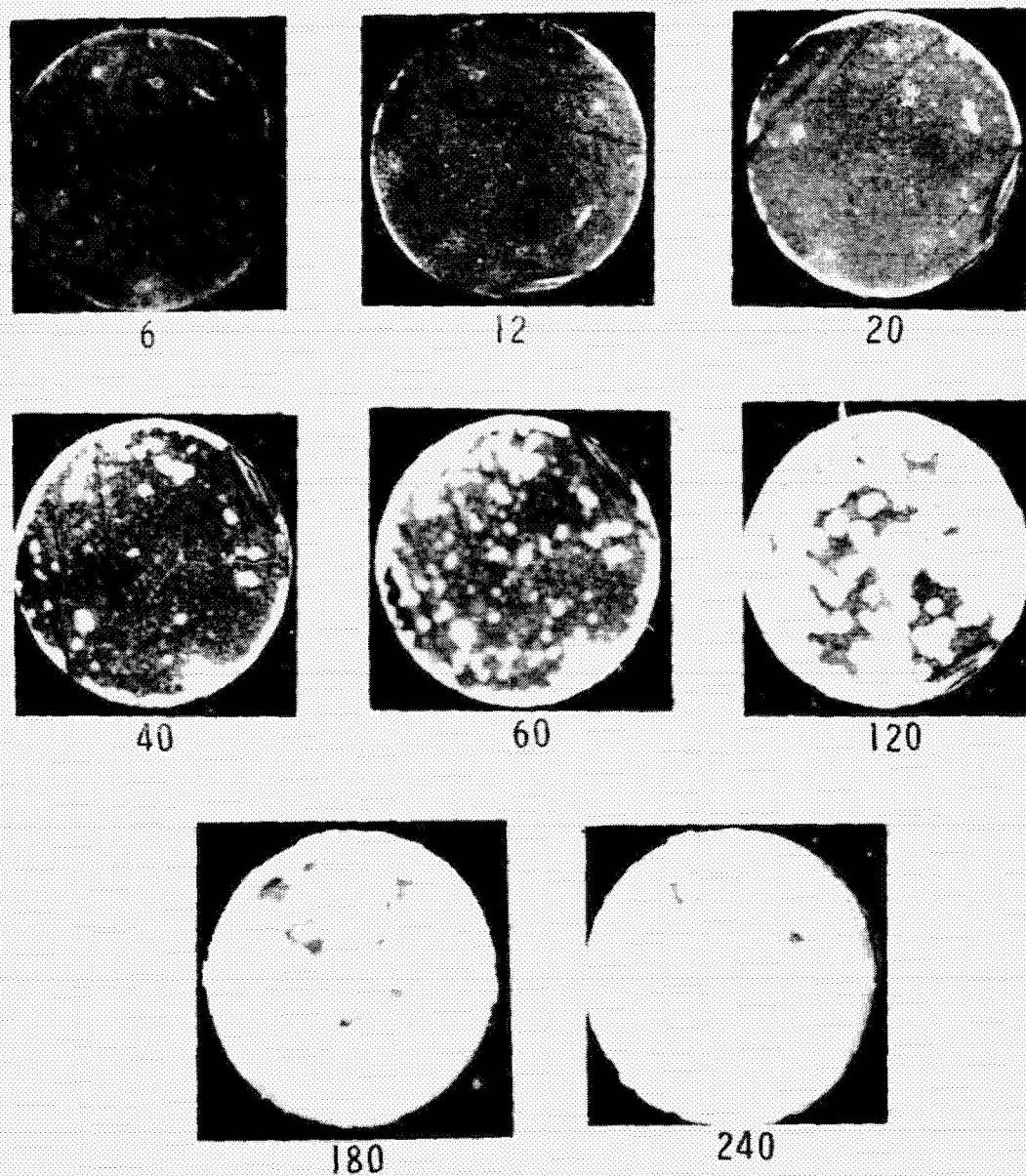


Figure 48. Static oxidation tests at 1000°C. 4X magnification.
Numbers indicate minutes at temperature

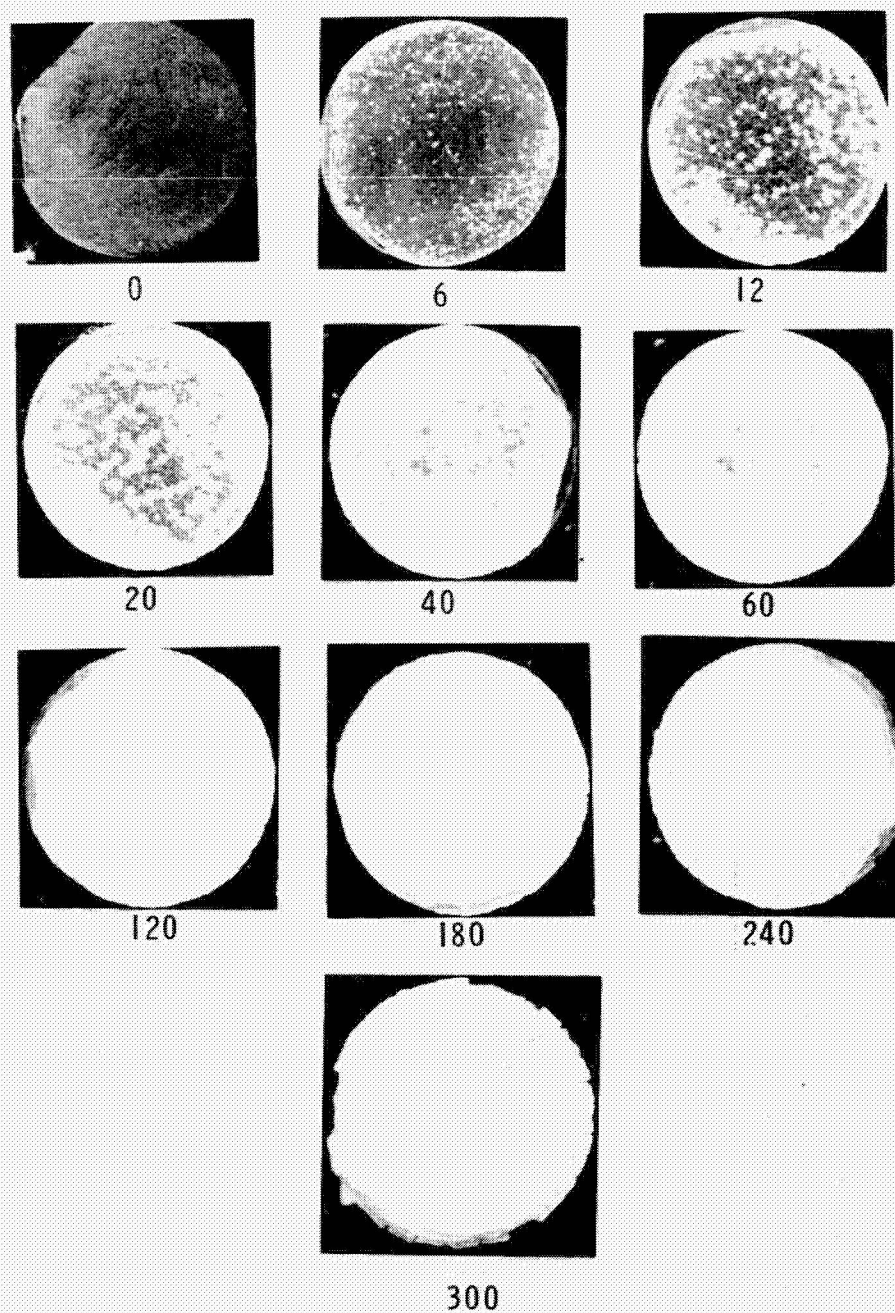


Figure 49. Static oxidation tests at 1255° C. 4X magnification.
Numbers indicate minutes at temperature

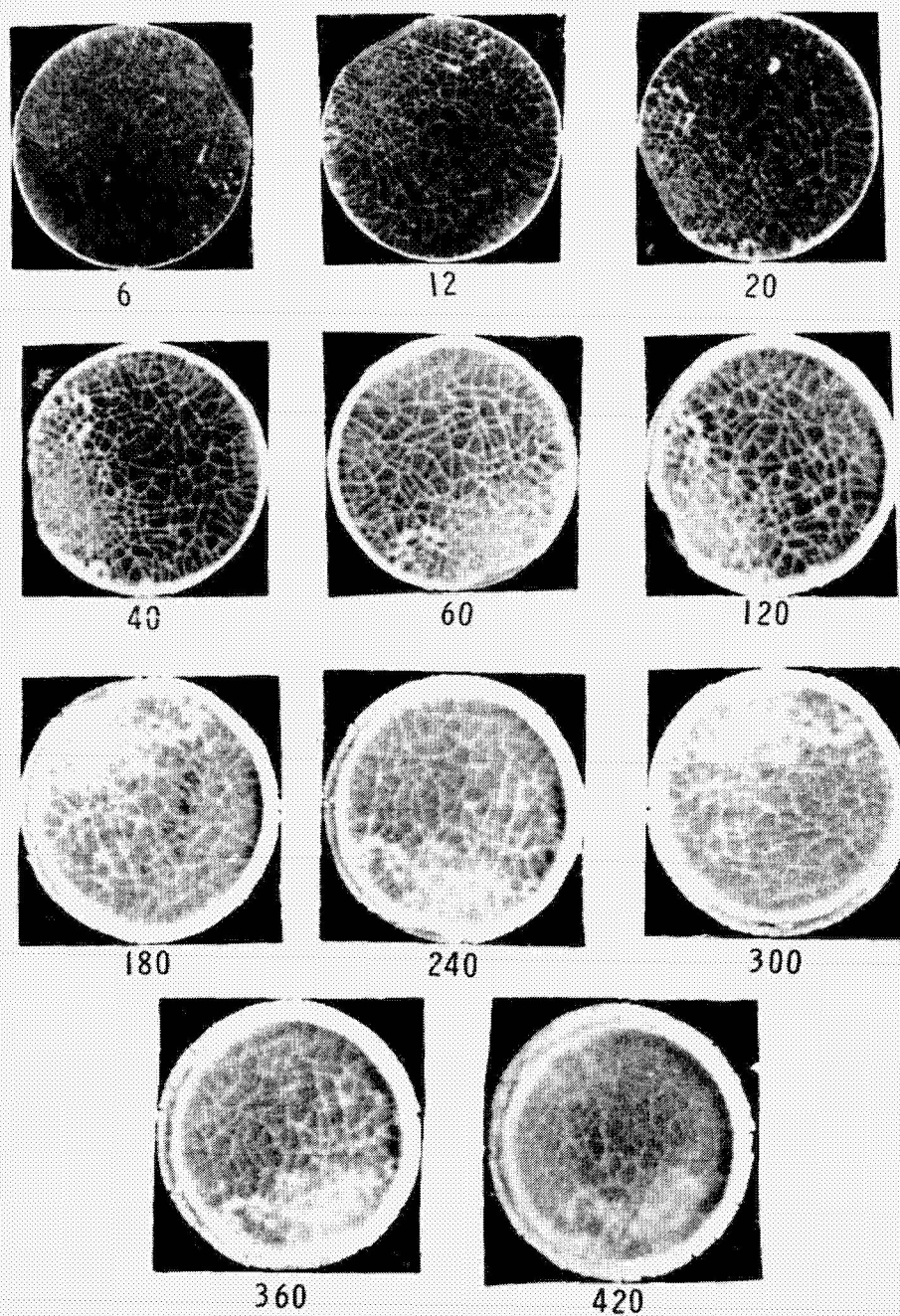


Figure 50. Static oxidation tests at 1470°C . $4\times$ magnification.
Numbers indicate minutes at temperature

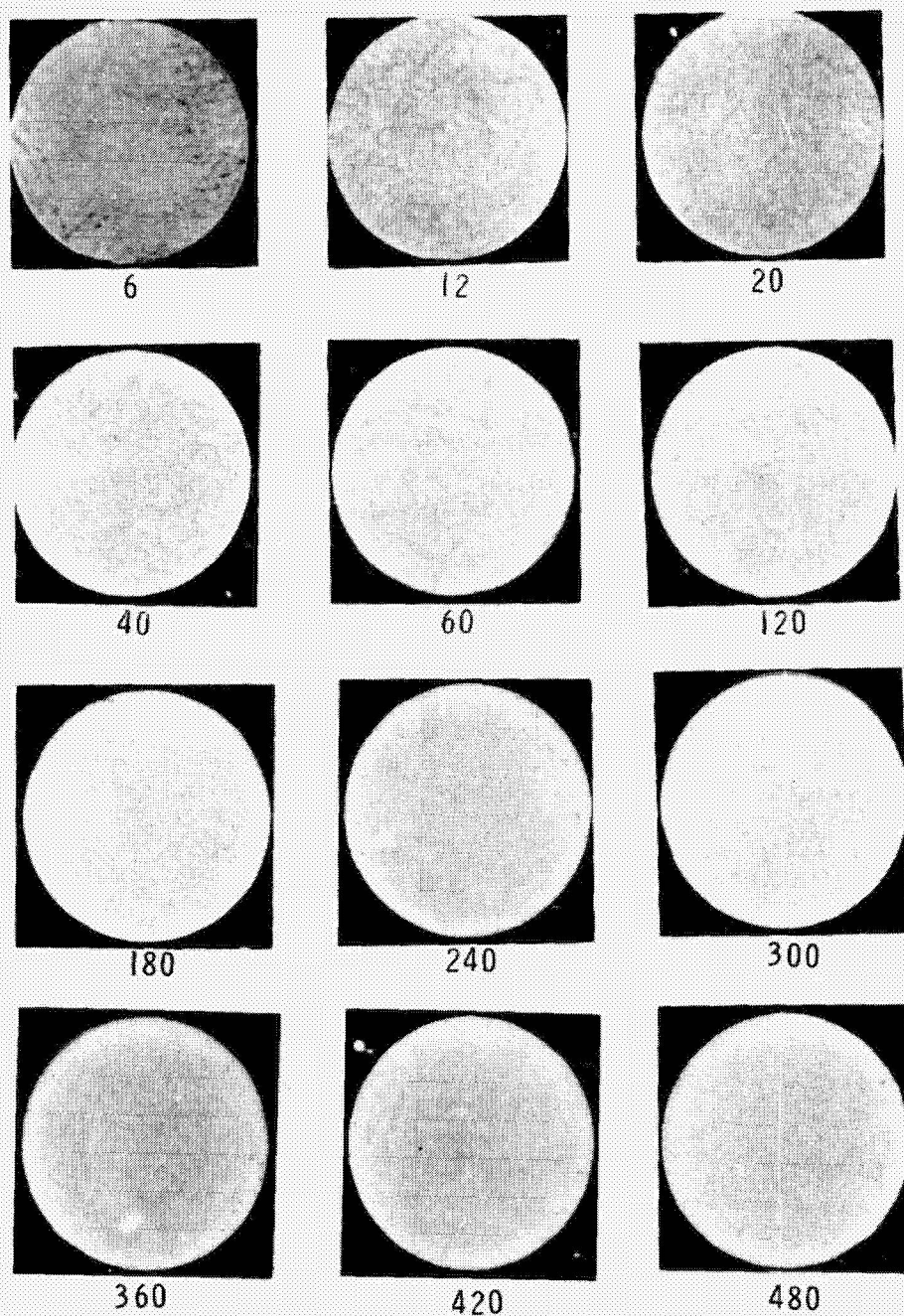


Figure 51. Static oxidation tests at 1688° C. 4X magnification.
Numbers indicate minutes at temperature

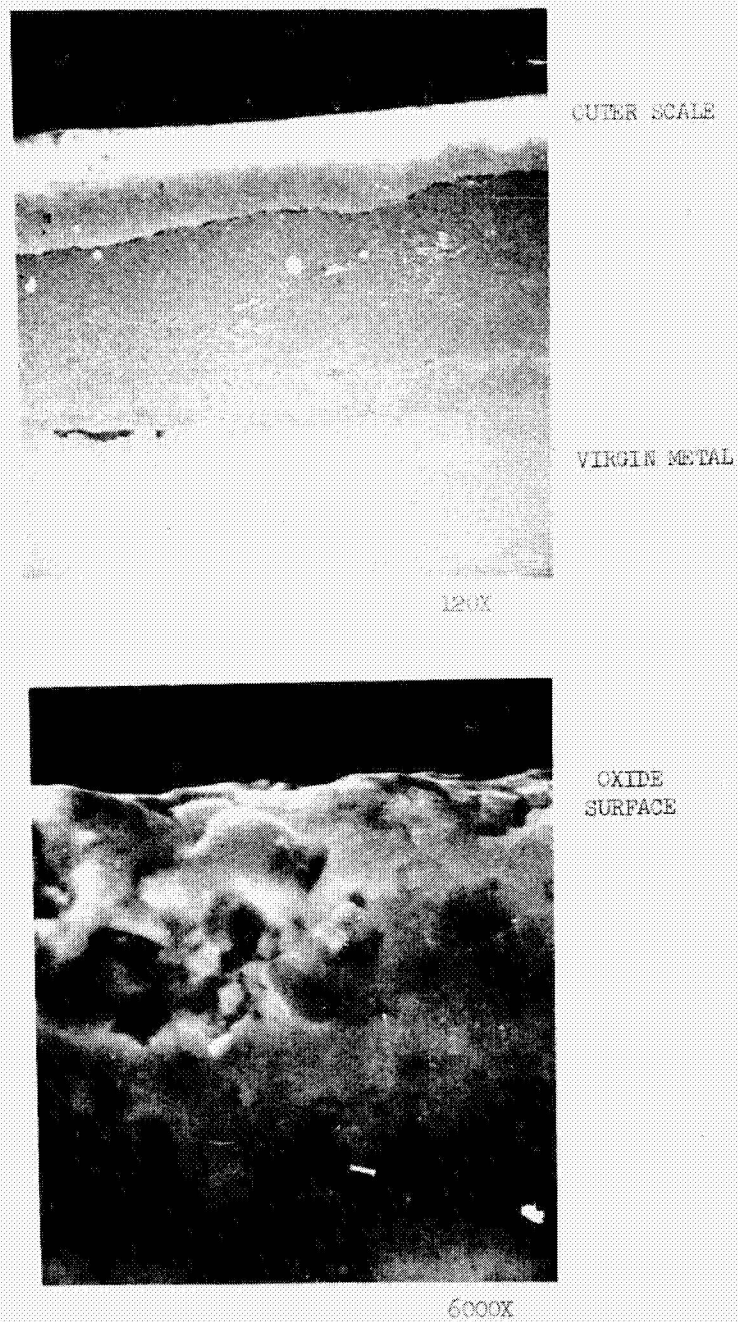


Figure 52. Scanning electron micrographs of cross section of specimen oxidized at 1688°C for 480 minutes

metal can be seen to penetrate to a depth of 0.016 inch below the surface. The outer surface as can be seen from the 6000X micrograph had a molten, glassy appearance and was bluish/gray in color. Voids can be seen below the surface in the oxide scale and a large crack parallel to the surface is seen to have formed during the exposure. Typical cross-section photographs of the oxide scale formed at 1000° C are shown in Figures 53 and 54. The outer scale is seen to be of a lower density than the oxide formed at the metal interface. As viewed by polarized light it can be seen that preferred oxidation does occur at the grain boundaries and is likely the cause for the ductile-to-brittle transition of the mechanical behavior of the alloy as seen in tensile tests conducted on the oxidized alloy.

Qualitative analysis of the oxides formed at 1000° C and 1700° C was performed using the X-ray analysis. Patterns obtained were quite complex as is the case for mixed oxides in general. Diffraction peaks from Ta_2O_5 , monoclinic and tetragonal HfO_2 are difficult to separate as they are coincident at the higher 2θ angles. The lower temperature 1000° C oxide indicated definite strong monoclinic peaks (111) with also the strong tetragonal peak at a d-spacing of 2.947 along with other tetragonal peaks and peaks of $\beta-Ta_2O_5$. This would indicate a partial stabilization of the high temperature form of hafnia by the Ta_2O_5 present in agreement with other investigators.

The higher temperature 1700° C oxide formed had the strongest monoclinic peaks (111) missing and showed a predominance of the high temperature tetragonal HfO_2 structure indicating almost complete stabilization at room temperature.

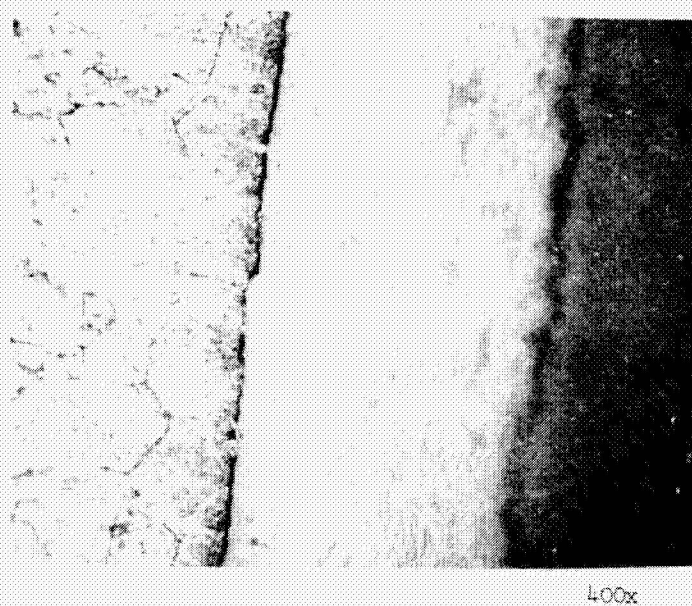


Figure 53. Microstructure of hafnium-20% tantalum oxidized at 1000° C

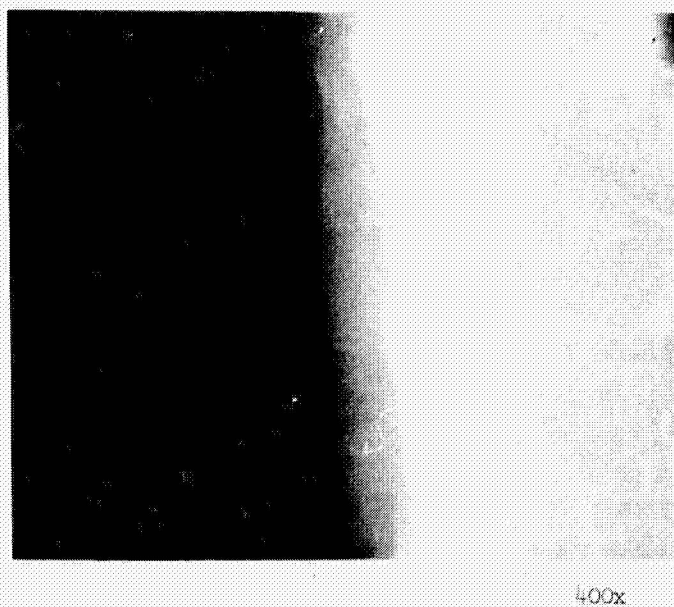


Figure 54. Microstructure of hafnium-20% tantalum oxidized at 1000° C using polarized light

Other investigators have indicated the possible existence of a complex oxide $6\text{HfO}_2 \cdot \text{Ta}_2\text{O}_5$; if indeed it does exist its pattern is very similar to that of a combination of monoclinic and tetragonal HfO_2 and it could not be positively identified by X-ray diffraction. Surface morphology studies discussed later do, however, provide some possible evidence for its existence.

Results of microhardness measurements on the high temperature 1700°C specimen oxidized for 30 minutes indicated an average Knoop hardness of about 1040 using a 700-gm load on the surface, increasing to 1225 using an 800-gm load at depth of 0.004 inch beneath the surface. At 0.008 inch below the surface the hardness drops to 685 using a 500-gm load decreasing down to a Knoop hardness of 500 at a depth of 0.012 below the surface. The corresponding X-ray patterns for each 0.004 inch below the surface showed increasing amounts of monoclinic HfO_2 being present which agrees with Marnoch's data (1965) in which he indicates that tantalum segregation depletes the amount of tantalum oxide available to stabilize the HfO_2 in the tetragonal structure.

In order to learn more about the protective nature of the oxide scale formed, the surface morphology was studied utilizing scanning electron microscopy techniques. Another series of static oxidation tests were conducted at similar temperatures to those used in the weight gain measurements. The sample was removed at various times during the heating cycle with electron micrographs taken of the surface. As the oxide coating developed on the surface, it became more difficult to get good photographs. An electronic charge would build up on the specimen in a localized area causing the specimen to burn in that area. A

conductive coating put on those specimens which were not to be returned to the furnace for further heating proved helpful in preventing the electronic charge build-up. From this problem it is evident that the HfO_2 coating is a very effective electrical insulator.

Figure 55 shows the individual oxide particle formation at temperatures up to about 1600°C for the first 3 minutes of heating time. These particles appear to have no particular size or shape and no individual grain or crystal structure can be detected. They form at random locations on the specimen surface and gradually cover the entire surface as time at temperature increases. In contrast, however, at temperatures approaching 1700°C - 1750°C , a definite oxide crystal structure formation can be detected. At 3 minutes heating at 1740°C distinct needle oxide crystals appear on the surface as can be seen from Figure 56. On close examination of the 5500X micrograph shown in Figure 56 some sintering or melting of the oxide needles appears. Figure 57 shows the surface of another specimen heated for 30 minutes at 1700°C . Examination of these micrographs reveal similar distinct needle-like oxide crystals over a portion of the surface. From these micrographs, it is seen that the individual oxide crystals have sintered together in some sectors of the specimen and apparently melted forming individual grain structures with a smooth, glassy appearance characterized by a bluish/gray color. This closed pore structure formed at temperatures approaching 1700°C is probably partially responsible for the protective nature of the tightly adherent oxide as it retards the diffusion of oxygen to the metallic virgin material below.



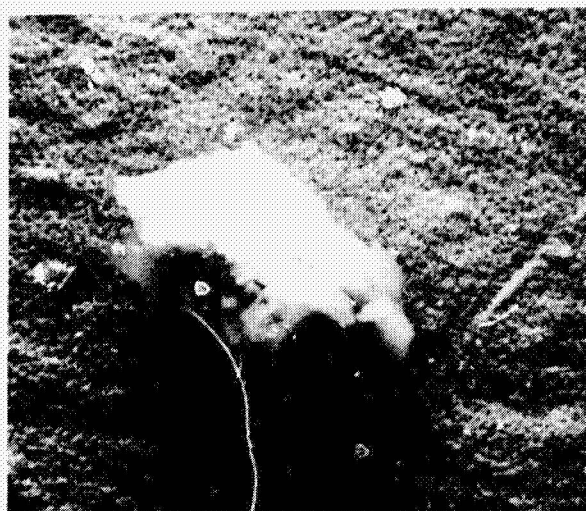
1000 C

5800x



1515 C

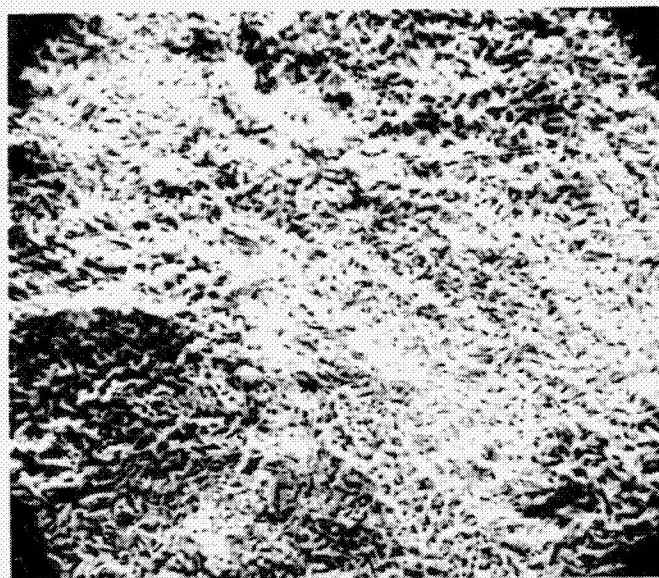
530x



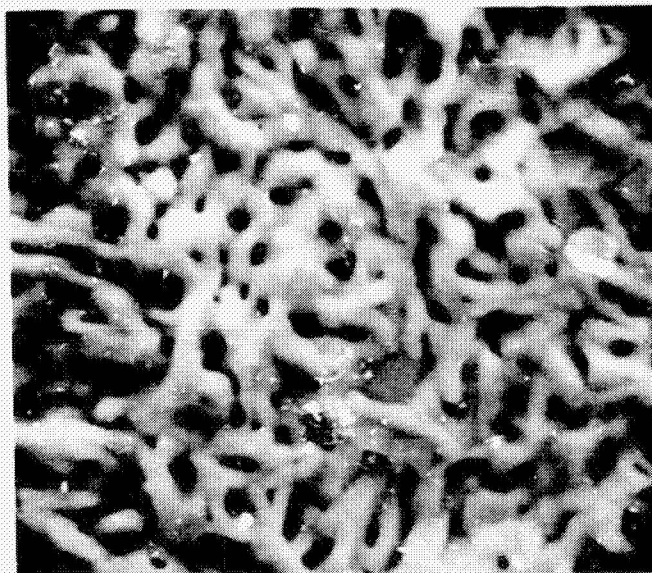
1600 C

1100x

Figure 55. Oxide particle formation on heating in air at temperature from 1000° C to 1600° C for 3 minutes

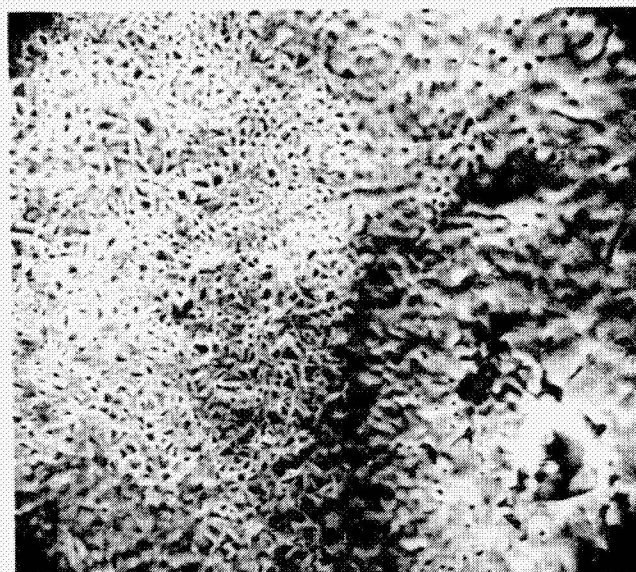


1100x



5500x

Figure 56. Needle-like oxide crystals formed at oxidation temperature of 1740°C for 3 minutes



1100x



5100x

Figure 57. Oxide crystals sintering at 1700°C after 30-minute exposure

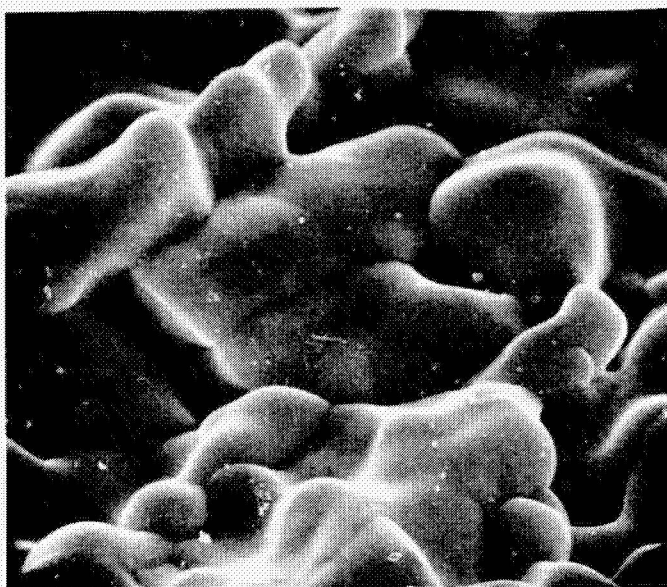
Evidence of internal oxidation of the hafnium-20% tantalum specimen is shown in Figure 58. This shows the formation of an oxide whisker below the surface of the specimen which burst through the surface with considerable force as indicated by the large hole in the surface and the raised area surrounding the whisker. A 5500X micrograph of the tip of the oxide whisker shows a dense oxide with some granular appearance. It should be noted that whiskers such as this one, formed during the 10-minute heating cycle at a temperature of 1685°C , could be detrimental to a protective coating. The hole formed by this whisker provides a more accessible route for rapid diffusion of oxygen to the virgin material below the surface thus increasing the rate of oxidation of the material.

Figure 59 shows the oxide coating formed after 30 minutes at 1150°C . No individual grain structure was discernible on this white oxide coating which appeared to form as small island particles on the surface. Even at 30 minutes at temperature the top of the specimen was not covered completely and the surface coating was not of uniform thickness. Large cracks developed in the coating, however, it is not known whether they developed during oxide formation or on removal from the furnace and subsequent cool down to room temperature.

The surface morphology studies indicate that at lower temperatures up to about 1600°C the oxidation kinetics are such that individual oxide needle crystals are not formed; however, as oxidation takes place at temperatures approaching 1700°C , definite needle-like oxide crystals are formed. As a function of time at temperatures between 3 and 30 minutes, sintering takes place between the oxide crystals forming a

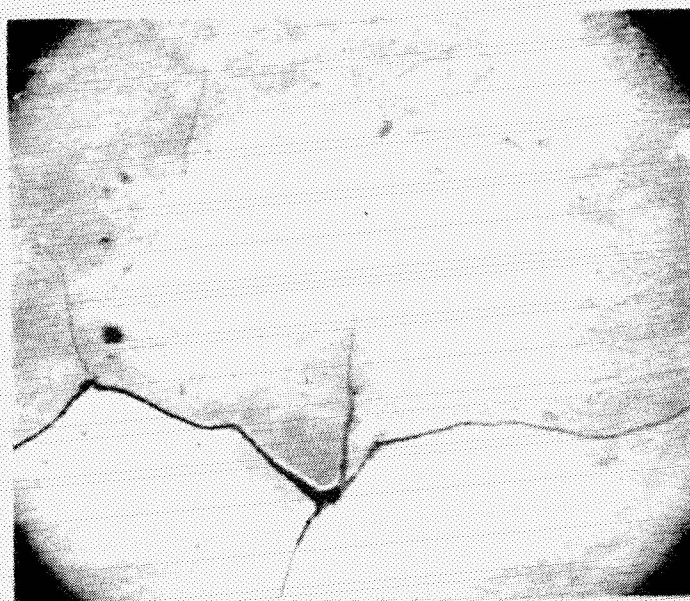


115x

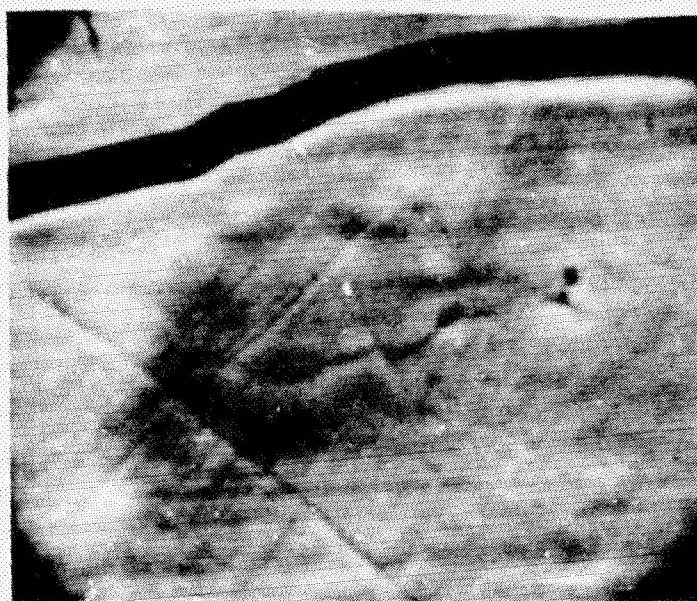


5500x

Figure 58. Oxide whisker formation at 1685°C after 10-minute exposure



115x



2350x

Figure 59. Cracking of oxide coating formed after 30-minute exposure at 1150° C in air

molten structure in which grain boundaries can be noted. The melting point of HfO_2 is 2777°C and 1890°C for tantalum oxide. As the test temperature did not exceed 1750°C this indicates that the oxide formed shows some visual signs of fluxing at a temperature lower than the melting point of either constituent. This may provide some support for the existence of the complex $6\text{HfO}_2 \cdot \text{Ta}_2\text{O}_5$ high temperature oxide which could not be confirmed by X-ray diffraction.

A check of the phase diagram for ZrO_2 and Ta_2O_5 indicates that in this system there exist certain compositions at which the melting point of the phases present is lower than either ZrO_2 and Ta_2O_5 .

CONCLUSIONS

The following are conclusions obtained from this investigation:

1. The elastic and shear moduli of the polycrystalline hafnium-20% tantalum alloy are lower at room temperature than the corresponding moduli of either of the major constituents of comparable purity and specimen form. This negative deviation of a rule of mixtures is in contrast to a positive deviation found in similar hafnium-27% tantalum alloy.
2. Fabrication of hafnium-20% tantalum by the Dynapack extrusion process leaves the rod with a highly preferred orientation. This preferred orientation is responsible for an alteration of the mechanical properties of the material.
3. The elastic and shear moduli of extruded hafnium-20% tantalum rod are lowered by this preferred orientation. The moduli can be recovered or increased on the order of 10 percent by vacuum annealing the alloy at 1200° C for 4 hours.
4. The dynamic mechanical resonance technique affords an excellent method for studying the annealing behavior of metals and alloys. This technique could be used for optimizing annealing time and temperature parameters for obtaining desired mechanical properties.
5. The rapid decrease of elastic and shear moduli above 1020° C limits usefulness of hafnium-20% tantalum as a load-carrying structural material in high temperature applications for which it could best take advantage of its oxidation resistance.

6. The sharp decrease in moduli above 1020°C denotes a structural phase transformation and is accompanied by a large increase in internal friction at this temperature. The high internal friction is likely a result of the viscous behavior of the grain boundaries which is partially responsible for the rapid decrease in mechanical properties.

7. Room temperature damping behavior of the hafnium-20% tantalum alloy is similar to other refractory metals such as molybdenum.

8. The unoxidized hafnium-20% tantalum is ductile, however, preferential oxidation at grain boundaries is responsible for the brittle behavior of oxidized material.

9. The $\alpha + \beta \text{Ta} \rightarrow \beta \text{Hf}$ phase transformation occurring in the hafnium-20% tantalum system on heating is not visible by hot stage metallography.

10. A martensitic-type, diffusionless phase transformation occurs on rapid cooling of the hafnium-20% tantalum alloy from above 1400°C to 1287°C . This transformation is visible using hot stage metallography techniques and is characterized by shear distortions of the surface and an increase in hardness of the material.

11. The oxide coating formed on pure hafnium up to 1000°C in static air is formed slower and is more adherent than that formed on the hafnium-20% tantalum alloy at that temperature.

12. Oxidation of the hafnium-20% tantalum alloy is parabolic from 1000°C to 1700°C for times approaching 3 hours, however, it tends to become linear beyond that point.

13. Internal oxidation of the hafnium-20% tantalum alloy at temperatures around 1700°C can result in whisker formations which

cause a break in the oxide coating. These formations could be detrimental to an oxidation resistant coating.

14. Surface oxide formed at temperatures up to 1400°C are predominantly white in color and consist of monoclinic HfO_2 , partially stabilized tetragonal HfO_2 , and $\beta\text{-Ta}_2\text{O}_5$.

15. Surface oxides formed at temperatures above 1400°C are blue/gray in color and analyzed as highly stabilized tetragonal HfO_2 with $\beta\text{-Ta}_2\text{O}_5$ present.

16. An increasing amount of monoclinic HfO_2 is formed as oxidation proceeds toward the oxide-metal interface in the static oxidation of the alloy at 1700°C .

17. Distinct needle-shaped oxide crystals are formed on the surface of the hafnium-20% tantalum alloy at static oxidation above 1700°C . These needle-like crystals are not formed in the coating below this temperature.

18. The oxide needles sinter together to form a smooth, molten coating as a function of time at temperature. The formation of this coating at temperatures below the melting point of either HfO_2 or Ta_2O_5 provides some evidence of the existence of a possible complex oxide, $6\text{HfO}_2 \cdot \text{Ta}_2\text{O}_5$.

19. The HfO_2 coating formed on the hafnium-20% tantalum alloy at temperatures $\leq 1000^{\circ}\text{C}$ appears to be brittle and to crack in thermal cycling from elevated temperatures to ambient conditions.

20. The HfO_2 coating appears to have excellent electrical insulative characteristics as evidenced by the electronic charge build-up during scanning electron microscopy studies.

21. Further developmental work is needed in inhibiting the rate of oxidation and strengthening the high temperature mechanical behavior of the alloy in order to realize its full potential.

22. The cost of the alloy at the present time will limit its use to all but the most specialized applications.

LIST OF REFERENCES

- Berkowitz-Matluck, J., L. Kaufman, and R. Hopper. 1967. Oxidation of Hf-Ta alloys. Transactions of the Metallurgical Society of AIME. 239:750-753.
- Berry, B. S. 1961. Review of internal friction due to point defects. Atomic Energy Commission Publication No. TID-15068.
- Bommel, H. E., W. P. Mason, and A. W. Warner. 1956. Dislocations, relaxations, and anelasticity of crystal quartz. Phys. Rev. 102:64-71.
- Bradfield, G., and H. Pursey. 1953. The role of preferred orientation in elasticity investigations. The Philosophical Magazine 44:437.
- Davies, R. M. 1938. The frequency of longitudinal and torsional vibration of loaded and unloaded bars. Philosophical Magazine 25:364-386.
- Dickinson, C. D., M. G. Nicholas, A. L. Prantis, and C. I. Whitman. 1963. Protective coatings for tungsten. Journal of Metals 15:787-792.
- Dickson, R. W., and S. Spinner. 1968. An improved method for the determination of torsional and flexural resonance frequencies of cylindrical specimens. J. of Materials 3(3):716.
- Dieter, G. E., Jr. 1961. Mechanical Metallurgy. McGraw-Hill Book Co., Inc., New York.
- Elliot, R. P. 1954. A study of a family of laves-type intermediate phases. Armour Research Foundation, Technical Rept. No. 1. OSR-TN-54-247.
- Förster, F. 1937. New methods for the determination of modulus of elasticity and damping. Z. Metallk. 29:109-115.
- Goens, E. 1931. Über die bestimmung des elastizitäts moduls von staben mit hilfe von biegungsschwingungen. Ann. Physik. Series 5(11):649-670.
- Granato, A., and K. Lucke. 1956. Application of dislocation theory to internal friction phenomena at high frequencies. J. Appl. Phys. 27:789-805.
- Granato, A., and K. Lucke. 1956. Theory of mechanical damping due to dislocations. J. Appl. Phys. 27:583-593.

- Hempel, Clifford A. 1961. Rare Metals Handbook. Reinhold Publishing Corporation, London.
- Hill, Maynard L. 1968. Materials for small radius leading edges for hypersonic vehicles. *Journal of Spacecraft* 4(1):55-61.
- Hill, V. L., and J. J. Rausch. 1966. Protective coatings for tantalum-base alloys. AFML-TR-354, Part II.
- Jeffries, Z., and R. S. Archer. 1924. The Science of Metals. McGraw-Hill Book Co., Inc., New York.
- Ke, T. S. 1947. Experimental evidence of the viscous behavior of grain boundaries in metals. *Phys. Review* 71:533-546.
- Ke, T. S. 1947. Stress relaxation across grain boundaries in metals. *Phys. Rev.* 72:41-46.
- Ke, T. S. 1949. On the structure of grain boundaries in metals. *Phys. Rev.* 73:267-268.
- Koehler, J. S. 1950. The influence of dislocations and impurities on the damping and elastic constants of metal single crystals. In W. Shockley, editor, *Imperfections in Nearly Perfect Crystals*. 197-216. John Wiley and Sons, Inc., New York.
- Kolsky, H. 1953. *Stress Waves in Solids*. Oxford University Press, London.
- Köster, W. 1940. Effects of phase transformations on internal friction of Ag-Zn alloys. *Z. Metallk* 32:151.
- Love, A. E. H. 1944. *A treatise on the mathematical theory of elasticity*. Dover Publications, New York.
- Lucke, K., and A. Granato. 1956. Internal friction phenomena due to dislocations. In Fisher, J. C., W. G. Johnston, R. Thomson, and T. Vreeland, Jr., editors. *Dislocations and Mechanical Properties of Crystals*. 425-457. John Wiley and Sons, Inc., New York.
- Marlowe, M. O., and D. R. Wilder. 1964. Elasticity and internal friction through the kilocycle range: Review and Annotated Bibliography. United States Atomic Energy Commission Report IS-925. Contract W-7405 eng-82. Ames Laboratory at Iowa State University of Science and Technology.
- Marnoch, K. 1965. High temperature oxidation resistant hafnium-tantalum systems. AFML-TR-65-240 under Air Force Contract No. AF 33(615)-1628.

- Marnoch, K. 1965. High temperature oxidation resistant hafnium-tantalum alloys. *Journal of Metals* 17(11):1225-1231.
- Marnoch, K. 1967. Some properties and applications of the hafnium-tantalum alloy. Paper prepared for the Thirteenth Refractory Composites Working Group Meeting, Seattle, Washington, July 1967. Work performed under Contract AF 33(615)-3734 for Air Force Aero Propulsion Laboratory, Ramjet Engine Division.
- Martin, Donald R., and Phillip J. Pizzozato. 1961. *Rare Metals Handbook*. Reinhold Publishing Corporation, London.
- Mash, D. R., D. C. Brillhart, and D. W. Bauer. 1968. Tantalum-hafnium metallurgical processing technology. Fansteel Metallurgical Corporation. First and Second Interim Reports, NASA Contract NAS 7-417.
- Mason, W. P. 1956. *J. Acoustic Society America* 28:1207.
- McLean, D. 1962. *Mechanical properties of metals*. John Wiley and Sons, Inc., New York.
- Niblett, D. H., and J. Wilks. 1960. Dislocation damping in metals. *Advances in Physics* 9(33):1-88.
- Norwick, A. S. 1953. Internal friction in metals. *Progress in Metal Physics* 4:1-70.
- Oden, L. L., D. K. Deardorff, M. I. Copeland, and H. Kato. 1964. The hafnium-tantalum equilibrium diagram. Bureau of Mines Report No. BM-RI-6521.
- Pickett, G. 1945. Equations for computing elastic constants from flexural and torsional resonant frequencies of vibration of prisms and cylinders. *Proceedings A.S.T.M.* 45:846-865.
- Pickett, G. 1945. Flexural vibration of unrestrained cylinders and disks. *Journal of Appl. Phys.* 16:821.
- Postnikov, V. S., F. N. Tavazde, and L. K. Gordiento. 1967. Internal friction in metals and alloys. A special Research Report translated from Russian by Consultants Bureau. Plenum Publishing Corp., New York.
- Potolskii, I. G., and N. S. Mordyuk. 1967. Mechanism of the damping of elastic vibrations in the case of phase transitions in copper and cobalt base alloys. In Postnikov, V. S., et al., editors, internal friction in metals and alloys. Special Research Report translated from Russian by Consultants Bureau. Plenum Publishing Corp., New York.

- Rayleigh, J. W. S. (Lord). 1877 (1945). The Theory of Sound, Vol. 1. Dover Publications, New York.
- Reed, T. A. 1940. The internal friction of single metal crystals. Phys. Rev. 58:371-380.
- Roderick, R. L., and R. Truett. 1952. The measurement of ultrasonic attenuation in solids by the pulse technique and some results in steel. J. Appl. Phys. 23:267-271.
- Rudy, E., and P. Stecher. 1963. Zum aufbau des systems hafnium-sauerstoff. Journal Les-Common Metals 5:78-89.
- Scheil, E., and G. Reinacher. 1944. Z. Metallk. 36:63.
- Smithhells, C. J. 1962. Metals Reference Book. Butterworths, Inc., Washington, D.C.
- Snoek, J. L. 1941. Effect of small quantities of carbon and nitrogen on the elastic and plastic properties of iron. Physica 8:711-713.
- Spinner, S., T. W. Reichard, and W. E. Tefft. 1960. Comparison of experimental and theoretical relations between Young's modulus and the flexural and longitudinal resonance frequencies of uniform bars. J. Research National Bureau of Standards 64A:147-155.
- Spinner, S., and W. E. Tefft. 1961. A method for determining mechanical resonance frequencies and for calculating elastic moduli from these frequencies. Proceedings A.S.T.M. 61:1221-1238.
- Spinner, S., and R. C. Valore, Jr. 1958. Comparison of theoretical and empirical relations between the shear modulus and torsional resonance frequencies for bars of rectangular cross section. Journal of Research, National Bureau of Standards 60:459-469.
- Svechnikov, V. N., A. K. Shurin, and G. P. Dmitrieva. 1964. Sb. Nauchn. Tr. Inst. Metallofiz., Akad. Nauk UKr. SSR. 19:206-211. Reproduced as NASA Technical Translation-TTF-10280.
- Tefft, W. E. 1960. Numerical solution of the frequency equations for the flexural vibration of cylindrical rods. Journal of Research of the National Bureau of Standards 64B(4):237-242.
- Timoshenko, S. 1937. Vibration Problems in Engineering. D. Van Nostrand Co., New York.
- Timoshenko, S., and J. N. Goodier. 1951. Theory of Elasticity. McGraw-Hill Publishing Co., Inc., New York.

- Van Thyne, R. J. 1966. Development of oxidation-resistant hafnium alloys. IIT Research Institute Report B6040-6. U.S. Naval Air Systems Command Contract 65-0301-f.
- Van Thyne, R. J., Alan L. Hess, and J. J. Rausch. 1966. Hafnium-tantalum alloy cladding as a protective coating system for rocket nozzles. Eighth Liquid Propulsion Symposium, Vol. II. Cleveland, Ohio. 395-419.
- Wachtman, J. B., Jr. 1963. Mechanical and electrical relaxation in ThO_2 containing CaO . Phys. Rev. 131:517-527.
- Wachtman, J. B., Jr., and W. E. Tefft. 1958. Effect of suspension position of apparent values of internal friction determined by Förster's method. Review of Scientific Instruments 29(6): 517-520.
- Wachtman, J. B., Jr., W. E. Tefft, D. G. Lam, Jr., and R. P. Stinchfield. 1960. Factors controlling resistance to deformation and mechanical failure in polycrystalline (glass free) ceramics. A.E.C. Publication No. 59-278. Also in Nuclear Science Abstracts 14:19443.
- Washburn, D. F., and F. K. Blechinger. 1966. Thermal expansion and temperature dependence of the elastic moduli of polycrystalline hafnium. United States A.E.C. Report KAPL-3112 by the General Electric Company.
- Zener, C. 1937. Internal friction in solids. Physical Review 52:230.
- Zener, C. 1947. Stress induced preferential orientation of pairs of solute atoms in metallic solid solution. Phys. Rev. 71:34.
- Zener, C. 1948. Elasticity and Anelasticity of Metals. University of Chicago Press, Chicago.